UNIVERSITÄT FÜR BODENKULTUR WIEN
University of Natural Resources
and Life Sciences, Vienna

Doctoral Dissertation

Impact of salts on protein-protein and protein-surface interactions

submitted by

DI Leo A. JAKOB, BSc

in partial fulfilment of the requirements for the academic degree
Doctor of Philosophy (PhD)

Vienna, January 2023

Supervisor:
Ao.Univ.Prof.i.R. DI Dr.nat.techn. Alois Jungbauer

Co-supervisors:
DI Dr. nat. techn. Nico Lingg
DI Dr. techn. Rupert Tschließnig

Institute of Bioprocess Science and Engineering
Department of Biotechnology

Affidavit

I hereby declare that I have authored this dissertation independently, and that I have not used any assistance other than that which is permitted. The work contained herein is my own except where explicitly stated otherwise. All ideas taken in wording or in basic content from unpublished sources or from published literature are duly identified and cited, and the precise references included. Any contribution from colleagues is explicitly stated in the authorship statement of the published papers.

I further declare that this dissertation has not been submitted, in whole or in part, in the same or a similar form, to any other educational institution as part of the requirements for an academic degree.

I hereby confirm that I am familiar with the standards of Scientific Integrity and with the guidelines of Good Scientific Practice, and that this work fully complies with these standards and guidelines.

Vienna, 18.01.2023   Leo A. JAKOB (*manu propia*)

Abstract

Salts, particularly dissolved as ions, are ubiquitous and serve crucial roles in regulating biological processes. Ions dictate phase behavior, protein-protein and protein-surface interactions of proteins which highlights their importance in bioprocessing. Mechanistic understanding of protein-salt interactions and their impact on interactions of proteins with various other targets allows rationalization of bioprocesses in general, maximizing the productivity and purity of each process step. In this work, the impact of salts on protein-protein and protein-surface interactions were investigated in the frame of two research problems. It is hypothesized that attractive protein-protein interactions have a positive impact on productivity but a negative impact on product purity. Furthermore, protein-protein interactions could have an impact on protein adsorption in chromatography. The first research problem concerned the investigation of protein binding of dual salt mixtures in hydrophobic interaction chromatography. In the second research problem, the cysteine-bearing CASPON enzyme was investigated for its multimerization properties in the presence of slightly repulsive and attractive protein-protein interactions. Altogether, protein-protein interactions correlated with dynamic binding capacities and thus productivities in hydrophobic interaction chromatography dual salt system for adalimumab and lysozyme. For these systems, non-Langmurian binding was observed in the adsorption isotherms, indicating that protein-protein interactions influence protein binding. Varying dynamic binding capacities when binding GFP could not be explained by protein-protein interactions. Product purity was impaired by the incubation of the CASPON enzyme under an attractive regime as multimerization is favored, both in free solution and on an IMAC stationary phase.

Kurzfassung

Salze, insbesondere in Form gelöster Ionen, sind allgegenwärtig und haben eine entscheidende Rolle in der Regulierung biologischer Prozesse. Ionen beeinflussen maßgeblich Phasentrennungen, Protein-Protein und Protein-Oberflächen Interaktionen und sind dementsprechend von enormer Bedeutung in der Bioverfahrenstechnik. Das mechanistische Verständnis von Protein-Salz Interaktionen und deren Auswirkungen auf Proteininteraktionen mit verschiedenen Molekülen oder Oberflächen verbessern das Verständnis von Bioprozessen im Allgemeinen, was die Produktivität und Reinheit in jedem Prozessschritt erhöhen kann. In dieser Dissertation wird der Einfluss von Salzen auf Protein-Protein und Protein-Oberflächen Interaktionen im Rahmen von zwei wissenschaftlichen Problemstellungen erörtert. Einerseits hypothetisieren wir, dass anziehende Protein-Protein Interaktionen die Produktivität von Chromatographieprozessen erhöht, aber andererseits negative Auswirkungen auf die Reinheit nach einem Downstream-Prozessschritt hat. In der ersten Problemstellung wurde die Verwendungen von binären Salzmischungen in der hydrophoben Interaktionschromatographie untersucht. Im Rahmen der zweiten Problemstellung wurde das cysteinhaltige CASPON Enzym und dessen Multimerisierungseigenschaften in der Gegenwart von anziehenden bzw. abstoßenden Protein-Protein Interaktionen untersucht. Im Falle von Lysozym und Adalimumab korrelieren anziehende Protein-Protein Interaktionen mit dynamischen Bindekapazitäten sowie der Produktivität in der hydrophoben Interaktionschromatographie. Für diese Systeme wich das Bindungsverhalten in den Adsorptionsisothermen vom Langmuir Model ab, was die Rolle von Protein-Protein Interaktionen unterstreicht. Unterschiedliche dynamische Bindekapazitäten bei der Beladung mit GFP können nicht durch Protein-Protein Interaktionen erklärt werden. Die Produktreinheit der CASPON Enzyms wurde bei

Inkubation unter anziehenden Interaktionen durch dessen starke Multimerisation verringert, sowohl in Lösung als auch auf IMAC stationären Phase.

Acknowledgements

First and foremost, I would like to express my deepest gratitude to my supervisor Alois Jungbauer. I feel honored to having had the opportunity to conduct my studies with such an excellent scientist and outstanding supervisor. His expertise, help and guidance helped me to become the scientist I am today.

Furthermore, I would like to thank Nico Lingg for his support and guidance during my time at BOKU. He was always eager to engage in discussions, being scientific or philosophical. He helped me to broaden my horizon and persevere.

I would also like to thank Rupert Tscheließnig, who not only helped me to tap into the nitty-gritty of biophysical chemistry, but also inspired me with his outside-the-box thinking.

I am also very grateful to having had the chance to work with Shekhar Garde at Rensselaer Polytechnic Institute. It was one of the most interesting and exciting experiences in my life.

Special thanks to my co-advisor Chris Oostenbrink, who gave valuable scientific input and offered guidance throughout my studies.

Thanks to all my colleagues at BOKU, to everyone in the BioToP PhD program and my group. It made the journey unforgettable.

Last but not least, I am thankful to have such great friends and family, supporting me relentlessly during all those years. Especially Theresa, who has supported me throughout my thesis, endured difficult times and celebrated my achievements with me.

Table of Contents

1 Introduction

Salts impact protein-protein and protein-surface interactions in downstream processing. A fundamental understanding is important for development of protein purification procedures, in general downstream processing and formulation of proteins. In aqueous solution, protein solubility varies significantly depending on the chemical makeup and structural properties of the protein of interest [1]. Salts generally increase protein solubility at low ionic strength due to charge screening [1], whereas higher ionic strength modulates protein solubility depending on the identity of the salt [2] (Figure 1). Moreover, salts influence the conformational stability of the protein [3]. The solubility and stability of the protein are affected by the accumulation and exclusion of ions on their surface [3, 4]. Salts also determine interactions of proteins to other interfaces, such as chromatographic stationary phases [5]. The solvent for all these processes is water. Due to its unique characteristics, water dictates solution properties and solvation of proteins [6].
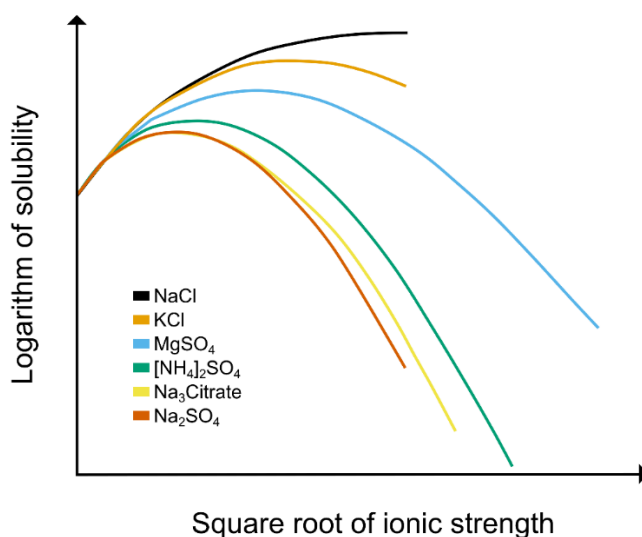

Figure 1. The effect of different salts on the solubility of carboxyhemoglobin, adapted from [7]

1.1 Hofmeister series

In biological systems, atomic and molecular ions play a crucial role in regulating biological processes and structures. Historically, Franz Hofmeister first systematically investigated the salting-out effect of cations and anions with several proteins. He proposed that ions can withdraw water molecules from proteins and thereby cause salting out [2, 8]. Hofmeister ordered ions concerning their ability to salt out proteins, dubbed the Hofmeister series (Table 1). Ions that cause salting out are often referred to as "kosmotropes," i.e., structure-making molecules that order water molecules around them [8, 9]. Indeed, classical kosmotropes such as F^- and SO_4^{2-} are strongly hydrated [8, 10]. However, their impact on water architecture might have been initially overestimated. Currently, there are debates about the impact of ions beyond their first hydration shell [10]. Ions at the other end of the series are referred to as "chaotropes", i.e., "disorder inducing", water structure breaking ions that are weakly hydrated [9].

Table 1. Hofmeister series adapted from [8]

Cations	NH_4^+	K^+	Na^+	Li^+	Mg^{2+}	Ca^{2+}	Guanidinium$^+$
Anions	SO_4^{2-}	HPO_4^{2-}	acetate$^-$	citrate$^-$	Cl^-	I^-	SCN^-
	Kosmotropic						Chaotropic

The Hofmeister series cannot be understood by their effects on water alone. For instance, the less hydrated cations, such as ammonium [11] show high salting out propensity and are therefore considered kosmotropic [12]. Ammonium is typically used as a sulfate salt as a protein precipitant. It has been reported that the ammonium ion has a high affinity towards carboxylate moieties and decreases carboxylate-carboxylate interactions after association, overall decreasing protein-protein

repulsion [12]. Calcium was shown to have concentration-dependent salting out and salting in effects through ion-bridging and overcharging, respectively [13].

Depending on the polarity and charge of the respective solute, the Hofmeister series is followed (direct series for negatively charged solutes), reversed (for positively charged solutes) or partially reversed [14]. The Hofmeister series can also change depending on the protein of interest [15].

Salting in and salting out aside, kosmotropes and chaotropes have a range of different effects on solute and solution, respectively. Kosmotropes increase the surface tension of the solution, free energy for cavity formation, protein stability and decrease protein denaturation, while chaotropes cause the opposite effects [9, 16]. The free energy of cavity formation is needed to create a cavity that accommodates the protein [16].

In water, cavity formation is also dependent on the degree of interference with the water network [17] and the impact of hydration free energy [18]. Solute size is essential for determining hydration-free energy and colloidal stability [17]. Small solutes do not interfere with the water network and are more favorably hydrated (< 0.5 nm), whereas larger solutes do interfere with the water network [17]. Recent studies have shown that surface curvature is decisive for disturbances of the water network, where concave surfaces are more likely to dewet, and convex surfaces are less likely to do so [19, 20]. This simple trend also explains why small solutes with a highly convex surface are more complex to dewet than larger solutes with a less convex surface. When imagining the rugged surface of a polymer such as a protein, one can understand why topology matters in ligand and salt binding. For instance, weakly hydrated ions such as SCN^- preferably bind to the chemically identical central region of polyethyleneglycol (PEG) over the termini, where convexity is smaller [20]. Similarly, ion-binding to polymers such as PEG might differ utterly

from chemically identical monomers due to their difference in water network disruption [21]. Another study has shown that weakly hydrated anions can bind to a curved amphiphile that resembles a hydrophobic cavity over amphiphilic adamantane carboxylic acid [22] which would be expected to have a higher binding affinity due to its hydrophobic region.

When the protein precipitates, proteins come in close contact and precipitate out of the solution as particles (salting out). Thermodynamically, preferential interaction theory can explain the effects of salting in and out [23]. Water, ions, and proteins are a weakly interactive system in which preferential interaction or exclusion of ions (or co-solutes, more broadly speaking) dictate phase behavior and stability of the protein [4, 24]. Structure-stabilizing, salting-out agents are typically excluded from the vicinity of the protein, resulting in preferential hydration of the protein [4, 25]. In such cases, the vicinity of the protein is deficient in ions compared to the bulk, and the precipitation of the protein reduces these thermodynamically unfavored zones.

On the contrary, they denaturing, destabilizing ions preferentially interacting with the protein [26, 27]. As ions bind to moieties that might be located internally in the protein's native fold, the surface accessible surface area is increased, and the protein unfolds [26]. For that matter, ion-protein interactions are essential to understand proteins' phase behavior and stability.

1.1.1 Site-specific interactions

Generally, ion-protein interactions can be categorized into amino acid side chains and protein backbone interactions. Isolated ion-amide interactions of the protein backbone can be investigated with butyramide as a proxy [28]. It was shown that soft (hence polarizable [29]) large anions such as SCN^- and I^- can bind to the formally positive amide nitrogen and slightly positively charged α-CH of the protein

backbone [30, 31]. Guanidium and thiocyanate can bind to the α-CH and α-CH$_2$ moieties of the protein backbone [12, 30, 32], and guanidinium can additionally bind to the carbonyl of the protein backbone [32]. According to preferential interaction theory, these ions then lead to salting in of the protein since they bind to protein moieties [26, 27]. To a lesser extent, the more strongly hydrated Cl$^-$ can bind to the amide nitrogen and α-CH, whereas the binding of the strongly hydrated SO$_4^{2-}$ to the protein backbone is even weaker [32]. Strongly hydrated cations such as Mg^{2+}, Ca^{2+}, and Li$^+$ can bind to an amide moiety of butyramide [28], therefore, they can interact with the protein backbone. Amide moieties were shown to bind Ca^{2+} and Li$^+$ as solvent-shared ion pairs [33]. Overall, cation-amide binding is weaker than anion-backbone binding, and most cations are excluded from the protein backbone compared to the bulk [30]. Interactions of cations with negatively charged amino acid sidechains (Asp and Glu) are more favorable, following the Hofmeister series [34, 35]. Furthermore, multivalent cations can cause attractive interactions by ion-bridging phenomena or repulsive interactions by overcharging, depending on the concentration of the multivalent ions [36, 37]. For instance, trivalent cations can bind to carboxylic side chains, leading to overcharging [38]. It was found that entropy drives cation-protein interactions, which increase with its valency [39]. Depending on the strength of the ion-protein binding, the counter-ion can bind to an ion bound to a protein which can lead to charge compensation [39].

Compared to a single negatively charged moiety (COO$^-$), there are three positively charged proteinogenic moieties: ammonium, imidazolium, and guanidium. Anions follow the reversed Hofmeister series at positively charged amino acid side chains, where strongly hydrated anions like F$^-$ and SO$_4^{2-}$ bind to said positively charged moieties [8]. A well-known example of the reversed Hofmeister series is lysozyme at low salt concentrations, a protein with a considerably high isoelectric point (pI)

of 10.7 and, therefore, positively charged in the acidic, neutral, and slightly basic range [40].

Originally, salt effects were believed to be additive, meaning that the overall salt effects are composed of the contributions of the individual salts [41-43]. Recently, it was shown that ion-ion interactions can modulate salting in and salting out effects beyond their individual contributions, respectively [32, 33, 44]. Poly(N-isopropyl acrylamide) (PNIPAM) is a polymer that serves as a proxy for protein backbone interactions due to its amide side chain. Using this model system, it was shown that I^- showed stronger binding to PNIPAM in the presence of Cs^+ compared to Li^+ and Na^+. This is due to stronger ion pairing of Cs^+ and I^- compared to the other two pairs, effectively causing ion depletion at the PNIPAM surface [45].

1.1.2 Protein unfolding and denaturation

Ions can bind to internal proteins' moieties and disrupt structural elements needed for protein conformation, which then causes either partial or complete unfolding and denaturation, respectively. Said internal moieties of proteins are primarily nonpolar and hydrophobic, whereas weakly hydrated anions and, to a lesser extent, strongly hydrated cations are typical denaturants (direct Hofmeister series). Weakly hydrated anions have been shown to bind to nonpolar interfaces [20] and thereby inhibit hydrophobic interactions needed for protein folding [46]. A prominent example is a guanidinium (Gdm^+), a chaotropic cation used for denaturation [47]. It is weakly hydrated and planar [46]. Therefore, it can bind to various amino acid side chains and stack with other planar molecules. Besides stacking with its solution, guanidium can stack with Arg, Trp, and Gln [48].

Furthermore, guanidium interacts with hydrophilic (Thr, Ser) as well as hydrophobic amino acids (Ala, Ile, Val) [48] and strongly with amino acids carrying a carboxylate moiety (Asp, Glu) [49]. Guanidium can neither form H-bonds with the amide

nitrogen nor the carbonyl oxygen, whereas chemically similar urea can bind to the protein backbone by hydrogen bonding [47]. The chaotropic effects of the guanidinium ion also heavily depend on the co-ion. Heyda et al. have shown that guanidinium is preferentially excluded from an elastin-like polypeptide when paired with sulfate and preferentially binding to it when thiocyanate is the co-ion [32]. Similarly, GdmSCN has a more significant denaturation effect on DNA than GdmCl and Gdm_2SO_4 [50]. Thiocyanate is an example of a well-studied denaturing anion. Like guanidium and urea, thiocyanate is a weakly hydrated, large, and soft ion [32]. It promotes protein denaturation due to its propensity to bind to α-CH and α-CH_2 moieties of the protein backbone [12].

1.2 Protein-protein interactions

In biology, protein-protein interactions occur via the interfaces of proteins. Interacting interfaces typically span 1500-3000 $Å^2$. Within those interfaces, so-called hot spots are responsible for the strongest interactions with an area of approximately 600 $Å^2$ [51]. For comparison purposes, amino acids have surface areas ranging from 75-255 $Å^2$ [52], therefore, a hot spot typically contains a few amino acids. Tyrosine, arginine, and tryptophane are overrepresented in hot spots compared to other amino acids [51]. As previously outlined, guanidine can interact with tryptophane and arginine, which at least partly explains the salting in the effect of guanidine and guanidinium moiety of arginine [48]. Typically, the protein-protein interactions encountered in bioprocessing are weak and unspecific [53, 54] unlike those found in biological complexes [51, 53, 54]. For many proteins, non-covalent self-association can indeed occur depending on the target protein and solution conditions [55-60]. When reversible self-association occurs, interacting proteins lock into a stable conformation detected in solution [55]. Protein-protein interactions

can also be enabled by ion-bridging, where ions facilitate interactions between like-charged moieties [13, 39]. Due to the therapeutic importance of monoclonal antibodies, their weak protein-protein interactions and their effect on solution behavior and protein stability are well studied [54-56, 60-63]. Ions and co-solutes can decrease protein-protein interactions, decrease solution viscosity and increase protein stability. This eases syringability [62, 64], prolongs its shelf life [65] and diminishes adverse effects [66]. However, in the presence of repulsive protein-protein interactions, the viscosity of protein formulations might still be elevated. The relationship between viscosity and protein-protein interactions is non-trivial [57]. Non-additive effects of salt mixtures can also impact protein-protein interactions. Generally, the solubility of proteins with regards to ion concentration either strictly increases (salting in) or increases at first and then decreases (salting in followed by salting out). In alkali iodide and alkali sulfate mixtures, the solubility of PNIPAM shows atypical behavior where solubility shows three distinct regions (I: salting out, II: salting in, III: salting out). When incubated with the individual salts alone, solubility either strictly decreases (sulfate) or shows a local maximum and decreases afterward (iodide) [44], which is most commonly observed for single salts [67]. The authors explain the presence of the three regions by competition of sulfate and iodide for the alkali counter-ion. In the first region, the more hydrated iodide is excluded from the surface and thus salts out since iodide binding does not occur. Due to the lower dissociation constant of the alkali sulfates, alkali-sulfate interactions are stronger and therefore sulfate binds to the respective alkali ion, hydrating iodide. With increasing alkali iodide concentration, sulfate reaches saturation, and hydration of iodide decreases, driving iodide towards the PNIPAM interface and thus causing salting in. In the last region, the PNIPAM interface becomes saturated with iodide, and salting out is caused by excluded volume effects [44].

1.2.1 Analytical techniques

A quantitative measure of protein-protein interactions is given by the second virial coefficient, B_{22}, which correlates to the potential of mean force of all possible interactions between two proteins [68]. B_{22} can be determined via static light scattering [60], small angle x-ray scattering (SAXS) [69] , or self-interaction chromatography (SIC) experiments [70]. For SIC measurements, the protein of interest is immobilized in the stationary phase. The ligand interacts with the same protein as the analyte in the mobile phase. When proteins exhibit attractive interactions, the analyte interacts with the ligand-protein bound to the stationary phase, thereby increasing retention. In that case, the resulting B_{22} is negative. In the presence of repulsive interactions retention is decreased, and retention time can be shorter than through size exclusion effects alone, resulting in a positive B_{22} [70].

When employing light scattering techniques such as multi-angle light scattering (MALS) and SAXS, visible light, and x-ray radiation are used to illuminate the sample, respectively. Depending on the intra- and intermolecular arrangement of the analyte, light scatters elastically from N points and can be detected at different angles [71]:

$$I(q) = \left| \sum_{i=1}^{N} e^{i\,\vec{q}\cdot\vec{r}_i} \right|^2 \qquad (1)$$

Where $\vec{r}$ is the position vector of the scattering element, $\vec{q}$ is the scattering wave vector, and q is the scattering vector:

$$q = 4\pi\,\lambda^{-1}\,sin(\theta/2) \qquad (2)$$

Where λ is the wavelength, and θ is the scattering angle.

In practice pair density distribution functions (p(r)) are used to calculate scattering curves [72]:

$$I(q) = 4\,\pi \int_0^{Dmax} p(r) \frac{sin(q\,r)}{q\,r}\,dr \tag{3}$$

Where r is the distance between two pairs.

Due to the different wavelengths employed in MALS and SAXS analyses, investigated length scales differ. MALS can be used for the determination of the radius of gyration (R_g), the weight average molar weight (M_w), and the second virial coefficient (B_{22}) [73]. SAXS experiments can provide information about protein-protein interactions and intramolecular structure. q-regions in SAXS traces correspond to different length scale according to Equation 4 [74]. Figure 2 shows a theoretical scattering plot of a monoclonal antibody and the corresponding q-regions for protein-protein interactions, intramolecular and surface structure.
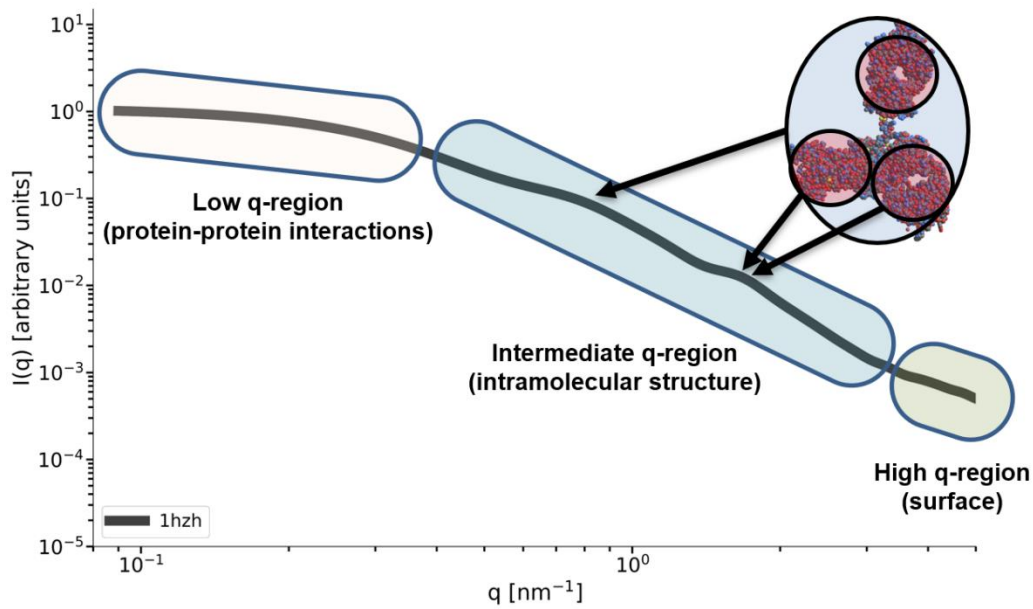
$$d = \frac{2\,\pi}{q} \tag{4}$$

Figure 2. Theoretical SAXS trace of a monoclonal antibody (PDB: 1hzh) with highlighted regions that are distinct for respective correlation distances. The pair distances of the atoms in the PDB have been transformed for the calculation of the scattering curve according to Equation 3.

Moreover, SAXS allows the investigation of r_g and B_{22}. SAXS is especially insightful for reversible self-association since the scattering trace can be fitted to the theoretical scattering data of different models of associated proteins [55]. If several different associated species are present in solution, data analysis is aggravated since scattering traces are obtained from the ensemble average in solution. This might result in many possible confirmations [56]. Generally, SAXS offers higher resolution and information content. However, the instrumentation is less accessible, and analytes suffer from radiation damage [75, 76].

Furthermore, protein-protein interactions can be quantified via dynamic light scattering (DLS). In DLS, light scattering fluctuations are measured to calculate the

diffusivity and, thus, the hydrodynamic radius of the analyte, assuming a spherical analyte [77]. The diffusion interaction parameter can be determined when measuring different protein concentrations [57, 78]. This is another parameter for protein-protein interactions, whereas values lower than -8 ml*g^{-1} are considered attractive [57, 61, 79].

In formulation science, there is extensive literature about the correlation between protein-protein interactions and protein aggregation [69], particularly for monoclonal antibodies [80-84]. According to the theory of slow coagulation, B_{22} correlates to protein aggregation for globular proteins that irreversibly bind after association [85]. However, protein-protein interaction effects in downstream processing are often neglected, rarely investigated, and discussed.

1.2.2   Model proteins

In this doctoral thesis lysozyme, adalimumab (a monoclonal antibody), green-fluorescent protein (GFP) and the CASPON enzyme have been investigated. They have been selected according to their differences in size (Figure 3 and Table 1), isoelectric points (Table 2), availability as model proteins (lysozyme and GFP), clinical relevance (adalimumab) [86] and high cysteine content (CASPON enzyme) [87].

Table 2. Molar mass and isoelectric point of the model proteins in this thesis. For the CASPON enzyme, the isoelectric point was calculated by Expasy ProtParam

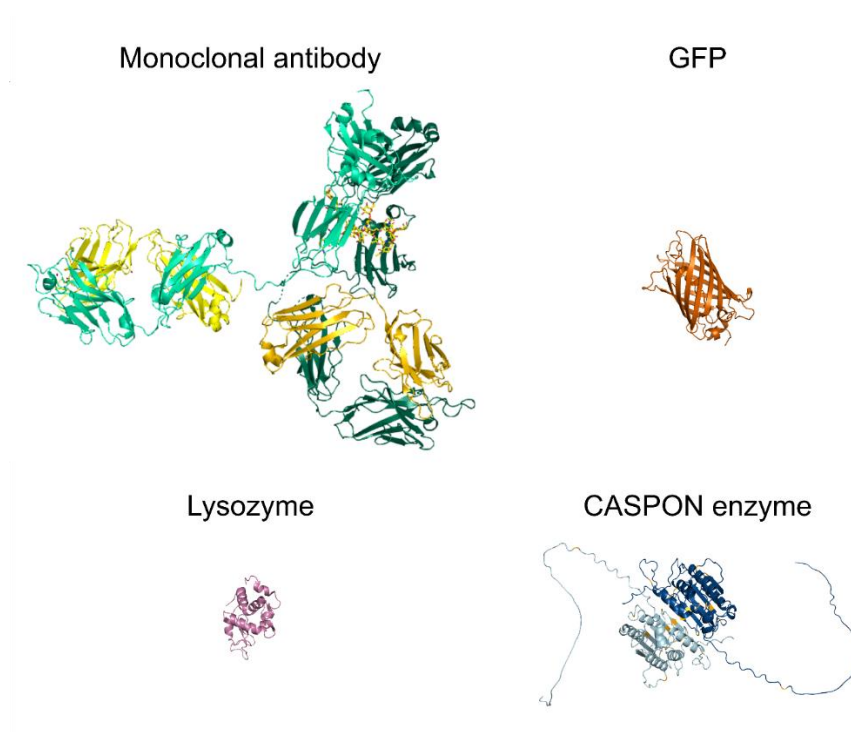| Model protein	Monoclonal antibody (adalimumab)	GFP	Lysozyme	CASPON enzyme
Molar mass [kDa]	148 [88]	26.9 [90]	14.3 [91]	70.6
Isoelectric point	7.9-9.1 [89]	5.8 [90]	10.7 [91]	6.2

Figure 3. Illustration of model proteins used. The corresponding PDB accession number are: 1hzh (monoclonal antibody), 1gfl (GFP), 1dpx (lysozyme). The CASPON enzyme [87] model was generated by AlphaFold [92, 93].

As a protein class, monoclonal antibodies are well-studied concerning protein-protein interactions [53, 56, 57, 60, 94-96]. Monoclonal antibodies consist of two heavy and two light chains that together form two antigen-binding fragment (Fab) arms and the crystallizable fragment (Fc) [97]. The apical part of the Fab arms contains the complementary-determining region (CDR) that binds to the antigen [98]. For monoclonal antibodies, protein-protein interactions are frequently mediated through Fab-Fab [99] and Fab-Fc interactions [100]. Fab-mediated interactions often involve the CDR [94, 100], where single mutations can significantly decrease attractive interactions [94]. Aromatic and hydrophobic residues have been shown to be crucial for hot spots in CDRs [63, 94, 101]. Mutation of those residues might

affect antigen binding significantly [94, 102], which aggravates the rational engineering of monoclonal antibodies regarding minimal protein-protein interactions. Minimizing protein-protein interactions would aid manufacturability and increases its shelf-life. Biotechnologically, the precipitation of monoclonal antibodies offers a low-cost alternative to Protein A chromatography capture. Polyethylene glycol (PEG) and zinc are added to the supernatant of the cell culture and precipitate the product. Precipitation of the monoclonal antibodies can be achieved by PEG [103] and zinc alone [104, 105], respectively, or a combination of both co-solutes [106, 107].

The CASPON enzyme is a circularly permuted mutant of the human caspase-2 protease [87, 108] and forms the centerpiece of the CASPON technology platform process [109]. The CASPON enzyme carries a solubility tag and a hexahistidine tag, making it a very soluble protein and facilitating manufacturing [87]. The protein of interest (POI) is expressed with a hexahistidine tag and a recognition site for the CASPON enzyme. The POI can be captured using immobilized metal ion affinity chromatography (IMAC). Subsequently, the hexahistidine tag and the recognition site are cleaved by the CASPON enzyme. After removing the cleaved tag and the CASPON enzyme by another subtractive IMAC step, high purities of the POI are achieved. For instance, when producing FGF2 with the CASPON technology, the final protein purity is 97.7 %, and HCP content is 40 ppm after two chromatography steps [109]. Besides its industrial potential, the CASPON enzyme is an interesting model protein due to its high number of cysteines. The active CASPON enzyme contains 26 cysteines (each monomer contains 13 cysteines) [87, 108].

Proteins containing cysteines are especially vulnerable under attractive protein-protein interactions as associations can be locked due to disulfide bond formation, e.g. for lysozyme [110]. In vitro, the formation of disulfide bonds is a pH-dependent

reaction. At basic pH, deprotonation of thiol moiety of cysteine (pKa = 8.5) occurs and forms the more nucleophilic thiolate anion. Free thiolate anions can bind other thiol moieties via a nucleophilic attack to form a disulfide bond [111, 112]. Surface-exposed, oxidized disulfides might also be involved in aggregation since existing intramolecular disulfide bridges can reshuffle intermolecularly to form multimers [11].

Due to its high crystallization propensity, lysozyme is an inexpensive, readily-available model protein for crystallization studies [113]. Crystallization of lysozyme occurs when the second virial coefficient is within the so-called "crystallization slot", which is in a slightly attractive regime [114]. More attractive conditions typically induce aggregation and fibrillation, respectively [110]. Another prominent model protein is a green fluorescent protein (GFP), a beta-barrel protein containing a fluorophore [115]. GFP is suitable for exploring interactions between different proteins in which it is fused to one of the interaction partners [13, 116].

1.3 Protein-surface interactions

1.3.1 Preparative chromatography

Protein-surface interactions dictate binding capacity and purification performance of chromatographic processes. Preparative chromatography is one of the most commonly applied unit operations in the manufacturing of biopharmaceuticals and recombinant proteins. It is a unit operation combining capacity, selectivity and versatility [5].

Most commonly, proteins are purified in bind and elute mode. In bind and elute mode, the chromatographic column is equilibrated in a suitable buffer that promotes protein binding. After equilibration, the protein of interest is first bound to the stationary phase, usually followed by a wash step. In the elution phase, the protein of interest is eluted by weakening the interaction of the protein with the stationary phase. This is achieved by either modulation of the ion concentration of the mobile phase or addition of an organic modifier and displacer, respectively. After elution of the protein of interest, the cleaning-in-place (CIP) procedure achieves sanitization and removal of strongly bound impurities [5].

The productivity of a chromatographic unit operation is given by Equation 5 [5]:

$$P = \frac{\eta_E * DBC_{10\%}}{\frac{DBC_{10\%}}{C_F}\frac{L}{u_{Load}} + t_{Wash} + t_{Elution} + t_{Equillibration} + t_{CIP}} \tag{5}$$

where η_E is the fraction of protein recovered in the elution phase, $DBC_{10\%}$ is the dynamic binding capacity at 10 % breakthrough, L is the length of the column, u_{Load} is the linear flow velocity to the flow rate, the ratio L/u_{Load} is the residence time, C_F is the protein feed concentration and t is the elapsed time of the corresponding phase.

Equation 5 demonstrates that the $DBC_{10\%}$ is a crucial parameter with regards to productivity of a chromatographic unit operation. In practice, it is sought to maximize $DBC_{10\%}$ to an extent where the desired protein purity is not compromised [5]. Figure 4 shows an illustration of two breakthrough curves where surface coverage of the stationary phase differs. In practice, the dynamic binding capacity at 10 % breakthrough is an easily obtainable parameter that can be used as a starting point for process development [117]. The equilibrium binding capacity (EBC) is the binding capacity of a column with infinite efficiency and its relation to the DBC depends on the respective dispersive mechanisms [5].
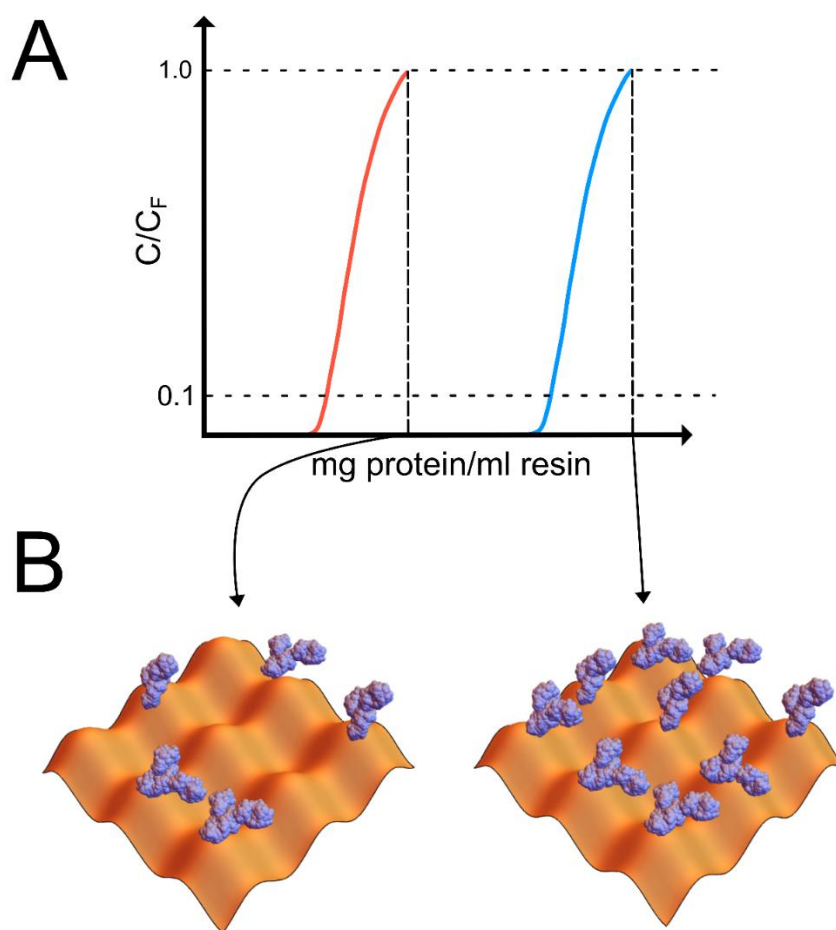
Figure 4. A: Illustration of breakthrough curves with different surface coverage. High surface coverage breakthrough curve indicated in blue, low surface coverage indicated in red. The column is fully saturated when the ratio $C/C_F = 1$, where C is the mobile phase concentration. $DBC_{10\%}$ occurs at $C/C_F = 0.1$. B: Illustration of the stationary phase and bound protein in the nanoscale, low surface coverage left, high surface coverage right.

Purity criteria for an individual process step depends on the application of the produced protein. For biopharmaceuticals, general guidelines for purity criteria exist, however, they are highly dependent on various factors such as the dose, risk-benefit ratio etc. Aggregates are among the critical product-related impurities as they can induce immunogenic reactions in patients and other side effects, respectively. Generally, dimer and higher order multimers content should be < 1 % of the specific protein content, highlighting the importance of avoiding aggregate formation and its effective purification during downstream processing [5].

1.3.2 Effects of salts on protein-surface interactions

Protein-surface interactions dictate the binding and elution behavior of proteins in chromatographic processes. Protein-surface interactions are driven by electrostatic interactions, hydrophobic interactions, complexations, or a combination thereof [5]. In hydrophobic interaction chromatography (HIC), binding is achieved at high salt concentrations where ideally only protein-surface interactions are increased, whereas elution is achieved at low salt concentrations. For ion-exchange chromatography (IEX), binding and elution are achieved at low and high salt concentrations, respectively. In both chromatography modes, ionic strength and identity of ions dictate chromatographic elution behavior [5]. In IEX, increasing ion concentration competes with proteinogenic moieties for ligand binding and causes the chromatographic velocity of the proteins to increase. Elution strength can be modulated depending on the ion identity [118-120]. Preferentially interacting salts, hence chaotropes, tend to have higher elution strength over preferentially excluded salts due to higher affinity towards the protein surface and chromatographic ligands [121].

Interestingly, the choice of co-ions also impacts elution behavior, therefore, anions in cation-exchange chromatography or vice versa. This was shown in a publication by Fuchs et al., where different sodium salts with different anions (citrate, chloride, sulfate, phosphate, and tartrate) induced significantly different retention factors in cation-exchange chromatography [120]. As previously outlined, ion-ion interactions might be a reasonable explanation for elution strength differences. Nevertheless, corresponding experimental evidence in chromatography is lacking up to this day.

For complexation and biospecific interactions of the protein and a stationary phase, the impact of salts depends heavily on the nature of the interaction. For affinity chromatography ligands such as Protein A and complexed Ni^{2+}, low to high concentrations (0.1-2 M) of sodium chloride are employed to suppress unspecific electrostatic interactions [122-124]. One of the most commonly employed ligands is the Protein A ligand from *Staphylococcus aureus*. Protein A affinity chromatography is the workhorse for manufacturing monoclonal antibodies [124], where the Protein A ligand interacts with the Fc region of the monoclonal antibody [125]. The interaction between the antibody and Protein A is disrupted by decreasing the pH below 3.5 [125]. In Protein A chromatography, monoclonal antibodies are loaded at low ionic strength and washed with 2 M NaCl to elute non-specifically interacting impurities [123], highlighting the minor role of ions in the interaction. Another prominent ligand for affinity chromatography is IMAC for purifying histidine-bearing proteins. In IMAC, Cu^{2+}, Zn^{2+}, $Co^{2+,}$ and Ni^{2+} are binding to immobilized chelators such as iminodiacetic acid (IDA) or nitrilotriacetic acid (NTA) [5, 126]. Said divalent cations can then complex proteinogenic histidines and cysteines, while interaction with histidine tags is especially strong [5]. Elution can be achieved by lowering the pH and thus protonating binding amino acids or adding a high concentration of competing imidazole [122]. 0.1-1 M NaCl is typically added

to decrease non-specific electrostatic interactions [122, 127, 128] whereas kosmotropic salts affect protein binding [128]. Interestingly, the addition of sodium sulfate can induce unspecific binding on a Ni-containing stationary phase, while the Ni-free control experiment only showed minimal binding [128]. This indicates that sodium sulfate increases unspecific protein binding only when a portion of the protein can bind to the stationary phase through complexation.

In hydrophobic interaction chromatography, protein-surface interactions are increased with increasing salt molality (m) and surface tension (γ) of the solution [129, 130]:

$$log \; \frac{k}{k_0} = E + F * \gamma + G * m \tag{6}$$

The surface tension of a salt solution depends on the concentration and surface tension increment (σ) of the respective salt [16]:

$$\gamma = \gamma_0 + \sigma \, m \tag{7}$$

Where γ_0 is the surface tension. This basic model does not factor in complex phenomena such as lateral protein-protein interactions in solution or when bound to the chromatographic resin. Furthermore, the surface tension of electrolyte mixtures cannot be calculated based on the properties of ideal binary salt systems alone, complicating the application of the model for dual salt systems [131].

The Hofmeister series can be constructed via the surface tension increment of the respective salt [16], which agrees overall well with salting out and in effects on proteins [2, 16, 132]. Salts with high surface tension increments increase the free energy of cavity formation of the respective solute and destabilize said solutes, causing a phase transition from the liquid phase to the solid phase [17, 129]. This ties back to the overall concept that hydrophobic interactions of proteins with stationary phases are linked to the free energy of cavity formation [124]. This is

conceptually true for proteins in free solution without any hydrophobic solid phase and in a chromatographic system.

One has to bear in mind that the surface tension of a solution is only a proxy for the aqueous/protein interface. From an experimentalist's point of view, it is a useful approximation since it is more easily examinable. Both the aqueous/air [133, 134] and the aqueous/analyte interface [35, 135] are influenced by the presence of ions [8]. Even for reasonably comparable interfaces, ions might experience different dynamics and have different characteristics in the aqueous/air interface compared to other interfaces, such as the aqueous/graphene interface [136]. As proteins are very heterogenous on their surface, ions are expected to deviate significantly in their behavior compared to the aqueous/air interface. This has to be kept in mind when deducing macroscopic solution properties to microscopic events such as hydrophobic interactions.

1.3.3   Chromatographic media as a self-avoiding random walk

The entire nanoscale surface morphology of chromatographic resins is not well documented, although several studies elucidate the upper nano- and micrometer scale of several chromatographic stationary phases [137, 138]. For synthetic polymers such as polymethylmethacrylate (PMMA), the backbone can be modeled as a self-avoiding random walk [139]. Conceptually, the easiest model of a self-avoiding random walk is a chain of non-interacting hard spheres (monomers) that grow successively. The entire polymer is self-avoiding, therefore single monomers are added to the polymer in a fashion that does not result in collisions [140]. This is an intuitive coarse-grained description of a polymer chain [139], such as a synthetic chromatographic resin.

Further, the spheres exclude their volume and an outer shell with a radius equal to their own, as shown in the shaded area in Figure 5. The overall spherical volume and the volume of this outer shell correspond to the excluded volume [141], which is a parameter describing the self-avoiding random walk [142]. Therefore, depending on the topology of the polymer, the excluded volume varies (Figure 5A). When applying this model to a stationary chromatographic phase with bound proteins, the excluded volume parameter offers a potential parameter for understanding the binding topology. Figure 5B shows the chromatographic resin binding an adsorbate (such as a protein) either on convex or concave parts of the stationary phase. Figure 5B also shows that the overall shaded area increases to a greater extent if the adsorbate binds to a convex region than a concave region.
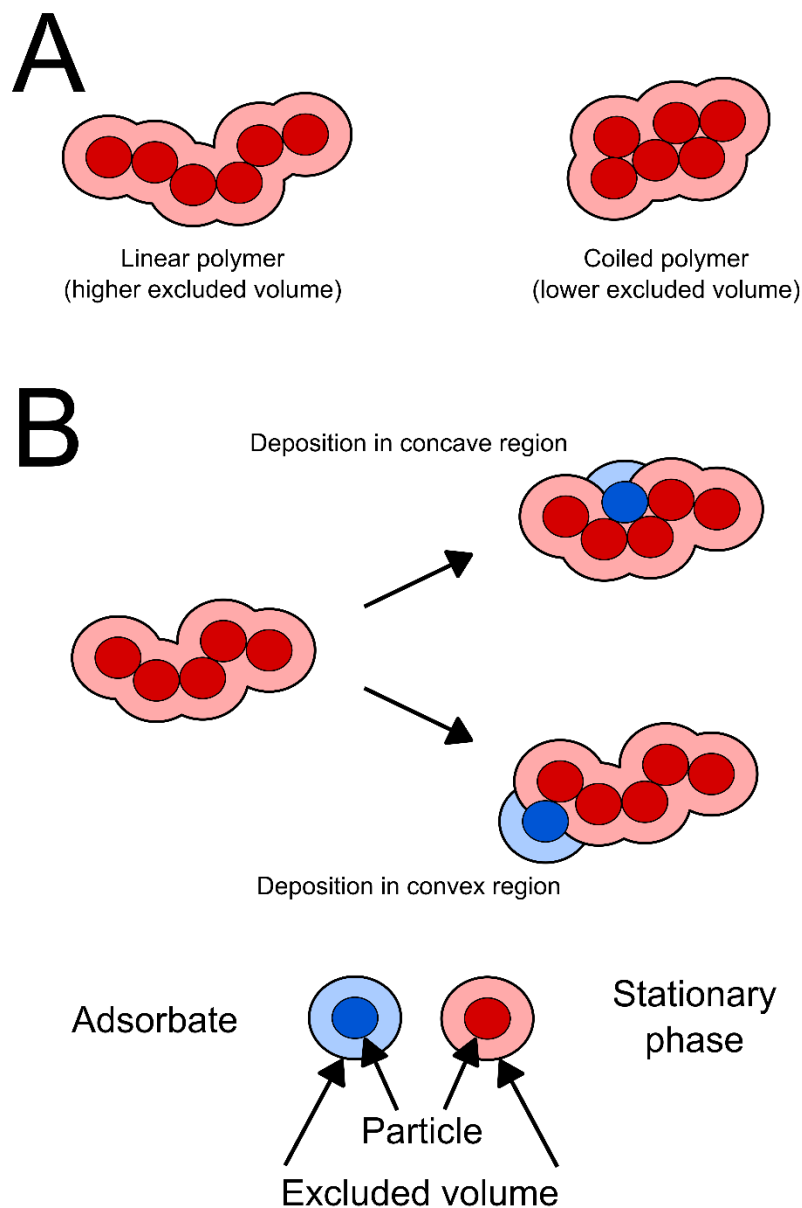
Figure 5. Self-avoiding random walk modeling a polymer with its excluded volume in the shaded area. A: Relatively linear self-avoiding random walk with a higher excluded volume than a coiled polymer. B: Depending on whether a single monomer is added to the convex or concave region of the polymer, the excluded volume parameter tends to decrease (concave) and increase (convex), respectively.

So-called mixed electrolytes or more specifically dual salt systems were shown to be beneficial in HIC. In dual salt systems, high concentrations of two different salts are used to facilitate binding, where conventionally, only a single salt is used. Senczuk et al. showed that a combination of two kosmotropic salts (sodium citrate and sodium phosphate) had increased dynamic binding capacities and protein solubilities for an IgG2 and an Fc-fusion protein on Toyopearl Butyl 650M [143]. In a later study, Müller et al. have shown that the combination of a chaotropic and kosmotropic (indicated by low and high surface tension increment) salt significantly increases dynamic binding capacities for lysozyme and a monoclonal antibody on Toyopearl Phenyl-600M, Butyl-600M, and PPG-600M in 21 out of 27 salt combinations tested. Generally, employing a combination of chaotropic and kosmotropic salts resulted in higher dynamic binding capacities compared to two kosmotropic or two chaotropic salts. The authors hypothesized that the chaotropic salt increased protein solubility, allowing for higher total salt concentrations. Higher total salt concentrations then increase interactions of the protein and the stationary phase, increasing overall dynamic binding capacities [130]. Therefore, mixing a chaotropic and a kosmotropic salt can be considered a rule of thumb in process development in dual salt HIC systems. Werner et al. have investigated lysozyme binding to mildly hydrophobic Toyopearl PPG-600M in different binary and trinary salt mixtures (ammonium chloride, sodium chloride, ammonium sulfate and sodium sulfate). When mixing different chloride and sulfate salts, synergistic improvement of binding capacities was observed compared to the single salt system. On the other hand, mixing different ammonium and sodium salts did not cause higher binding capacities compared to the individual salts [144]. Hackemann et al. have investigated BSA as a model protein in binary and trinary mixtures at different operating pH, resulting in different net charges of the protein. The employed salts were sodium

chloride, sodium sulfate, ammonium chloride and ammonium sulfate. They reported that these salt mixtures can have positive, neutral or negative effects on binding capacities compared to the corresponding single salt. Interestingly, relative binding capacities were inverted qualitatively when incubating at pH 7.0 (net negative charge of BSA) compared to pH 4.0 (net positive charge of BSA), emphasizing the importance of protein charge in dual salt HIC systems. As for lysozyme, BSA exhibited positive or negative cooperative behavior in mixtures of sulfate and chloride, whereas ammonium and sodium salt mixtures exhibited linear change of the binding capacity [145]. Baumgartner et al. followed a practical approach to study dynamic binding capacities of dual salt HIC systems. Different ratios of a rather chaotropic (sodium chloride) to a kosmotropic salt (ammonium sulfate or sodium sulfate) were employed and solubility of lysozyme in these systems were investigated. A concentration close to the solubility of lysozyme was selected as the salt concentration for protein binding in HIC, namely 90 % of the salt concentration were precipitation was observed [146]. Selecting a salt concentration that is close to salting out of the protein of interest is a common approach in HIC process development [147]. Ultimately, dynamic binding capacities for both dual salt systems did not show clear trends. For both systems, dynamic binding capacities showed a maximum at higher proportions of the chaotropic salts. These maximum dynamic binding capacities were also higher compared to the single salt systems. Furthermore, dynamic binding capacities showed a minimum at a higher proportion of the kosmotropic salt for the sodium chloride and ammonium sulfate system[146]. Moreover, the authors could show that DBCs correlated well to ionic strength, but not to the surface tension of the solution [146].

Altogether, dual salt systems are not well understood and increase of binding capacity cannot be predicted a priori. However, one can conclude general guidelines.

Firstly, mixtures of kosmotropic and chaotropic salts seem to be generally more beneficial with regards to dynamic binding capacities compared to mixtures of only kosmotropic and only chaotropic salts, respectively [130]. Secondly, ionic strength seems to be the more decisive parameter governing dynamic binding capacities compared to surface tension as indicated by Baumgartner et al [146]. Thirdly, ionic strength seems to be a decisive parameter for static binding capacities, however, they are not solely responsible for differences in binding capacities [144, 145]. This phenomenon was not reported for dynamic binding capacities yet.

1.3.5 Lateral interactions of proteins bound to a stationary phase

Lateral protein-protein interactions add additional complexity to protein-surface interactions. They potentially modulate binding capacities [121, 148] and potentially cause protein aggregation, as described in formulation sciences [121]. The most common binding model for proteins on stationary phases is the Langmurian model [149]. Here, the protein binds to the surface modeled by a grid with equal adsorption energy without any lateral protein-protein interactions. Naturally, said assumptions and prerequisites might not be applicable depending on the surface and presence of protein-protein interactions [149]. For instance, BSA was shown to either form clusters or bind as a monomer at surface coverage below monolayer adsorption levels on a PEG-modified surface. BSA monomers laterally move on the surface and reversibly associate with existing clusters. The residence time of the monomeric BSA at the clusters was below 2 s for 90 % of the associations. [150] Surface hydrophobicity might also have an impact on lateral interactions. On a hydrophobic surface, fibrinogen was shown to have higher mobility and self-association than the hydrophilic oligo ethylene glycol surface [151]. Generally, protein-protein interactions in solution potentially indicate lateral protein interactions in the bound

state. However, protein-surface interactions might catalyze protein aggregation through either partial unfolding and subsequent exposure of hydrophobic regions or by arranging proteins in an aggregation-prone orientation. For recombinant human leukin-1 receptor antagonists at the silicone oil-water interface, the aggregate formation was only observed at the interface and not in bulk solution. Aggregate formation at the surface occurred even though the recombinant protein binding at the interface was low. In this study, protein-protein interactions correlated with gel strength [152]. High ionic strength might favor lateral interactions, particularly in HIC. For HIC, another complication is the potential unfolding of the target protein [153-158]. The unfolding degree depends on the stationary phase's hydrophobicity [154] and the target protein [159].

Regarding the protein, the adiabatic compressibility was correlated to the extent of unfolding in HIC [154]. Furthermore, more labile regions of proteins unfold to a greater extent than more stable regions, as indicated by isothermal titration calorimetry [154]. Together with attractive conditions induced by high ionic strength, the unfolding of proteins might cause an even higher degree of irreversible aggregation under crowded conditions and partial unfolding of the protein of interest. In such instances, the stationary phase would catalyze irreversible aggregation. Ultimately, HIC is an interesting but complex unit operation for studying different salts. Other chromatography modes do not employ conditions favoring protein-protein interactions, such as affinity chromatography (AC) and ion-exchange chromatography.

Several adsorption models implicitly or explicitly account for protein-protein interactions. The Brunauer-Emmett-Teller (BET) adsorption isotherm accounts for multilayer formation in which the bound analyte serves as a new binding site [160]. The Oberholzer and Lenhoff isotherm models the adsorption of small, globular

proteins through colloidal energetics [161]. In that model, an electrostatic interaction parameter for protein-protein interaction is included. The Freundlich isotherm assumes adsorption sites with different adsorption energies [149, 162, 163]. Concerning lateral protein-protein interactions, heterogeneous adsorption energies could be induced by concentration-dependent protein-protein interactions, a common phenomenon for proteins in solution [164, 165]. Figure 6 exemplifies lateral protein-protein interactions that could lead to higher surface coverage compared to non-interactive systems. Dependent on the surface concentration of the protein, protein-surface interactions are facilitated in the case of attractive interactions and attenuated in the case of repulsive interactions.
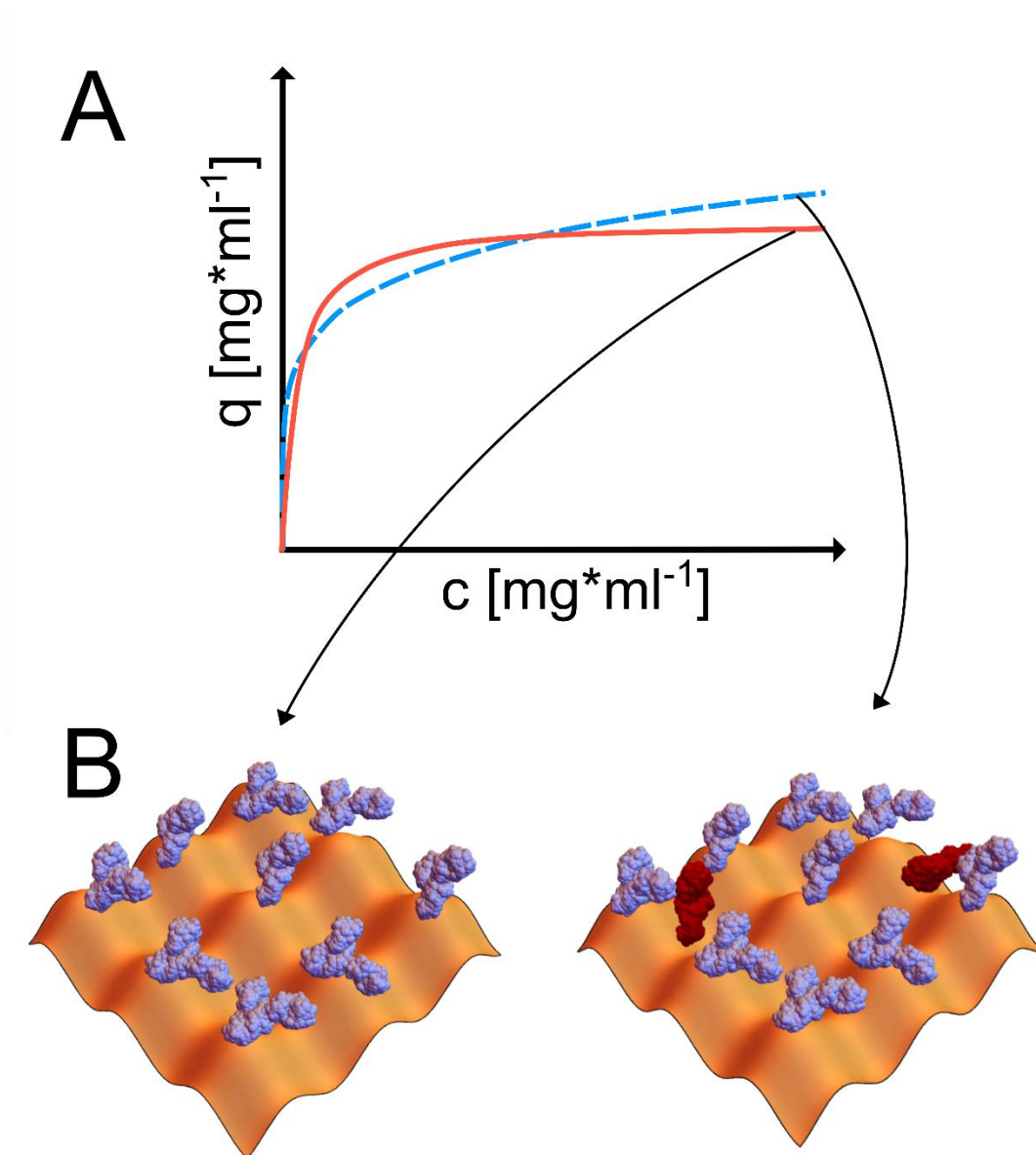
Figure 6. A: Illustration of the Langmuir model (red) where saturation (q_{max}) is reached vs. the Freundlich model (blue, dashed) where the binding capacity q steadily increases. B: Illustration of a stationary phase (orange) and bound proteins (light purple and red). Potential reasons for differences in binding capacities data that follows Freundlich vs. Langmuir models could be protein-protein interactions that facilitate the accommodation of additional proteins (dark red).

2 Aims & Hypothesis

The aim of the thesis was to elucidate the impact of salts on protein-protein as well as protein-surface interactions within the frame of two research problems. The first research problem covered different dual salt hydrophobic interaction chromatography systems. The second research problem concerned multimerization of a labile cysteine-bearing protease in free solution as well as when bound to an affinity chromatography stationary phase. In the first research problem, the aim was also to investigate the impact of surface tension and ionic strength on dynamic binding capacities of dual salt hydrophobic interaction chromatography systems. Furthermore, I aimed to gain a deeper understanding of dual salt systems in the molecular- and mesoscale by an in-depth small-angle x-ray scattering analysis of the model proteins in solution as well when bound to the stationary phase. In the second research problem, the aim was to study the multimerization behavior of a labile, cysteine-bearing protease in solution and its correlation to multimerization on a chromatographic stationary phase. This work should contribute to rationalize downstream process development and to gain a deeper understanding of the effects of employed salts when proteins are separated by chromatography. In particular, knowledge-based guidelines should be established for manufacturing cysteine-bearing proteins in the presence of attractive protein-protein interactions.

The main hypotheses were:

- I hypothesize that attractive and repulsive protein-protein interactions have a positive and negative impact on productivity depending on the employed salts, respectively. Vice versa, product quality is hypothesized to be diminished and improved for attractive and repulsive interactions, respectively.

- I hypothesize that the combination of different salt mixtures modulate the binding capacity in hydrophobic interaction chromatography due to changes in surface coverage and multilayer formation, respectively. This modulation occurs in the presence of protein-protein interactions.
- Alternatively, I hypothesize that dynamic binding capacities are altered due to changes of the footprint of the proteins which allows more protein to bind to the surface compared to single salt systems. The footprint of the proteins might be altered by expansion, collapse or change of the hydration shell of the protein, respectively.
- I hypothesize that the multimerization mechanism of a protein in free solution can serve as a proxy for multimerization on a chromatographic surface, in particular for proteins prone to multimerization.

3   Extended discussion

As previously reported, dynamic binding capacities in dual salt HIC systems can differ vastly whereas mechanistic understanding of the phenomenon is lacking [130, 143-145, 166, 167]. Initially, I have studied the effect of ionic strength and surface tension of HIC buffers on dynamic binding capacities for a selected set of model proteins and dual salt systems. Baumgartner et al. [146] already showed that ionic strength seems to be more decisive than surface tension which I confirmed for two different model proteins (adalimumab and lysozyme) in a set of three different dual salt systems (sodium citrate with either sodium phosphate, sulfate or acetate as a secondary salt). Furthermore, I could demonstrate that ionic strength is more decisive, however, it is not sufficient to describe dynamic binding capacities. This was already indicated by Werner et al. [144] and Hackemann et al. [145, 166] for static binding capacities and is now also confirmed for dynamic binding capacities. Thereafter, I investigated potential reasons for differences in dynamic binding capacities for buffers of equal ionic strength with a small-angle x-ray scattering analysis. Small-angle x-ray scattering experiments for the proteins in solution revealed differences in protein-protein interactions for adalimumab and lysozyme in the dual salt systems. For adalimumab and lysozyme, attractive protein-protein interactions correlated qualitatively with dynamic binding capacities in dual salt HIC systems. As dynamic binding capacities are increased for these model proteins, the productivity of the loading phase is boosted accordingly as more protein can be bound per volume and time. For GFP, protein-protein interactions are in the neutral range and cannot explain differences in dynamic binding capacities. A potential explanation for the absence of repulsive or attractive interactions might be the different surface properties of the model proteins. Unlike adalimumab and lysozyme, the pI of GFP is acidic and below the operating pH of 6, leading to a net negative

charge in all experiments. Since several multivalent anions have been employed, particularly the divalent anions citrate^{2-}, SO_4^{2-}, and HPO_4^{2-} could cause protein-protein interactions through ion-bridging phenomena of the net positively charged adalimumab and lysozyme. Vice versa, GFP would experience ion-bridging phenomena to a smaller extent.

Although protein-protein interactions can be correlated to the binding capacity for adalimumab and lysozyme, there is no explanation for the decreased binding capacities of the single salt citrate system. Non-additive salt effects could modulate the activity of either citrate or the secondary ion, leading to stronger hydration and hence the exclusion of the ions from the protein. This would, in turn, favor hydrophobic interactions of the dual salt systems over the single citrate system. Alternatively, higher citrate concentrations could cause overcharging of the protein and thus induce repulsive and less attractive protein-protein interactions. Overcharging phenomenon could occur preferably in the single salt citrate buffer due to the presence of higher concentrations of the trivalent citrate anion at pH 6. Another possible explanation for decreased attraction in the citrate system would be diminished ion-bridging by citrate over to the secondary ions. As the five-carbon backbone of citrate is large compared to sulfate, phosphate, and acetate, citrate could cause higher steric hindrance while binding to cationic amino acid residues. If citrate causes steric hindrance and thus decreases protein-protein interactions, different salt combinations could cause repulsive interactions. Thus, dual salt systems do not necessarily cause attractive interactions, higher binding capacities, and higher productivity in the loading phase. Altogether, rationalizing dual salt effects is fairly difficult and employing a secondary salt adds additional complexity to HIC.

Experiments with GFP indicate that protein-protein interaction does not contribute significantly to dynamic binding capacities for all model proteins. The employed

salts rather induce different protein-surface interactions that would be needed to be investigated separately. The experimental setup did not allow the investigation of protein-surface effects alone since all the measurements were conducted in a crowded environment where lateral interactions contribute to binding capacities. Since binding capacities and protein-protein interactions correlated with the kosmotropicity of the secondary salt, it could be speculated that protein-surface interactions are increased accordingly.

In adsorption conditions exhibiting protein-protein interactions, the adsorption isotherms deviated from the typical Langmurian shape and they could be approximated by BET or Freundlich isotherms. This could be explained by multilayer formation where bound proteins serve as new binding sites. The energy of adsorption sites could be increased and decreased depending on whether adjacent binding sites accommodate proteins that induce repulsive and attractive protein-protein interactions, respectively [148]. Conclusively, it seems likely that changes in dynamic binding capacities are mostly dictated by protein-protein interactions for adalimumab and lysozyme. SAXS analysis of the protein in solution revealed that the internal protein structure is comparable for all model proteins in all investigated buffers. This is an indication that the footprint on the stationary phase is comparable. Nevertheless, changes in the footprint of the investigated systems cannot be ruled out since we did not perform experiments for determination of the binding orientation, surface coverage or unfolding of the protein.

Moreover, a SAXS analysis was performed to understand preferred binding location of the protein on the stationary phase. A self-avoiding random walk model was derived and fitted to the scattering data of the resin slurry incubated with protein. The excluded volume parameter decreased upon binding of the protein, and its decrease correlated with the binding capacity of the resin. The decrease in excluded

volume parameter was interpreted as successive deposition of the protein in the cavities of the chromatographic resin (Figure 5B). The concept of a perturbed water network near the concave regions of an adsorbent also supports the deposition in the cavities of the stationary phase. The perturbed water network then decreases the energy of cavity formation needed to accommodate the protein. A decreased excluded volume parameter correlates with a lower surface accessible area [141]. On the macroscopic level, the reduced surface accessible area also reduces the overall surface energy of the two-phase system since a surface area and surface tension correlate to the surface energy. Attractive protein-protein interactions might facilitate the population of cavities, whereas repulsive protein-protein interactions potentially inhibit the binding of other proteins in an already occupied cavity.

The second research problem allows better insights into the impact of protein-protein interactions on protein purity. Cysteine-dependent multimerization was observed in free solution correlating qualitatively with attractive protein-protein interactions. Multimerization was also observed after binding the CASPON enzyme to an IMAC stationary phase under attractive conditions. This suggests that multimerization might also occur throughout manufacturing under attractive regimes, decreasing product purity and recovery. Throughout all experiments in free solution, the protein was incubated at a concentration of 1 mg*ml^{-1}, so concentration effects have not been evaluated. Increased protein concentrations might enhance multimerization which would be especially relevant for hold steps at high ionic strength [80]. For chromatographic processes, high local protein concentration could also cause increased multimerization; therefore, decreased loading densities should be considered at the expense of productivity. For the CASPON enzyme, it was demonstrated that understand the multimerization pathway in free solution can correlate to multimerization on surfaces and therefore help to avoid conditions

favoring multimerization. Incubation with chaotropic agents such as guanidium favored monomerization through denaturing and should be avoided completely in case of the CASPON enzyme as not only multimerization occurs, but also these multimers are partly non-reducible. Hence, these multimers could not be recycled in the process. Protein-surface interactions of the CASPON enzyme and the IMAC stationary phase have not been investigated in detail in this work. Preferential binding of the CASPON enzyme could lead to an orientation that actually favors cysteine-dependent multimerization. As reported in literature, the addition of kosmotropic sodium sulfate might increase binding capacities of IMAC stationary phases [128]. It seems likely that binding capacities might be at least in part be increased due to protein-protein interactions that facilitate higher surface coverage. Cysteine-dependent multimerization can be avoided entirely when surface-exposed cysteines are mutated in protein engineering. When a protein of interest is known to aggregate via cysteine-dependent multimerization, disulfide bonds to host cell proteins might also occur. This would not only immediately lead to product loss, but also produce potentially co-eluting impurities in the following process steps. Adducts of large proteins of interest and small cysteine-bearing impurities could be particularly problematic. Removal of these adducts is more difficult since they contain surface properties resembling the protein of interest. Consequently, different immunogenic reactions could be triggered when these adducts are present in the drug product.

We have discussed the introduction of additional reductants to buffers throughout the process to decrease multimer content. Besides the target protein, the reductant could adversely affect employed materials such as complexed Ni^{2+} in IMAC purifications. The half-life of reductants and their reactivity towards oxygen should be considered, as they might be depleted during the process and thus require several

additions. Reductants also show pH-dependent activity, which could limit their application to selected unit operations [168]. On the downside, chemical modifications could be introduced [169]. The CASPON enzyme is an interesting model protein for cysteine-bearing multimerization and a model protein for protein-protein interaction research in general. Assuming a cysteine-depending multimerization pathway, protein-protein interactions correlate with multimerization, and multimers are easily detected using SE-HPLC.

4 Summary and conclusion

In short, the impact of different salts on protein-protein and protein-surface interactions was investigated within the frame of two different research problems. Furthermore, the impact of protein-protein interactions on productivity and purity was demonstrated with regards to two different interaction mechanisms and stationary phases: reversible vs. irreversible associations and in HIC vs. in IMAC, respectively. The irreversible association of the CASPON enzyme was also investigated in free solution. For the dual salt systems, it was confirmed that ionic strength is a more decisive parameter compared to surface tension for dynamic binding capacities. However, ionic strength alone is not sufficient to understand differences in dynamic binding capacities. Moreover, it was shown that protein-protein interactions correlate with binding capacities and, thus, the productivity of the loading phase for adalimumab and lysozyme. Furthermore, protein-protein interactions and dynamic binding capacities align with the Hofmeister series for adalimumab and lysozyme. For GFP with a pI close to the operating pH, protein-protein interactions were neutral, and protein-surface interactions are most likely responsible for differences in dynamic binding capacities. For the CASPON enzyme, it was demonstrated that attractive protein-protein interactions can have adverse effects on product purity. Multimer content increases when incubating in the presence of ammonium sulfate in free solution and on a chromatographic stationary phase, inducing attractive protein-protein interactions. For the CASPON enzyme, multimerization pathways in free solution can aid to avoid process conditions that favor multimerization.

The investigation of different dual salt systems in HIC also gave valuable insights into the binding behavior with regards to protein-protein interactions. For adalimumab and lysozyme, the SAXS analysis of the proteins in free solution

indicated the presence of protein-protein interactions. In the presence of protein-protein interactions, adsorption isotherm experiments showed non-Langmurian binding behavior. Corresponding adsorption isotherms were fitted with either the Freundlich or the BET model. Therefore, protein-protein interactions likely lead to increased surface coverage and thus higher binding capacities. The intramolecular structure of the model proteins did not change in the presence of different dual salt systems, indicating that the footprint of the protein did neither. The SAXS analysis of the adduct of stationary phase and protein revealed that binding capacities and protein-protein interactions correlated negatively with the excluded volume parameter. This indicates the deposition of the proteins in the cavities of the chromatographic resin, which also decreases the overall surface energy of the system.

Lastly, a guideline for the manufacturing of cysteine-bearing enzymes was outlined. This was achieved by investigating the multimerization properties of the CASPON enzyme in the presence of different salts and rationalizing their occurrence in downstream processing. Attractive protein-protein interactions in the presence of a kosmotrope, such as ammonium sulfate, increase protein aggregation, which is relevant for process steps such as loading in HIC or elution in IEX. These conditions should be avoided throughout the process.

5 References

[1] T.E. Creighton, Proteins: structures and molecular properties, 1993.

[2] F. Hofmeister, Zur Lehre von der Wirkung der Salze, Archiv für experimentelle Pathologie und Pharmakologie 24(4) (1888) 247-260. https://doi.org/10.1007/BF01918191.

[3] S.N. Timasheff, H. Inoue, Preferential binding of solvent components to proteins in mixed water-organic solvent systems, Biochemistry 7(7) (1968) 2501-2513. https://doi.org/10.1021/bi00847a009.

[4] T. Arakawa, R. Bhat, S.N. Timasheff, Preferential interactions determine protein solubility in three-component solutions: the magnesium chloride system, Biochemistry 29(7) (1990) 1914-1923. https://doi.org/10.1021/bi00459a036.

[5] G. Carta, A. Jungbauer, Protein Chromatography: Process Development and Scale-Up, 2010. https://doi.org/10.1002/9783527630158.

[6] F.H. Stillinger, Water Revisited, Science 209(4455) (1980) 451-457. https://doi.org/doi:10.1126/science.209.4455.451 %U https://www.science.org/doi/abs/10.1126/science.209.4455.451.

[7] A.A. Green, STUDIES IN THE PHYSICAL CHEMISTRY OF THE PROTEINS: X. THE SOLUBILITY OF HEMOGLOBIN IN SOLUTIONS OF CHLORIDES AND SULFATES OF VARYING CONCENTRATION, Journal of Biological Chemistry 95(1) (1932) 47-66. https://doi.org/https://doi.org/10.1016/S0021-9258(18)76355-2.

[8] H.I. Okur, J. Hladilkova, K.B. Rembert, Y. Cho, J. Heyda, J. Dzubiella, P.S. Cremer, P. Jungwirth, Beyond the Hofmeister Series: Ion-Specific Effects on Proteins and Their Biological Functions, The journal of physical chemistry. B 121(9) (2017) 1997-2014. https://doi.org/10.1021/acs.jpcb.6b10797.

[9] Y. Zhang, P.S. Cremer, Interactions between macromolecules and ions: The Hofmeister series, Curr Opin Chem Biol 10(6) (2006) 658-63. https://doi.org/10.1016/j.cbpa.2006.09.020.

[10] K.P. Gregory, G.R. Elliott, H. Robertson, A. Kumar, E.J. Wanless, G.B. Webber, V.S.J. Craig, G.G. Andersson, A.J. Page, Understanding specific ion effects and the Hofmeister series, Physical chemistry chemical physics : PCCP 24(21) (2022) 12682-12718. https://doi.org/10.1039/d2cp00847e.

[11] A. Villard, O. Bernard, J.-F. Dufrêche, Non-additivity of ionic radii in electrolyte solutions: Hofmeister effect on mixtures modeled by an Associated MSA model, Journal of Molecular Liquids 270 (2018) 30-39. https://doi.org/10.1016/j.molliq.2018.01.125.

[12] O.A. Francisco, C.J. Clark, H.M. Glor, M. Khajehpour, Do soft anions promote protein denaturation through binding interactions? A case study using ribonuclease A, RSC Adv 9(6) (2019) 3416-3428. https://doi.org/10.1039/c8ra10303h.

[13] H. Batoulis, T.H. Schmidt, P. Weber, J.G. Schloetel, C. Kandt, T. Lang, Concentration Dependent Ion-Protein Interaction Patterns Underlying Protein Oligomerization Behaviours, Sci Rep 6 (2016) 24131. https://doi.org/10.1038/srep24131.

[14] D. Bastos-González, L. Pérez-Fuentes, C. Drummond, J. Faraudo, Ions at interfaces: the central role of hydration and hydrophobicity, Current Opinion in Colloid & Interface Science 23 (2016) 19-28. https://doi.org/10.1016/j.cocis.2016.05.010.

[15] R.L. Baldwin, How Hofmeister ion interactions affect protein stability, Biophysical journal 71(4) (1996) 2056-2063.

[16] W. Melander, C. Horváth, Salt effects on hydrophobic interactions in precipitation and chromatography of proteins: An interpretation of the lyotropic series, Archives of Biochemistry and Biophysics 183(1) (1977) 200-215. https://doi.org/https://doi.org/10.1016/0003-9861(77)90434-9.

[17] D. Chandler, Interfaces and the driving force of hydrophobic assembly, Nature 437(7059) (2005) 640-7. https://doi.org/10.1038/nature04162.

[18] A.J. Patel, P. Varilly, S.N. Jamadagni, H. Acharya, S. Garde, D. Chandler, Extended surfaces modulate hydrophobic interactions of neighboring solutes, Proceedings of the National Academy of Sciences of the United States of America 108(43) (2011) 17678-83. https://doi.org/10.1073/pnas.1110703108.

[19] E. Xi, V. Venkateshwaran, L. Li, N. Rego, A.J. Patel, S. Garde, Hydrophobicity of proteins and nanostructured solutes is governed by topographical and chemical context, Proceedings of the National Academy of Sciences of the United States of America 114(51) (2017) 13345-13350. https://doi.org/10.1073/pnas.1700092114.

[20] B.A. Rogers, H.I. Okur, C. Yan, T. Yang, J. Heyda, P.S. Cremer, Weakly hydrated anions bind to polymers but not monomers in aqueous solutions, Nat Chem 14(1) (2022) 40-45. https://doi.org/10.1038/s41557-021-00805-z.

[21] A.U. Thosar, A.J. Patel, Hydration determines anion accumulation, Nature Chemistry 14(1) (2022) 8-10. https://doi.org/10.1038/s41557-021-00864-2.

[22] C.L. Gibb, B.C. Gibb, Anion binding to hydrophobic concavity is central to the salting-in effects of Hofmeister chaotropes, Journal of the American Chemical Society 133(19) (2011) 7344-7. https://doi.org/10.1021/ja202308n.

[23] S.N. Timasheff, THE CONTROL OF PROTEIN STABILITY AND ASSOCIATION BY WEAK INTERACTIONS WITH WATER: How Do Solvents Affect These Processes?, Annu. Rev. Biophys. Biomol. Struct. (1993).

[24] T. Arakawa, R. Bhat, S.N. Timasheff, Why preferential hydration does not always stabilize the native structure of globular proteins, Biochemistry 29(7) (1990) 1924-1931. https://doi.org/10.1021/bi00459a037.

[25] T. Arakawa, S.N. Timasheff, Preferential interactions of proteins with salts in concentrated solutions, Biochemistry 21(25) (2002) 6545-6552. https://doi.org/10.1021/bi00268a034.

[26] H. Inoue, S.N. Timasheff, Interaction of beta-lactoglobulin with solvent components in mixed water-organic solvent systems, Journal of the American Chemical Society 90(7) (1968) 1890-1897. https://doi.org/10.1021/ja01009a037.

[27] M.E. Noelken, S.N. Timasheff, Preferential Solvation of Bovine Serum Albumin in Aqueous Guanidine Hydrochloride, Journal of Biological Chemistry 242(21) (1967) 5080-5085. https://doi.org/10.1016/s0021-9258(18)99478-0.

[28] H.I. Okur, J. Kherb, P.S. Cremer, Cations bind only weakly to amides in aqueous solutions, Journal of the American Chemical Society 135(13) (2013) 5062-7. https://doi.org/10.1021/ja3119256.

[29] L. Vrbka, M. Mucha, B. Minofar, P. Jungwirth, E.C. Brown, D.J. Tobias, Propensity of soft ions for the air/water interface, Current Opinion in Colloid & Interface Science 9(1-2) (2004) 67-73. https://doi.org/10.1016/j.cocis.2004.05.028.

[30] K.B. Rembert, J. Paterova, J. Heyda, C. Hilty, P. Jungwirth, P.S. Cremer, Molecular mechanisms of ion-specific effects on proteins, Journal of the American Chemical Society 134(24) (2012) 10039-46. https://doi.org/10.1021/ja301297g.

[31] K.B. Rembert, H.I. Okur, C. Hilty, P.S. Cremer, An NH moiety is not required for anion binding to amides in aqueous solution, Langmuir : the ACS journal of surfaces and colloids 31(11) (2015) 3459-64. https://doi.org/10.1021/acs.langmuir.5b00127.

[32] J. Heyda, H.I. Okur, J. Hladilkova, K.B. Rembert, W. Hunn, T. Yang, J. Dzubiella, P. Jungwirth, P.S. Cremer, Guanidinium can both Cause and Prevent the Hydrophobic Collapse of Biomacromolecules, Journal of the American Chemical Society 139(2) (2017) 863-870. https://doi.org/10.1021/jacs.6b11082.

[33] E.E. Bruce, H.I. Okur, S. Stegmaier, C.I. Drexler, B.A. Rogers, N.F.A. van der Vegt, S. Roke, P.S. Cremer, Molecular Mechanism for the Interactions of Hofmeister Cations with Macromolecules in Aqueous Solution, Journal of the American Chemical Society 142(45) (2020) 19094-19100. https://doi.org/10.1021/jacs.0c07214.

[34] O. Becconi, E. Ahlstrand, A. Salis, R. Friedman, Protein-ion Interactions: Simulations of Bovine Serum Albumin in Physiological Solutions of NaCl, KCl and LiCl, Israel Journal of Chemistry 57(5) (2017) 403-412. https://doi.org/10.1002/ijch.201600119.

[35] L. Vrbka, J. Vondrášek, B. Jagoda-Cwiklik, R. Vácha, P. Jungwirth, Quantification and rationalization of the higher affinity of sodium over potassium to protein surfaces, Proceedings of the National Academy of Sciences of the United States of America 103(42) (2006) 15440-15444. https://doi.org/10.1073/pnas.0606959103.

[36] C. Pasquier, M. Vazdar, J. Forsman, P. Jungwirth, M. Lund, Anomalous Protein-Protein Interactions in Multivalent Salt Solution, The journal of physical chemistry. B 121(14) (2017) 3000-3006. https://doi.org/10.1021/acs.jpcb.7b01051.

[37] O. Matsarskaia, F. Roosen-Runge, F. Schreiber, Multivalent ions and biomolecules: Attempting a comprehensive perspective, Chemphyschem 21(16) (2020) 1742-1767. https://doi.org/10.1002/cphc.202000162.

[38] A. Kubickova, T. Krizek, P. Coufal, M. Vazdar, E. Wernersson, J. Heyda, P. Jungwirth, Overcharging in biological systems: reversal of electrophoretic mobility of aqueous polyaspartate by multivalent cations, Phys Rev Lett 108(18) (2012) 186101. https://doi.org/10.1103/PhysRevLett.108.186101.

[39] A.K. Sahoo, F. Schreiber, R.R. Netz, P.K. Maiti, Role of entropy in determining the phase behavior of protein solutions induced by multivalent ions, Soft Matter 18(3) (2022) 592-601. https://doi.org/10.1039/d1sm00730k.

[40] Y. Zhang, P.S. Cremer, The inverse and direct Hofmeister series for lysozyme, Proceedings of the National Academy of Sciences of the United States of America 106(36) (2009) 15249-15253. https://doi.org/10.1073/pnas.0907616106.

[41] K.D. Collins, M.W. Washabaugh, The Hofmeister effect and the behaviour of water at interfaces, Quarterly Reviews of Biophysics 18(4) (1985) 323-422. https://doi.org/10.1017/S0033583500005369.

[42] E.A. Guggenheim, L.The specific thermodynamic properties of aqueous solutions of strong electrolytes, The London, Edinburgh, and Dublin Philosophical Magazine and Journal of Science 19(127) (2009) 588-643. https://doi.org/10.1080/14786443508561403.

[43] J.N. Brönsted, Studies on solubility. IV. The principle of the specific interaction of ions, Journal of the American Chemical Society 44(5) (1922) 877-898. https://doi.org/10.1021/ja01426a001.

[44] P.T. Bui, P.S. Cremer, Cation Identity Affects Nonadditivity in Salt Mixtures Containing Iodide and Sulfate, Journal of Solution Chemistry 50(11-12) (2021) 1443-1456. https://doi.org/10.1007/s10953-021-01125-z.

[45] E.E. Bruce, P.T. Bui, M. Cao, P.S. Cremer, N.F.A. van der Vegt, Contact Ion Pairs in the Bulk Affect Anion Interactions with Poly(N-isopropylacrylamide), The journal of physical chemistry. B 125(2) (2021) 680-688. https://doi.org/10.1021/acs.jpcb.0c11076.

[46] P.E. Mason, G.W. Neilson, C.E. Dempsey, A.C. Barnes, J.M. Cruickshank, The hydration structure of guanidinium and thiocyanate ions: Implications for protein stability in aqueous solution, Proceedings of the National Academy of Sciences of the United States of America 100(8) (2003) 4557-4561. https://doi.org/10.1073/pnas.0735920100.

[47] W.K. Lim, J. Rösgen, S.W. Englander, Urea, but not guanidinium, destabilizes proteins by forming hydrogen bonds to the peptide group, Proceedings of the National Academy of Sciences of the United States of America 106(8) (2009) 2595-2600. https://doi.org/10.1073/pnas.0812588106.

[48] P.E. Mason, J.W. Brady, G.W. Neilson, C.E. Dempsey, The interaction of guanidinium ions with a model peptide, Biophysical journal 93(1) (2007) L04-6. https://doi.org/10.1529/biophysj.107.108290.

[49] A.N. Muttathukattil, S. Srinivasan, A. Halder, G. Reddy, Role of Guanidinium-Carboxylate Ion Interaction in Enzyme Inhibition with Implications for Drug Design, The journal of physical chemistry. B 123(44) (2019) 9302-9311. https://doi.org/10.1021/acs.jpcb.9b06130.

[50] M. Hanke, N. Hansen, E. Tomm, G. Grundmeier, A. Keller, Time-Dependent DNA Origami Denaturation by Guanidinium Chloride, Guanidinium Sulfate, and Guanidinium Thiocyanate, Int J Mol Sci 23(15) (2022). https://doi.org/10.3390/ijms23158547.

[51] H. Lu, Q. Zhou, J. He, Z. Jiang, C. Peng, R. Tong, J. Shi, Recent advances in the development of protein-protein interactions modulators: mechanisms and clinical trials, Signal Transduct Target Ther 5(1) (2020) 213. https://doi.org/10.1038/s41392-020-00315-3.

[52] C. Chothia, The nature of the accessible and buried surfaces in proteins, Journal of Molecular Biology 105(1) (1976) 1-12. https://doi.org/10.1016/0022-2836(76)90191-1.

[53] S.K. Chaturvedi, A. Parupudi, K. Juul-Madsen, A. Nguyen, T. Vorup-Jensen, S. Dragulin-Otto, H. Zhao, R. Esfandiary, P. Schuck, Measuring aggregates, self-association, and weak interactions in

concentrated therapeutic antibody solutions, MAbs 12(1) (2020) 1810488. https://doi.org/10.1080/19420862.2020.1810488.

[54] B.D. Connolly, C. Petry, S. Yadav, B. Demeule, N. Ciaccio, J.M. Moore, S.J. Shire, Y.R. Gokarn, Weak interactions govern the viscosity of concentrated antibody solutions: high-throughput analysis using the diffusion interaction parameter, Biophysical journal 103(1) (2012) 69-78. https://doi.org/10.1016/j.bpj.2012.04.047.

[55] P.D. Godfrin, I.E. Zarraga, J. Zarzar, L. Porcar, P. Falus, N.J. Wagner, Y. Liu, Effect of Hierarchical Cluster Formation on the Viscosity of Concentrated Monoclonal Antibody Formulations Studied by Neutron Scattering, The journal of physical chemistry. B 120(2) (2016) 278-91. https://doi.org/10.1021/acs.jpcb.5b07260.

[56] W.G. Lilyestrom, S. Yadav, S.J. Shire, T.M. Scherer, Monoclonal antibody self-association, cluster formation, and rheology at high concentrations, The journal of physical chemistry. B 117(21) (2013) 6373-84. https://doi.org/10.1021/jp4008152.

[57] A.Y. Xu, N.J. Clark, J. Pollastrini, M. Espinoza, H.J. Kim, S. Kanapuram, B. Kerwin, M.J. Treuheit, S. Krueger, A. McAuley, J.E. Curtis, Effects of Monovalent Salt on Protein-Protein Interactions of Dilute and Concentrated Monoclonal Antibody Formulations, Antibodies (Basel) 11(2) (2022). https://doi.org/10.3390/antib11020024.

[58] L. Silvestrini, N. Belhaj, L. Comez, Y. Gerelli, A. Lauria, V. Libera, P. Mariani, P. Marzullo, M.G. Ortore, A. Palumbo Piccionello, C. Petrillo, L. Savini, A. Paciaroni, F. Spinozzi, The dimer-monomer equilibrium of SARS-CoV-2 main protease is affected by small molecule inhibitors, Sci Rep 11(1) (2021) 9283. https://doi.org/10.1038/s41598-021-88630-9.

[59] K. Sakurai, M. Oobatake, Y. Goto, Salt-dependent monomer-dimer equilibrium of bovine β-lactoglobulin at pH 3, Protein Science 10(11) (2001) 2325-2335. https://doi.org/10.1110/ps.17001.

[60] W. Wang, W.G. Lilyestrom, Z.Y. Hu, T.M. Scherer, Cluster Size and Quinary Structure Determine the Rheological Effects of Antibody Self-Association at High Concentrations, The journal of physical chemistry. B 122(7) (2018) 2138-2154. https://doi.org/10.1021/acs.jpcb.7b10728.

[61] D.S. Tomar, S. Kumar, S.K. Singh, S. Goswami, L. Li, Molecular basis of high viscosity in concentrated antibody solutions: Strategies for high concentration drug product development, MAbs 8(2) (2016) 216-28. https://doi.org/10.1080/19420862.2015.1128606.

[62] J.C. Geoghegan, R. Fleming, M. Damschroder, S.M. Bishop, H.A. Sathish, R. Esfandiary, Mitigation of reversible self-association and viscosity in a human IgG1 monoclonal antibody by rational, structure-guided Fv engineering, MAbs 8(5) (2016) 941-50. https://doi.org/10.1080/19420862.2016.1171444.

[63] C. Tilegenova, S. Izadi, J. Yin, C.S. Huang, J. Wu, D. Ellerman, S.G. Hymowitz, B. Walters, C. Salisbury, P.J. Carter, Dissecting the molecular basis of high viscosity of monospecific and bispecific IgG antibodies, MAbs 12(1) (2020) 1692764. https://doi.org/10.1080/19420862.2019.1692764.

[64] V. Burckbuchler, G. Mekhloufi, A.P. Giteau, J.L. Grossiord, S. Huille, F. Agnely, Rheological and syringeability properties of highly concentrated human polyclonal immunoglobulin solutions, European journal of pharmaceutics and biopharmaceutics : official journal of Arbeitsgemeinschaft fur Pharmazeutische Verfahrenstechnik e.V 76(3) (2010) 351-6. https://doi.org/10.1016/j.ejpb.2010.08.002.

[65] W.F.t. Weiss, T.M. Young, C.J. Roberts, Principles, approaches, and challenges for predicting protein aggregation rates and shelf life, Journal of pharmaceutical sciences 98(4) (2009) 1246-77. https://doi.org/10.1002/jps.21521.

[66] K.D. Ratanji, J.P. Derrick, R.J. Dearman, I. Kimber, Immunogenicity of therapeutic proteins: influence of aggregation, J Immunotoxicol 11(2) (2014) 99-109. https://doi.org/10.3109/1547691X.2013.821564.

[67] A.A. Green, W.L. Hughes, Protein fractionation on the basis of solubility in aqueous solutions of salts and organic solvents, Methods in Enzymology 1(C) (1955) 67-90. https://doi.org/10.1016/0076-6879(55)01014-8.

[68] W.G. McMillan, J.E. Mayer, The Statistical Thermodynamics of Multicomponent Systems, The Journal of Chemical Physics 13(7) (1945) 276-305. https://doi.org/10.1063/1.1724036.

[69] P. Sonderby, J.T. Bukrinski, M. Hebditch, G.H.J. Peters, R.A. Curtis, P. Harris, Self-Interaction of Human Serum Albumin: A Formulation Perspective, ACS Omega 3(11) (2018) 16105-16117. https://doi.org/10.1021/acsomega.8b02245.

[70] T. Ahamed, M. Ottens, G.W. van Dedem, L.A. van der Wielen, Design of self-interaction chromatography as an analytical tool for predicting protein phase behavior, Journal of chromatography. A 1089(1-2) (2005) 111-24. https://doi.org/10.1016/j.chroma.2005.06.065.

[71] C.M. Sorensen, Light Scattering by Fractal Aggregates: A Review, Aerosol Science and Technology 35(2) (2001) 648-687. https://doi.org/10.1080/02786820117868.

[72] O. Glatter, A new method for the evaluation of small-angle scattering data, Journal of Applied Crystallography 10(5) (1977) 415-421. https://doi.org/https://doi.org/10.1107/S0021889877013879.

[73] P.J. Wyatt, The "SIZE" of Macromolecules and Some Observations on Their Mass, Journal of Liquid Chromatography 14(12) (1991) 2351-2372. https://doi.org/10.1080/01483919108049696.

[74] M.A. Blanco, H.W. Hatch, J.E. Curtis, V.K. Shen, Evaluating the Effects of Hinge Flexibility on the Solution Structure of Antibodies at Concentrated Conditions, Journal of pharmaceutical sciences 108(5) (2019) 1663-1674. https://doi.org/10.1016/j.xphs.2018.12.013.

[75] J.B. Hopkins, R.E. Thorne, Quantifying radiation damage in biomolecular small-angle X-ray scattering, J Appl Crystallogr 49(Pt 3) (2016) 880-890. https://doi.org/10.1107/S1600576716005136.

[76] S. Skou, R.E. Gillilan, N. Ando, Synchrotron-based small-angle X-ray scattering of proteins in solution, Nat Protoc 9(7) (2014) 1727-39. https://doi.org/10.1038/nprot.2014.116.

[77] J. Stetefeld, S.A. McKenna, T.R. Patel, Dynamic light scattering: a practical guide and applications in biomedical sciences, Biophysical reviews 8(4) (2016) 409-427. https://doi.org/10.1007/s12551-016-0218-6.

[78] A.S. Parmar, M. Muschol, Hydration and hydrodynamic interactions of lysozyme: effects of chaotropic versus kosmotropic ions, Biophysical journal 97(2) (2009) 590-8. https://doi.org/10.1016/j.bpj.2009.04.045.

[79] J. Jayaraman, J. Wu, M.C. Brunelle, A.M. Cruz, D.S. Goldberg, B. Lobo, A. Shah, P.M. Tessier, Plasmonic measurements of monoclonal antibody self-association using self-interaction nanoparticle spectroscopy, Biotechnol Bioeng 111(8) (2014) 1513-20. https://doi.org/10.1002/bit.25221.

[80] A.Y. Xu, M.M. Castellanos, K. Mattison, S. Krueger, J.E. Curtis, Studying Excipient Modulated Physical Stability and Viscosity of Monoclonal Antibody Formulations Using Small-Angle Scattering, Mol Pharm 16(10) (2019) 4319-4338. https://doi.org/10.1021/acs.molpharmaceut.9b00687.

[81] S. Saito, J. Hasegawa, N. Kobayashi, N. Kishi, S. Uchiyama, K. Fukui, Behavior of monoclonal antibodies: relation between the second virial coefficient (B (2)) at low concentrations and aggregation propensity and viscosity at high concentrations, Pharmaceutical research 29(2) (2012) 397-410. https://doi.org/10.1007/s11095-011-0563-x.

[82] C.R. Mosbaek, P.V. Konarev, D.I. Svergun, C. Rischel, B. Vestergaard, High concentration formulation studies of an IgG2 antibody using small angle X-ray scattering, Pharmaceutical research 29(8) (2012) 2225-35. https://doi.org/10.1007/s11095-012-0751-3.

[83] F. Zhang, G. Richter, B. Bourgeois, E. Spreitzer, A. Moser, A. Keilbach, P. Kotnik, T. Madl, A General Small-Angle X-ray Scattering-Based Screening Protocol for Studying Physical Stability of Protein Formulations, Pharmaceutics 14(1) (2021). https://doi.org/10.3390/pharmaceutics14010069.

[84] M.J. Scannell, M.W. Hyatt, I.L. Budyak, M.A. Woldeyes, Y. Wang, Revisit PEG-Induced Precipitation Assay for Protein Solubility Assessment of Monoclonal Antibody Formulations, Pharmaceutical research 38(11) (2021) 1947-1960. https://doi.org/10.1007/s11095-021-03119-4.

[85] C. Kalonia, V. Toprani, R. Toth, N. Wahome, I. Gabel, C.R. Middaugh, D.B. Volkin, Effects of Protein Conformation, Apparent Solubility, and Protein-Protein Interactions on the Rates and Mechanisms of Aggregation for an IgG1Monoclonal Antibody, The journal of physical chemistry. B 120(29) (2016) 7062-75. https://doi.org/10.1021/acs.jpcb.6b03878.

[86] B. Bain, M. Brazil, Adalimumab, Nat Rev Drug Discov 2(9) (2003) 693-94. https://doi.org/10.1038/nrd1182.

[87] N. Lingg, C. Kross, P. Engele, C. Ohlknecht, C. Koppl, A. Fischer, B. Lier, J. Loibl, B. Sprenger, J. Liu, P. Scheidl, M. Berkemeyer, W. Buchinger, C. Brocard, G. Striedner, C. Oostenbrink, R. Schneider, A. Jungbauer, M. Cserjan-Puschmann, CASPON platform technology: Ultrafast circularly permuted caspase-2 cleaves tagged fusion proteins before all 20 natural amino acids at the N-terminus, N Biotechnol 71 (2022) 37-46. https://doi.org/10.1016/j.nbt.2022.07.002.
[88] W. Wang, S. Singh, D.L. Zeng, K. King, S. Nema, Antibody structure, instability, and formulation, Journal of pharmaceutical sciences 96(1) (2007) 1-26. https://doi.org/10.1002/jps.20727.
[89] L. Magnenat, A. Palmese, C. Fremaux, F. D'Amici, M. Terlizzese, M. Rossi, L. Chevalet, Demonstration of physicochemical and functional similarity between the proposed biosimilar adalimumab MSB11022 and Humira(R), MAbs 9(1) (2017) 127-139. https://doi.org/10.1080/19420862.2016.1259046.
[90] A.M. dos Santos, Thermal effect on Aequorea green fluorescent protein anionic and neutral chromophore forms fluorescence, J Fluoresc 22(1) (2012) 151-4. https://doi.org/10.1007/s10895-011-0941-0.
[91] T. Sakaguchi, T. Wada, T. Kasai, T. Shiratori, Y. Minami, Y. Shimada, Y. Otsuka, K. Komatsu, S. Goto, Effects of ionic and reductive atmosphere on the conformational rearrangement in hen egg white lysozyme prior to amyloid formation, Colloids Surf B Biointerfaces 190 (2020) 110845. https://doi.org/10.1016/j.colsurfb.2020.110845.
[92] J. Jumper, R. Evans, A. Pritzel, T. Green, M. Figurnov, O. Ronneberger, K. Tunyasuvunakool, R. Bates, A. Zidek, A. Potapenko, A. Bridgland, C. Meyer, S.A.A. Kohl, A.J. Ballard, A. Cowie, B. Romera-Paredes, S. Nikolov, R. Jain, J. Adler, T. Back, S. Petersen, D. Reiman, E. Clancy, M. Zielinski, M. Steinegger, M. Pacholska, T. Berghammer, S. Bodenstein, D. Silver, O. Vinyals, A.W. Senior, K. Kavukcuoglu, P. Kohli, D. Hassabis, Highly accurate protein structure prediction with AlphaFold, Nature 596(7873) (2021) 583-589. https://doi.org/10.1038/s41586-021-03819-2.
[93] M. Mirdita, K. Schutze, Y. Moriwaki, L. Heo, S. Ovchinnikov, M. Steinegger, ColabFold: making protein folding accessible to all, Nature methods 19(6) (2022) 679-682. https://doi.org/10.1038/s41592-022-01488-1.
[94] C. Mieczkowski, A. Cheng, T. Fischmann, M. Hsieh, J. Baker, M. Uchida, G. Raghunathan, C. Strickland, L. Fayadat-Dilman, Characterization and Modeling of Reversible Antibody Self-Association Provide Insights into Behavior, Prediction, and Correction, Antibodies (Basel) 10(1) (2021). https://doi.org/10.3390/antib10010008.
[95] M. Hebditch, A. Roche, R.A. Curtis, J. Warwicker, Models for Antibody Behavior in Hydrophobic Interaction Chromatography and in Self-Association, Journal of pharmaceutical sciences 108(4) (2019) 1434-1441. https://doi.org/10.1016/j.xphs.2018.11.035.
[96] L. Gentiluomo, D. Roessner, W. Streicher, S. Mahapatra, P. Harris, W. Friess, Characterization of Native Reversible Self-Association of a Monoclonal Antibody Mediated by Fab-Fab Interaction, Journal of pharmaceutical sciences 109(1) (2020) 443-451. https://doi.org/10.1016/j.xphs.2019.09.021.
[97] J.G. Elvin, R.G. Couston, C.F. van der Walle, Therapeutic antibodies: market considerations, disease targets and bioprocessing, Int J Pharm 440(1) (2013) 83-98. https://doi.org/10.1016/j.ijpharm.2011.12.039.
[98] M.L. Chiu, G.L. Gilliland, Engineering antibody therapeutics, Curr Opin Struct Biol 38 (2016) 163-73. https://doi.org/10.1016/j.sbi.2016.07.012.
[99] S. Kanai, J. Liu, T.W. Patapoff, S.J. Shire, Reversible self-association of a concentrated monoclonal antibody solution mediated by Fab-Fab interaction that impacts solution viscosity, Journal of pharmaceutical sciences 97(10) (2008) 4219-27. https://doi.org/10.1002/jps.21322.
[100] J. Arora, Y. Hu, R. Esfandiary, H.A. Sathish, S.M. Bishop, S.B. Joshi, C.R. Middaugh, D.B. Volkin, D.D. Weis, Charge-mediated Fab-Fc interactions in an IgG1 antibody induce reversible self-association, cluster formation, and elevated viscosity, MAbs 8(8) (2016) 1561-1574. https://doi.org/10.1080/19420862.2016.1222342.
[101] J.D. Schrag, M.E. Picard, F. Gaudreault, L.P. Gagnon, J. Baardsnes, M.S. Manenda, J. Sheff, C. Deprez, C. Baptista, H. Hogues, J.F. Kelly, E.O. Purisima, R. Shi, T. Sulea, Binding symmetry and surface

flexibility mediate antibody self-association, MAbs 11(7) (2019) 1300-1318. https://doi.org/10.1080/19420862.2019.1632114.

[102] C. Chen, V.A. Roberts, M.B. Rittenberg, Generation and analysis of random point mutations in an antibody CDR2 sequence: Many mutated antibodies lose their ability to bind antigen, Journal of Experimental Medicine 176(3) (1992) 855-866. https://doi.org/10.1084/jem.176.3.855.

[103] S.L. Sim, T. He, A. Tscheliessnig, M. Mueller, R.B. Tan, A. Jungbauer, Branched polyethylene glycol for protein precipitation, Biotechnol Bioeng 109(3) (2012) 736-46. https://doi.org/10.1002/bit.24343.

[104] G. Dutra, D. Komuczki, A. Jungbauer, P. Satzer, Continuous capture of recombinant antibodies by ZnCl 2 precipitation without polyethylene glycol, Eng Life Sci 20(7) (2020) 265-274. https://doi.org/10.1002/elsc.201900160.

[105] G. Recanati, R. Coca-Whiteford, P. Scheidl, B. Sissolak, A. Jungbauer, Redissolution of recombinant antibodies precipitated by ZnCl2, Process Biochemistry 118 (2022) 145-153. https://doi.org/10.1016/j.procbio.2022.04.023.

[106] D. Burgstaller, A. Jungbauer, P. Satzer, Continuous integrated antibody precipitation with two-stage tangential flow microfiltration enables constant mass flow, Biotechnol Bioeng 116(5) (2019) 1053-1065. https://doi.org/10.1002/bit.26922.

[107] Z. Li, Q. Gu, J.L. Coffman, T. Przybycien, A.L. Zydney, Continuous precipitation for monoclonal antibody capture using countercurrent washing by microfiltration, Biotechnol Prog 35(6) (2019) e2886. https://doi.org/10.1002/btpr.2886.

[108] A. Schweizer, C. Briand, M.G. Grutter, Crystal structure of caspase-2, apical initiator of the intrinsic apoptotic pathway, J Biol Chem 278(43) (2003) 42441-7. https://doi.org/10.1074/jbc.M304895200.

[109] N. Lingg, M. Cserjan-Puschmann, A. Fischer, P. Engele, C. Kröß, R. Schneider, C. Brocard, M. Berkemeyer, G. Striedner, A. Jungbauer, Advanced purification platform using circularly permuted caspase-2 for affinity fusion-tag removal to produce native fibroblast growth factor 2, Journal of Chemical Technology & Biotechnology (2021). https://doi.org/10.1002/jctb.6666.

[110] R. Swaminathan, V.K. Ravi, S. Kumar, M.V. Kumar, N. Chandra, Lysozyme: a model protein for amyloid research, Adv Protein Chem Struct Biol 84 (2011) 63-111. https://doi.org/10.1016/B978-0-12-386483-3.00003-3.

[111] L.B. Poole, The basics of thiols and cysteines in redox biology and chemistry, Free Radic Biol Med 80 (2015) 148-57. https://doi.org/10.1016/j.freeradbiomed.2014.11.013.

[112] M.V. Trivedi, J.S. Laurence, T.J. Siahaan, The role of thiols and disulfides on protein stability, Current Protein and Peptide Science 10(6) (2009) 614-625. https://doi.org/10.2174/138920309789630534.

[113] N.C. Strynadka, M.N. James, Lysozyme: a model enzyme in protein crystallography, EXS 75 (1996) 185-222. https://doi.org/10.1007/978-3-0348-9225-4_11.

[114] D. Takahashi, E. Nishimoto, T. Murase, S. Yamashita, Protein-protein interaction on lysozyme crystallization revealed by rotational diffusion analysis, Biophysical journal 94(11) (2008) 4484-92. https://doi.org/10.1529/biophysj.107.111872.

[115] D.P. Myatt, L. Hatter, S.E. Rogers, A.E. Terry, L.A. Clifton, Monomeric green fluorescent protein as a protein standard for small angle scattering, Biomedical Spectroscopy and Imaging 6(3-4) (2017) 123-134. https://doi.org/10.3233/bsi-170167.

[116] S.H. Park, R.T. Raines, Green fluorescent protein as a signal for protein-protein interactions, Protein Science 6(11) (1997) 2344-2349. https://doi.org/10.1002/pro.5560061107.

[117] R. Hahn, Methods for characterization of biochromatography media, J Sep Sci 35(22) (2012) 3001-32. https://doi.org/10.1002/jssc.201200770.

[118] G. Malmquist, N. Lundell, Characterization of the influence of displacing salts on retention in gradient elution ion-exchange chromatography of proteins and peptides, Journal of Chromatography A 627(1-2) (1992) 107-124. https://doi.org/10.1016/0021-9673(92)87191-A.

[119] S. Al-Jibbouri, The influence of salt type on the retention of bovine serum albumin in ion-exchange chromatography, Journal of chromatography. A 1139(1) (2007) 57-62. https://doi.org/10.1016/j.chroma.2006.10.079.

[120] T. Fuchs, A. Jupke, Comparison of the impact of anion and cation selection onto cation exchange chromatography of model proteins, Journal of chromatography. A 1673 (2022) 463054. https://doi.org/10.1016/j.chroma.2022.463054.

[121] K. Tsumoto, D. Ejima, A.M. Senczuk, Y. Kita, T. Arakawa, Effects of salts on protein-surface interactions: applications for column chromatography, Journal of pharmaceutical sciences 96(7) (2007) 1677-90. https://doi.org/10.1002/jps.20821.

[122] R. Gutiérrez, E.M. Martín del Valle, M.A. Galán, Immobilized Metal-Ion Affinity Chromatography: Status and Trends, Separation & Purification Reviews 36(1) (2007) 71-111. https://doi.org/10.1080/15422110601166007.

[123] N. Walch, T. Scharl, E. Felfoldi, D.G. Sauer, M. Melcher, F. Leisch, A. Durauer, A. Jungbauer, Prediction of the Quantity and Purity of an Antibody Capture Process in Real Time, Biotechnology journal 14(7) (2019) e1800521. https://doi.org/10.1002/biot.201800521.

[124] A.M. Ramos-de-la-Pena, J. Gonzalez-Valdez, O. Aguilar, Protein A chromatography: Challenges and progress in the purification of monoclonal antibodies, J Sep Sci 42(9) (2019) 1816-1827. https://doi.org/10.1002/jssc.201800963.

[125] W. Choe, T. Durgannavar, S. Chung, Fc-Binding Ligands of Immunoglobulin G: An Overview of High Affinity Proteins and Peptides, Materials 9(12) (2016). https://doi.org/10.3390/ma9120994.

[126] N. Lingg, C. Ohlknecht, A. Fischer, M. Mozgovicz, T. Scharl, C. Oostenbrink, A. Jungbauer, Proteomics analysis of host cell proteins after immobilized metal affinity chromatography: Influence of ligand and metal ions, Journal of chromatography. A 1633 (2020) 461649. https://doi.org/10.1016/j.chroma.2020.461649.

[127] J.J. Winzerling, P. Berna, J. Porath, How to use immobilized metal ion affinity chromatography, Methods 4(1) (1992) 4-13. https://doi.org/https://doi.org/10.1016/1046-2023(92)90052-A.

[128] J. Porath, B. Olin, Immobilized Metal Ion Affinity Adsorption and Immobilized Metal Ion Affinity Chromatography of Biomaterials. Serum Protein Affinities for Gel-Immobilized Iron and Nickel Ions, Biochemistry 22(7) (1983) 1621-1630. https://doi.org/10.1021/bi00276a015.

[129] J.L. Fausnaugh, F.E. Regnier, Solute and mobile phase contributions to retention in hydrophobic interaction chromatography of proteins, Journal of Chromatography A 359(C) (1986) 131-146. https://doi.org/10.1016/0021-9673(86)80068-1.

[130] E. Muller, J. Vajda, D. Josic, T. Schroder, R. Dabre, T. Frey, Mixed electrolytes in hydrophobic interaction chromatography, J Sep Sci 36(8) (2013) 1327-34. https://doi.org/10.1002/jssc.201200704.

[131] P. Wang, A. Anderko, R.D. Young, Modeling Surface Tension of Concentrated and Mixed-Solvent Electrolyte Systems, Industrial & Engineering Chemistry Research 50(7) (2011) 4086-4098. https://doi.org/10.1021/ie101915n.

[132] C. Drummond, L. Pérez-Fuentes, D. Bastos-González, Can Polyoxometalates Be Considered as Superchaotropic Ions?, The Journal of Physical Chemistry C 123(47) (2019) 28744-28752. https://doi.org/10.1021/acs.jpcc.9b08324.

[133] M. Boström, W. Kunz, B.W. Ninham, Hofmeister effects in surface tension of aqueous electrolyte solution, Langmuir : the ACS journal of surfaces and colloids 21(6) (2005) 2619-2623. https://doi.org/10.1021/la047437v.

[134] A.P. Dos Santos, A. Diehl, Y. Levin, Surface tensions, surface potentials, and the hofmeister series of electrolyte solutions, Langmuir : the ACS journal of surfaces and colloids 26(13) (2010) 10778-10783. https://doi.org/10.1021/la100604k.

[135] E. Lee, J.H. Choi, M. Cho, The effect of Hofmeister anions on water structure at protein surfaces, Physical chemistry chemical physics : PCCP 19(30) (2017) 20008-20015. https://doi.org/10.1039/c7cp02826a.

[136] D.L. McCaffrey, S.C. Nguyen, S.J. Cox, H. Weller, A.P. Alivisatos, P.L. Geissler, R.J. Saykally, Mechanism of ion adsorption to aqueous interfaces: Graphene/water vs. air/water, Proceedings of the National Academy of Sciences of the United States of America 114(51) (2017) 13369-13373. https://doi.org/10.1073/pnas.1702760114.

[137] S. Zhang, T. Iskra, W. Daniels, J. Salm, C. Gallo, R. Godavarti, G. Carta, Structural and performance characteristics of representative anion exchange resins used for weak partitioning chromatography, Biotechnol Prog 33(2) (2017) 425-434. https://doi.org/10.1002/btpr.2412.

[138] Y. Wu, D. Abraham, G. Carta, Comparison of perfusion media and monoliths for protein and virus-like particle chromatography, Journal of chromatography. A 1447 (2016) 72-81. https://doi.org/10.1016/j.chroma.2016.03.077.

[139] M.E. Fisher, Shape of a Self-Avoiding Walk or Polymer Chain, The Journal of Chemical Physics 44(2) (1966) 616-622. https://doi.org/10.1063/1.1726734.

[140] G. Beaucage, Determination of branch fraction and minimum dimension of mass-fractal aggregates, Physical Review E 70(3) (2004) 031401. https://doi.org/10.1103/PhysRevE.70.031401.

[141] T.J. Richmond, Solvent accessible surface area and excluded volume in proteins: Analytical equations for overlapping spheres and implications for the hydrophobic effect, Journal of Molecular Biology 178(1) (1984) 63-89. https://doi.org/https://doi.org/10.1016/0022-2836(84)90231-6.

[142] B. Hammouda, Small-Angle Scattering From Branched Polymers, Macromolecular Theory and Simulations 21(6) (2012) 372-381. https://doi.org/10.1002/mats.201100111.

[143] A.M. Senczuk, R. Klinke, T. Arakawa, G. Vedantham, Y. Yigzaw, Hydrophobic interaction chromatography in dual salt system increases protein binding capacity, Biotechnol Bioeng 103(5) (2009) 930-5. https://doi.org/10.1002/bit.22313.

[144] A. Werner, H. Hasse, Experimental study and modeling of the influence of mixed electrolytes on adsorption of macromolecules on a hydrophobic resin, Journal of chromatography. A 1315 (2013) 135-44. https://doi.org/10.1016/j.chroma.2013.09.071.

[145] E. Hackemann, H. Hasse, Influence of mixed electrolytes and pH on adsorption of bovine serum albumin in hydrophobic interaction chromatography, Journal of chromatography. A 1521 (2017) 73-79. https://doi.org/10.1016/j.chroma.2017.09.024.

[146] K. Baumgartner, S. Amrhein, S.A. Oelmeier, J. Hubbuch, The influence of mixed salts on the capacity of HIC adsorbers: A predictive correlation to the surface tension and the aggregation temperature, Biotechnol Prog 32(2) (2016) 346-54. https://doi.org/10.1002/btpr.2166.

[147] J.F. Kramarczyk, B.D. Kelley, J.L. Coffman, High-throughput screening of chromatographic separations: II. Hydrophobic interaction, Biotechnol Bioeng 100(4) (2008) 707-20. https://doi.org/10.1002/bit.21907.

[148] Q. Meng, J. Wang, G. Ma, Z. Su, Isotherm type shift of hydrophobic interaction adsorption and its effect on chromatographic behavior, J Chromatogr Sci 51(2) (2013) 173-80. https://doi.org/10.1093/chromsci/bms123.

[149] R.A. Latour, The Langmuir isotherm: a commonly applied but misleading approach for the analysis of protein adsorption behavior, J Biomed Mater Res A 103(3) (2015) 949-58. https://doi.org/10.1002/jbm.a.35235.

[150] B.B. Langdon, M. Kastantin, R. Walder, D.K. Schwartz, Interfacial protein-protein associations, Biomacromolecules 15(1) (2014) 66-74. https://doi.org/10.1021/bm401302v.

[151] B.B. Langdon, M. Kastantin, D.K. Schwartz, Surface Chemistry Influences Interfacial Fibrinogen Self-Association, Biomacromolecules 16(10) (2015) 3201-8. https://doi.org/10.1021/acs.biomac.5b00869.

[152] L.L. Sorret, M.A. DeWinter, D.K. Schwartz, T.W. Randolph, Protein-protein interactions controlling interfacial aggregation of rhIL-1ra are not described by simple colloid models, Protein Sci 27(7) (2018) 1191-1204. https://doi.org/10.1002/pro.3382.

[153] R.W. Deitcher, J.P. O'Connell, E.J. Fernandez, Changes in solvent exposure reveal the kinetics and equilibria of adsorbed protein unfolding in hydrophobic interaction chromatography, Journal of chromatography. A 1217(35) (2010) 5571-83. https://doi.org/10.1016/j.chroma.2010.06.051.

[154] B. Beyer, A. Jungbauer, Conformational changes of antibodies upon adsorption onto hydrophobic interaction chromatography surfaces, Journal of chromatography. A 1552 (2018) 60-66. https://doi.org/10.1016/j.chroma.2018.04.009.

[155] S.L. Wu, A. Figueroa, B.L. Karger, Protein conformational effect in hydrophobic interaction chromatography. Retention characterization and the role of mobile phase additives and stationary phase hydrophobicity, Journal of Chromatography A 371(C) (1986) 3-27. https://doi.org/10.1016/S0021-9673(01)94689-8.

[156] T. Tibbs Jones, E.J. Fernandez, α-Lactalbumin tertiary structure changes on hydrophobic interaction chromatography surfaces, Journal of Colloid and Interface Science 259(1) (2003) 27-35. https://doi.org/10.1016/s0021-9797(02)00180-7.

[157] Y. Xiao, T.T. Jones, A.H. Laurent, J.P. O'Connell, T.M. Przybycien, E.J. Fernandez, Protein instability during HIC: hydrogen exchange labeling analysis and a framework for describing mobile and stationary phase effects, Biotechnol Bioeng 96(1) (2007) 80-93. https://doi.org/10.1002/bit.21186.

[158] A. Jungbauer, C. Machold, R. Hahn, Hydrophobic interaction chromatography of proteins. III. Unfolding of proteins upon adsorption, Journal of chromatography. A 1079(1-2) (2005) 221-8. https://doi.org/10.1016/j.chroma.2005.04.002.

[159] R. Ueberbacher, E. Haimer, R. Hahn, A. Jungbauer, Hydrophobic interaction chromatography of proteins V. Quantitative assessment of conformational changes, Journal of chromatography. A 1198-1199 (2008) 154-63. https://doi.org/10.1016/j.chroma.2008.05.062.

[160] S. Brunauer, P.H. Emmett, E. Teller, Adsorption of Gases in Multimolecular Layers, Journal of the American Chemical Society 60(2) (1938) 309-319. https://doi.org/10.1021/ja01269a023.

[161] M.R. Oberholzer, A.M. Lenhoff, Protein Adsorption Isotherms through Colloidal Energetics, Langmuir : the ACS journal of surfaces and colloids 15(11) (1999) 3905-3914. https://doi.org/10.1021/la981199k.

[162] H. Freundlich, Über die Adsorption in Lösungen, 57U(1) (1907) 385-470. https://doi.org/doi:10.1515/zpch-1907-5723.

[163] S. Sharma, G.P. Agarwal, Interactions of proteins with immobilized metal ions: a comparative analysis using various isotherm models, Anal Biochem 288(2) (2001) 126-40. https://doi.org/10.1006/abio.2000.4894.

[164] T.M. Scherer, J. Liu, S.J. Shire, A.P. Minton, Intermolecular interactions of IgG1 monoclonal antibodies at high concentrations characterized by light scattering, Journal of Physical Chemistry B 114(40) (2010) 12948-12957. https://doi.org/10.1021/jp1028646.

[165] T.M. Scherer, Role of Cosolute-Protein Interactions in the Dissociation of Monoclonal Antibody Clusters, The journal of physical chemistry. B 119(41) (2015) 13027-38. https://doi.org/10.1021/acs.jpcb.5b07568.

[166] E. Hackemann, A. Werner, H. Hasse, Influence of mixed electrolytes on the adsorption of lysozyme, PEG, and PEGylated lysozyme on a hydrophobic interaction chromatography resin, Biotechnol Prog 33(4) (2017) 1104-1115. https://doi.org/10.1002/btpr.2474.

[167] N. Galeotti, E. Hackemann, F. Jirasek, H. Hasse, Prediction of the elution profiles of proteins in mixed salt systems in hydrophobic interaction chromatography, Separation and Purification Technology 233 (2020). https://doi.org/10.1016/j.seppur.2019.116006.

[168] I.B. Santarino, S.C.B. Oliveira, A.M. Oliveira-Brett, Protein reducing agents dithiothreitol and tris(2-carboxyethyl)phosphine anodic oxidation, Electrochemistry Communications 23(1) (2012) 114-117. https://doi.org/10.1016/j.elecom.2012.06.027.

[169] L. Grassi, C. Cabrele, Susceptibility of protein therapeutics to spontaneous chemical modifications by oxidation, cyclization, and elimination reactions, Amino Acids 51(10-12) (2019) 1409-1431. https://doi.org/10.1007/s00726-019-02787-2.

6 Publications

Protein-protein interactions and reduced excluded volume increase dynamic binding capacity of dual salt systems in hydrophobic interaction chromatography

Leo A. Jakob, Beate Beyer, Catarina Janeiro Ferreira, Nico Lingg, Alois Jungbauer, Rupert Tscheließnig

Journal of Chromatography A, 2021, 1649, 462231

doi.org/10.1016/j.chroma.2021.462231

Processing status: **published**.

Declaration of Authorship: Conceptualization, Methodology, Formal analysis, Investigation, Data curation, Writing – original draft, Visualization.

Increase in cysteine-mediated multimerization under attractive protein–protein interactions

Leo A. Jakob, Tomás Mesurado, Alois Jungbauer, Nico Lingg

Preparative Biochemistry & Biotechnology, 2022 (online publication)

doi.org/10.1080/10826068.2022.2158471

Processing status: **published**.

Declaration of Authorship: Conceptualization, Methodology, Formal analysis, Investigation, Data curation, Writing – original draft, Writing – review & Editing, Visualization.

Additional Publications

Productivity for free: Residence time gradients during loading increase dynamic binding capacity and productivity

Declaration of Authorship: Methodology, Investigation, Writing – review & Editing,

From strain engineering to process development: monoclonal antibody production with an unnatural amino acid in Pichia pastoris

Declaration of Authorship: Methodology, Investigation

Protein-protein interactions and reduced excluded volume increase dynamic binding capacity of dual salt systems in hydrophobic interaction chromatography

Leo A. Jakob[a], Beate Beyer[a,b], Catarina Janeiro Ferreira[b], Nico Lingg[a,b], Alois Jungbauer[a,b,*], Rupert Tscheließnig[a]

[a] Department of Biotechnology, University of Natural Resources and Life Sciences, Vienna, Muthgasse 18, A-1190, Austria
[b] Austrian Centre of Industrial Biotechnology, Muthgasse 18, Vienna A-1190, Austria

ABSTRACT

Deploying two salts in hydrophobic interaction chromatography can significantly increase dynamic binding capacities. Nevertheless, the mechanistic understanding of this phenomenon is lacking. Here, we investigate whether surface tension or ionic strength govern dynamic binding capacities of the chromatographic resin Toyopearl Butyl-650 M in dual salt systems. Small-angle X-ray scattering was employed to analyze the model proteins and the protein-resin adduct in the respective dual salt systems. The dual salt systems incorporate sodium citrate and a secondary sodium salt (acetate, sulfate, or phosphate). As model proteins, we used lysozyme, GFP, and a monoclonal antibody (adalimumab).

Moreover, for the protein-resin adduct, we determined the model parameters of a self-avoiding random walk model fitted into the pair density distribution function of the SAXS data. Ionic strength is more predictive for dynamic binding capacities in HIC dual salt systems than surface tension. However, dynamic binding capacities still differ by up to 30 % between the investigated dual salt systems. The proteins exhibit extensive protein-protein interactions in the studied dual salt HIC buffers. We found a correlation of protein-protein interactions with the well-known Hofmeister series. For systems with elevated protein-protein interactions, adsorption isotherms deviate from Langmuirian behavior. This highlights the importance of lateral protein-protein interactions in protein adsorption, where monomolecular protein layers are usually assumed. SAXS analysis of the protein-resin adduct indicates an inverse correlation of the binding capacity and the excluded volume parameter. This is indicative of the deposition of proteins in the cavities of the stationary phase. We hypothesize that increasing protein-protein interactions allow the formation of attractive clusters and multilayers in the cavities, respectively.

1. Introduction

Senczuk *et al.* (2009) described the positive effect of so-called dual salt buffer systems on dynamic binding capacities (DBC) in hydrophobic interaction chromatography (HIC). Those dual salt systems showed increased dynamic binding capacities compared to a single salt system [1] which has been confirmed by other groups [2–4]. Hackemann et al. [5] has shown that dual salt systems can either synergistically increase or decrease binding capacities in adsorption isotherms. Altogether, a fundamental understanding

of how two different buffers promote better binding than a single one has not yet been provided. Commonly, a kosmotropic buffer is added to the protein solution to promote binding. The addition of a chaotropic salt would be counterintuitive according to the current theory explaining the adsorption of proteins in HIC [6]. Both Müller et al. [2] and Baumgartner et al. [3] postulated that mixing a kosmotropic salt for promoting binding to the hydrophobic stationary phase surface and chaotropic salt, which is possibly increasing the protein solubility, should be the preferred strategy when setting up mixed salt buffer systems for chromatography. The current understanding is lacking a fundamental explanation of the mechanism.

The surface tension increment of the salt in the binding buffer and the salting in and out properties govern the adsorption of proteins in HIC, as described in the solvophobic theory [6]. In gen-

eral, this theory describes the interaction behavior of a more polar solvent, in this case the mobile phase and a less polar solute, the sample protein, by considering the changes in the system's free energy caused by the individual processes involved. The structural forces of water formed by hydrogen bonding, in this context, represent a low energy state. In contrast, the water molecules near the stationary phase's hydrophobic surface are in an energetically "loaded" state. The protein binding to the hydrophobic surface reduces the surface area in contact with the water molecules. The energy released as a consequence of this can be described as a function of the change in available free surface area ΔA and the surface tension of the mobile phase γ:

$$Energy = \Delta A * \gamma \tag{1}$$

This means that the retention in both reversed-phase chromatography and HIC increases with the mobile phase's surface tension [6,7]. Based on this concept, higher hydrophobic energy and thus a higher surface tension of the mobile phase should also translate into higher protein binding capacities of the column.

Another parameter that could influence retention and binding capacity in HIC is ionic strength. This parameter describes the total concentration of ions in a solution. Thus, it can be vastly different for solutions containing identical molar concentrations of different salts depending on the valences of the salts in question. The ionic strength I of a solution can be calculated based on the Lewis and Randall equation:

$$I = \frac{1}{2}\sum_{i}^{n} c_i z_i^2 \tag{2}$$

with n representing the number of ions in the solution, i representing one specific ion, c_i being the corresponding concentration of ion i in mol*l^{-1}, and z_i denoting the valence of ion i.

In order to determine the ionic strength, the concentration of the ions has to be determined using the Henderson-Hasselbalch equation, defined as:

$$pH = pK_a + log\frac{[A^-]}{[HA]} \tag{3}$$

where $[HA]$ is the molar concentration of the unassociated weak acid and $[A^-]$ is the molar concentration of the acid's conjugate base.

Apart from interactions between the protein and the HIC stationary phase [8,9], it is well known that ions modulate protein-protein interactions [10–14]. Although speculations about protein-protein interaction-based multilayer formation [15] and cluster formation [16] can be found in literature, experimental evidence is scarce for those phenomena in HIC. However, interactive protein clusters have already been reported for other surfaces. Langdon et al. [17] showed that attractive protein-protein interactions responsible for cluster formation of BSA on a hydrophilic surface. In the case of the presence of protein-protein interactions, the Langmuir adsorption isotherm model is no longer valid since the non-interactivity of the adsorbate is a prerequisite for its applicability [18]. Meng et al. [19] have shown that the isotherm type shifted between Langmuir and Freundlich type depending on the salt concentration. Moreover, they have hypothesized that protein-protein interaction is responsible for Freundlich type isotherms. Besides Freundlich type isotherms, the Brunauer-Emmett-Teller (BET) theory describes multilayer adsorption protein chromatography [20,21].

As an analytical tool, small-angle x-ray scattering (SAXS) gives a unique insight into the native solution structure of proteins. It allows the investigation of the intramolecular and intermolecular structure of proteins, such as the medium resolution protein conformation [22,23] and protein-protein interactions [12,14], respectively. More recently, SAXS has been utilized for online monitor-

ing of the protein layer thickness [24] and binding conformations [25] in chromatographic systems. In classical polymer chemistry, SAXS experiments allow the characterization of polymers. Fractal models can be used to describe linear and branched polymers, characterizing the polymer's inter-monomer conformational distribution. This includes several parameters, such as the excluded volume and the path length in-between the monomers [26] In this work, we model the chromatographic resin as a self-avoiding random walk (SARW) with and without proteins bound. The resulting parameters are then interpreted to gain an understanding of the binding topology. These experiments are performed with resin slurries using a pipetting robot [27].

As model proteins for this study, a monoclonal antibody (adalimumab), lysozyme, and Green Fluorescent Protein (GFP) were used, since they have previously been described in dual salt systems. Senczuk et al. postulated that their observations might be due to specific interactions of the antibodies with the stationary phase [1]. Lysozyme was first proposed by Müller et al. as an additional model protein for studying dual salt buffer systems. It has a basic pI (10.7 [28]), similar to most monoclonal antibodies [2] and adalimumab's (7.9-9.1 [29]). GFP was added because of its acidic range (pI = 5.8 [30]). Thus, if the claim of increased binding capacity with dual salt systems also holds for GFP, this would strongly indicate that the pI of the sample protein does not influence stationary phase binding in mixed salt systems. Furthermore, the chosen model proteins differ significantly in regards to their molar mass, having molar masses of 14.3 kDa (lysozyme [28]), 26.9 kDa (GFP [30]) and 148 kDa (adalimumab [31]).

Ultimately, this study aims to identify whether surface tension or ionic strength is the primary driving force for dynamic binding capacities in HIC. For that purpose, we prepared citrate buffers containing a secondary salt (acetate, phosphate, or sulfate) and varied the concentrations of these salts to obtain buffers with identical surface tension. Dynamic binding capacities of a Toyopearl Butyl-650M HIC column were determined for the systems with identical surface tension. Similarly, we prepared buffers with more or less the same ionic strength by variation of the citrate concentration. For those systems, the equilibrium and dynamic binding capacities were determined. SAXS was used to investigate the impact on the model protein solution structure (such as the protein structure and protein-protein interaction) and the protein-resin topology when bound to the chromatographic resin. For modelling the protein-chromatographic resin adduct, we have derived a SARW model that was then fitted to the pair density distribution function (PDDF) of the adduct.

2. Theory

2.1. SARW model

We follow the arguments of Hammouda [26], Zimm [32], and Beaucage [33]. We consider a linear polymer chain first; it consists of n elements. First, we define a segment of reference. It can be any segment, i. The probability of finding another segment, j of the same molecule is [26]:

$$\pi_{ij}^1(r) = 4\pi r^2 (3/2\langle \pi r \rangle^{-2})^{3/2} exp\left(-3/2r^2\langle r\rangle^{-2}\right). \tag{4}$$

Then, we link the inter-segment distance, r, and the average inter-monomer distance, $\langle r\rangle$. We follow Hammouda and put it $\langle r^2 \rangle = a^2 |i - j|^{2\nu}$ [26]. Herein r resembles the inter-segment distance, and ν gives the excluded volume parameter while a is the statistical segment length. If we put the excluded volume parameter to 1, we get the probability to find two pairs i, j of a non-self-avoiding random chain. It is easy to show that the Eq. (4) is normalized to one, $\int_0^\infty dr\pi_{ij}^1(r) = 1$. The linear polymer chain is finite and consists of N segments; still following the argument of

Zimm, we give the PDDF of this particular construct:

$$p(r) = \int_0^N dn(N-n)\pi_n^1(r).\qquad(5)$$

The norm of it equals $\Gamma = \int_0^\infty dr p(r) = N^2/2$. It seems incorrect as from any N segment long chain, random, or random self-avoiding can pair N(N-1)/2 nonidentical segments. Thus, we correct the norm and find the PDDF:

$$p'(r) = \frac{(N-1)}{N} p(r).\qquad(6)$$

The equation is still inappropriate as in nonidentical pairs, the lower boundary of the integration over n must read one and not 0. Then the appropriate PDDF reads:

$$p''(r) = \frac{N}{N-1} \int_1^N dn(N-n)\pi(n)\pi_n^1(r)\qquad(7)$$

Please note one important thing. The segments are equally distributed, $\pi(n) = 1$. What if they are not? What if specific segment pairs are not to be taken into account? What if the segments are fractally distributed, and their probability is given by $\pi(n) = (n\lambda)^c$? We follow the arguments of Hammouda [26], we introduce a fractal distribution of n. Moreover, we compute the norm:

$$\int_0^\infty dr p_\lambda^c(\ldots|r) = \lambda^c \frac{\left(c+1-N\left(c+2-N^{c+1}\right)\right)}{(c+1)(c+2)}\qquad(8)$$

It is straightforward to show that in $c=0$, the norm equals: N(N-1)/2. We proceed and give pair density of a self-avoiding random walk explicitly. Therefore, we introduce a set of abbreviations: $\alpha = \frac{c - \frac{\nu}{2} + 1}{\nu}$, $\alpha' = \alpha + \frac{1}{\nu}$, $\beta = \frac{3r^2}{2b^2}$, $\beta' = \beta N^{-\nu}$, $\gamma = \sqrt{\frac{3}{\pi}}\frac{3r^2}{b^3}\frac{(c^2+3c+2)(1-N)N^{1-\frac{3}{2}\nu}}{\nu(N+c+1)}$, and then find for the PDDF for an ensemble of self-avoiding random walks, with fractal distributed pairs:

$$p_\lambda^c(b,N,\nu,c|r)=\gamma N^{c+2}\left(E_{\alpha'}\left(\beta'\right)-E_\alpha\left(\beta'\right)\right)+N^{\frac{3}{2}\nu}(NE_\alpha(\beta)-E_{\alpha'}(\beta))\qquad(9)$$

Therein $E_n(z) = \int_1^\infty dt t^{-n}\exp(-zt)$ is the exponential integral function.

$\pi(n) = (n\lambda)^c$ accounts, within the integral for the average number of minimum paths with a path length n [3].

2.2. Chromatographic stationary phase as a SARW

If we embed a random walk in a spherical volume, we assume that a spherical PDDF distributes the minimum paths' average number with a path length n. Think of a sphere that is filled by random points, up to infinite density. Then any randomly chosen pair will have a minimum path that equals their Euclid net distance. This is true for a hypothetical resin absent of any pore. The introduction of pores and their decoration by proteins is then measurable by the difference in their particular PDDF. We introduce the normalized probability to identify minimum paths of length n, $r \propto \lambda n$, and $R \propto \lambda N$

$$\pi(n) = \lambda^{-1}\left(\frac{3n^5}{16N^6} - \frac{9n^3}{4N^4} + \frac{3n^2}{N^3}\right)\qquad(10)$$

Finally, we obtain the PDDF for a hypothetical resin. It resembles a resin absent of pores.

$$p_{SARW}(b,N,\nu|r) \propto 1/16/N^6 p_\lambda^c(b,N,\nu,5|r)+3/4/N^4 p_\lambda^c(b,N,\nu,3|r)$$
$$+1/N^3 p_\lambda^c(b,N,\nu,2|r)\qquad(11)$$

With the PDDF describing the SARW model (Eq. (11)), the experimental PDDF p(r) can be fitted. The fitting procedure minimizes the difference between the experimental PDDF and the PDDF describing the SARW by adjusting

$$\text{minarg}_r \| p(r) - \left(a\ p_{SARW}(b,N,\nu r) + c_B\ r^D\right)\|_2\qquad(12)$$

While parameters a, c_B, and D are due to the norm and the overall stochastic background, parameters b, N and ν characterize the system's morphology on a smaller scale.

3. Material & methods

3.1. Buffer preparation

The salts used for the buffers tested in the experiments were supplied by Merck (Germany) and were all of analytical grade. All buffers were prepared from stock solutions of 1.5 M of sodium citrate monobasic, 1 M of sodium phosphate, 0.6 M of sodium sulfate, 2 M of sodium acetate, and then adjusted to pH 6 with NaOH. The specific dual salt mixtures of 0.329 M of citrate + 0.5 M of sulfate were prepared from a 0.8 M sodium sulfate stock solution. The buffer preparation was followed by filtration using a 0.22 μm filter supplied by Merck Millipore (Ireland).

3.2. Model proteins

Lysozyme was obtained from Merck in the crystalline state. GFP and the antibody were produced in-house and kept as low ionic strength stock solutions at 4°C for the experiments' duration. GFP was previously expressed in *E. coli* and purified in a three-step chromatographic process. In contrast, the monoclonal antibody (mAb), an in-house produced adalimumab, was expressed in CHO and purified solely by protein A capture. For the SAXS experiments analyzing the protein in solution, the monoclonal antibody was purified using a HiLoad 26/600 Superdex 200 pg (Cytiva, Sweden). The model proteins have been analyzed with high-performance size exclusion chromatography (HP-SEC). The corresponding chromatograms can be found in the Supplementary Material (Fig. S1).

3.3. Measurement of surface tension

The surface tension measurements were performed using the pendant drop (PD) method, an optical method for determining the surface tension of a drop of liquid by using the drop profile's curvature. The measurements of the different salt buffers were performed using the Drop Shape Analyzer (Krüss, Germany) instrument. The determination of the surface tension using the PD requires the drop to be distorted by gravity, which is ensured by using a tip large enough to support the needed drop size (in this case, the needle had a diameter of 1.835 mm). Water was used as a reference at the beginning of all sets of experiments. Its surface tension is between 72 and 73 mN*m^{-1}, depending on the surrounding temperature and humidity conditions. The measurements were repeated at least three times each (each one is already the average of one minute of measurements). The system was always flushed with the intended test buffer between different buffers' measurements for fifteen minutes to ensure that there were no traces of other buffers left in the tubes. As determined by a pycnometer, both the buffers' density and the temperature of the room were measured and taken into account by the software Krüss Advanced (Krüss, Germany) to get the most accurate results possible.

For obtaining buffers with comparable surface tension, the surface tension value measured for 0.55 M citrate was used as a reference point. The other buffers' salt concentrations, as previously

Table 1

Surface tension of the buffers used by Senczuk et al. [1] (left-hand side), buffers with adjusted salt concentrations that resulted in similar surface tension values (right-hand side).

Starting Buffers as used by Senczuk et al. [1]	Surface Tension [mN*m^{-1}]	Buffers with adjusted salt concentrations to achieve similar surface tension	Surface Tension [mN*m^{-1}]
Citrate 0.55 M	73.5	Citrate 0.55 M	73.5
Citrate 0.55 M + 1 M Acetate	70.4	Citrate 0.55 M + 0.5 M Acetate	73.4
Citrate 0.55 M + 0.5 M Phosphate	74.7	Citrate 0.35 M + 0.5 M Phosphate	74.3
Citrate 0.55 M + 0.3 M Sulfate	73.7	Citrate 0.55 M + 0.3 M Sulfate	73.7

described by Senczuk *et al.*, were adjusted to achieve either a decrease or an increase in surface tension, which was then confirmed by pendant drop measurements. Based on these measurements, the buffers listed in Table 1 were used for chromatographic experiments.

3.4. Measurement of dynamic binding capacities

Dynamic binding capacity measurements for protein samples in the different high salt buffers were performed using a Toyopearl Butyl-650 M (Tosoh Bioscience, Germany) column. A 4.8 × 0.5 cm column with a column volume (CV) of 0.94 ml and a 1.3 × 1.0 cm column with a CV of 1.02 ml were used for the breakthrough (BT) experiments. To test packing quality, 1 % acetone (v/v) was injected to evaluate the peak asymmetry. The asymmetry ranged from 1.2-1.6. All chromatographic experiments were carried out on an ÄKTA^{TM} Pure 25 chromatography system (Cytiva, Sweden).

3.4.1. Column packing

A 10/20 tricorn column housing (Cytiva, Sweden) was packed with TOYOPEARL Butyl-650M (Tosoh Cooperation, Japan) resin using 50 mM phosphate buffer with 1 M of NaCl as packing buffer. A 5 ml*min^{-1} flow rate was chosen for packing based on the manufacturer's instruction manual. Once the packing operation was completed, the column was equilibrated with 5 – 10 CVs of low ionic strength buffer (50 mM of phosphate buffer). While not in use, both columns were stored in 20 % (v/v) ethanol at room temperature.

3.4.2. Breakthrough curves and calculation of DBC

All samples were transferred into the corresponding high salt buffer before the experiment either by resolubilizing the crystallized protein in the buffer (in the case of lysozyme) or diluting the sample protein from a stock solution (for the mAb and GFP). The stock solution concentrations were set so that the protein was diluted at least 1:5 in the experimental buffer to achieve a final load concentration of approximately 5 g*l^{-1}. The precise concentration of the sample solution was then determined spectrophotometrically by measuring the absorbance at 280 nm.

For the chromatographic runs, the column was first equilibrated in the corresponding high salt experiment buffer. The flow rate for the loading step was set to achieve a residence time of 10 min. Sample loading was followed by a 5–10 CV wash step with the experiment buffer. For elution, a linear gradient from 0-100 % B was performed with water as buffer B over 10 CV, followed by 5 CV at 100 % buffer B. For column CIP, 0.1 M NaOH was used. All experiments were performed in a temperature-controlled room with a temperature ranging from 21–25°C.

For DBC calculations, the load's absorbance value was determined in a by-pass experiment on the Äkta system. This value was then treated as a 100 % breakthrough. The volume was then determined, at which 10 % of the absorbance value at 100 % breakthrough was reached (*loaded volume$_{10\%BT}$*). Absorbance at 10 % breakthrough was below 1 AU for all breakthrough experiments. From the volume at 10 % breakthrough, the void volume of the column and system were subtracted. The resulting value times the concentration of the load (c_{load}) divided by the volume of the column was treated as the DBC at 10 % breakthrough ($DBC_{10\%}$):

$$DBC_{10\%} = \frac{(loaded\ volume_{10\%BT} - void\ volume)*c_{load}}{column\ volume} \quad (13)$$

3.5. Calculation of buffer ionic strength

The tested buffers' ionic strength was calculated using Eqs. (2) and (3). For preparing buffers with comparable ionic strengths, the ionic strength value obtained for 0.55 M citrate was again used as a reference point. The salt concentrations of the other buffers were adjusted to match that value. Since significant amounts of NaOH had to be used to adjust the experiment buffers to a pH of 6, this also had to be considered. Based on these calculations, the buffers listed in Table 1 were used for the chromatographic experiments investigating ionic strength as a possible driving force.

3.6. Adsorption isotherms

The procedure for the adsorption isotherms was based on a previous publication [25]. Protein stock solutions were prepared by mixing a concentrated protein stock (> 60 mg*ml^{-1}), dH$_2$O, and salt stock solutions to achieve the desired buffer composition and a protein concentration of approximately 7 mg*ml^{-1}. The protein stock solution was then further diluted in a 96 UV Star Microplate (Greiner Bio-One, Austria) to achieve a final concentration range of 0.5 mg*ml^{-1} – 5 mg*ml^{-1} with a total of ten different concentrations. Before adding the chromatographic resin, the resin slurry was set to the concentration of 50 % and washed two times with dH$_2$O and six times with the corresponding buffer. 50 µl of the 50 % slurry were added to the protein solutions to achieve a total volume of 250 µl and a slurry concentration of 10 %. The chromatographic resin and the corresponding model protein were incubated for 24 h on a thermomixer (Thermo Fisher Scientific, Waltham, MA) at 950 rpm and 21.5°C. The resulting supernatant was analyzed spectrophotometrically via absorbance at 280 nm to determine the protein concentration. When the plateau in the adsorption isotherm was not reached, additional measurements were performed with a 3 - 4.5 mg*ml^{-1} mobile phase concentration at a resin concentration of 5 %. Adsorption isotherms incorporating such data points are marked in the corresponding figure.

The Langmuir (Eq. (14)) [18], BET (Eq. (15)) [20] and Freundlich (16) [19] models were used to describe the adsorption isotherm data:

$$q = c\frac{q_{max}*K_a}{1 + q_{max}*K_a} \quad (14)$$

$$q = \frac{q_{mono}K_S c}{(1 - K_L c)(1 - K_L c + K_S c)} \quad (15)$$

$$q = K_F * c^{n_F} \quad (16)$$

where q describes the binding capacity in mg protein per ml resin, c the mobile phase concentration in mg*ml^{-1}, q_{max} the maximum binding capacity in mg protein per ml resin, K_a the affinity

constant of the protein towards the stationary phase in ml*mg^{-1}, q_{mono} the binding capacity of a monolayer, K_S the affinity constant towards the stationary phase (equivalent to Langmuir K_A), K_L the affinity constant towards deposited layers [20], K_F the adsorption constant in ml*mg^{-1} and n_F the adsorption exponent [19].

In the case of a distinct plateau, the Langmuir isotherm model was used to fit the data. Data with a second liftoff was fitted with the BET adsorption isotherm model. Data that showed neither a second liftoff nor a plateau was fitted with the Freundlich isotherm. The fitted adsorption isotherm model was evaluated based on trends in residuals. Since protein-protein interaction must not be negligible for the validity of the Langmuir model [18] and present in the case of the BET model [21], protein-protein interactions were evaluated from SAXS analytics of the model proteins in solution (Section 2.7.1).

3.7. SAXS

All SAXS experiments were performed at the Elettra synchrotron in Trieste, Italy. The scattering vector q ($q = 4\,\pi\,\sin(\Theta)\,\lambda^{-1}$, where Θ is the scattering angle) ranged from 0.896–6.998 nm^{-1} at a wavelength of $\lambda = 0.154$ nm. All protein solutions were prepared from dH$_2$O, protein, and salt stock solutions. The recently described high throughput robot was used for all SAXS experiments [27].

3.7.1. Proteins in solution
The resulting protein concentration was 5 mg*ml^{-1} for the proteins' measurements in solution.

20 μl of the protein solution was pipetted into the measuring cell, and a total of 12 images were measured. For each image, the exposure time was 10 s followed by a 2 s pause between every image. For each sample, the respective buffer was measured without an analyte for background subtraction.

3.7.2. Protein-chromatographic resin suspension
For the suspension experiments, the protein concentration was 5 mg*ml^{-1}, and the chromatographic resin slurry was prepared as described in Section 2.6. The model proteins were GFP and the monoclonal antibody. The adsorption experiments were performed at a protein concentration of 5 mg*ml^{-1} and a slurry concentration of 5 % to achieve the chromatographic resin's full saturation. The reaction was conducted in 2 ml Eppendorf reaction tubes (Eppendorf GmbH, Germany) at a total volume of 1 ml. The reaction was incubated for 15 h on a thermomixer (Thermo Fisher Scientific, Waltham, MA) at 900 rpm and room temperature. After incubation, the resin slurry was briefly washed two times with the respective buffer. For the measurements, the slurry concentration was set to 40 %. The samples were prepared in triplicates.

For the measurement, 25 μl of a slurry suspension was pipetted into the measuring cell. To increase the throughput and keep the time between the protein incubation and the actual measurement to a minimum, 20 images were recorded in a total time of 20 s. The exposure time was 950 ms for each image, followed by a 50 ms pause between the measurements. For each sample, the respective buffer was measured without an analyte for background subtraction.

3.7.3. Data treatment
Data evaluation was performed using the program Mathematica 12.1 (Wolfram Research, Inc., USA). Intensities were averaged over all 20 images for the sample and the background, respectively. After normalization at 4.95-5.05 nm^{-1}, the background was subtracted from the scattering data, resulting in the background corrected scattering data. Q values of distinctive features and regions of the reciprocal space were converted to the real-space via Eq. 17 ([34]).

$$\boldsymbol{d} = \frac{2\,\pi}{\boldsymbol{q}} \tag{17}$$

where d is the real-space distance in nm and q is the scattering vector in nm^{-1}.

3.7.4. Plotting of the background-corrected scattering data
For the measurements of the protein in solution, the background-corrected scattering data were normalized to q = 0.55 nm^{-1} and plotted to facilitate the comparison of the low and high q-range. For the measurements of the protein-chromatographic resin suspension, the background-corrected scattering data were normalized to q = 0.09 nm^{-1}. The curves of the triplicates were stacked by multiplying the intensity by 1, 10^1, and 10^2, respectively, to facilitate the comparison between the measurements.

3.7.5. Pair density distribution function
The PDDF p(r) of scattering data was calculated via an inverse Fourier transform [35]:

$$I(q) = 4\,\pi \int_0^{Dmax} p(r) \frac{\sin(q\,r)}{q\,r}\,dr \tag{18}$$

I(q) is the scattering intensity at the scattering vector q. D_{max} is the maximum dimension of correlated pairs and r is the distance between the correlated pairs.

The scattering data of the protein-chromatographic resin suspension was transformed to fit the SARW model. The scattering data after background subtraction ($I_e(q)$) was fitted to the PDDF p(r) via Eq. (19):

$$\text{minarg} \parallel I(q) - I_e(q)) \parallel_2 \tag{19}$$

where I(q) is calculated according to Eq. (18) to find the PDDF describing our data (p(r)). The minimum of the argument was determined by applying the Mathematica FindArgMin function. Only $0 \leq p(r)$ were accepted in the inverse Fourier transform. D_{max} was set to 70 and p(r) contained a total of 70 data points (r=1, 2, 3… 70). This fitting procedure resulted in excellent fits throughout all protein-chromatographic resin suspension experiments, as seen in the overlay of the experimental data and the produced fit (Supplementary Material, Fig. S3, left-hand side).

The resulting PDDF (p(r)) is then further used to fit the SARW model derived in Section 3. Again, the difference between p(r) (the experimental PDDF) and the PDDF of the SARW model is minimized (Eq. (12)). Minimization is achieved by applying the FindArgMin function. This results in considerably good fits for distances up to 45 nm (Supplementary Material, Fig. S3, right-hand side)

For calculation of the theoretical scattering curves, the atomic coordinates of the PDBs of lysozyme (1dpx), an IgG1 monoclonal antibody (1hzh), and GFP (1gfl) were used to calculate the theoretical PDDF by summing up all pair distances of all atoms. The intensities were calculated for every scattering angle between 0.896 and 3.000 nm^{-1} according to Eq. (18). The theoretical scattering curves were used as a benchmark for attractive and repulsive interactions in the low q-range.

4. Results & discussion

4.1. Determination of buffer surface tension

The buffers tested in Senczuk *et al.* (2009) were replicated and their surface tension was measured (Table 1). Since the surface tension values varied greatly between buffers, the concentration of one of the salts in the dual salt mixtures was adjusted until similar surface tension values were reached using the surface tension measured for 0.55 M citrate (73.5 mN*m^{-1}) as a reference point
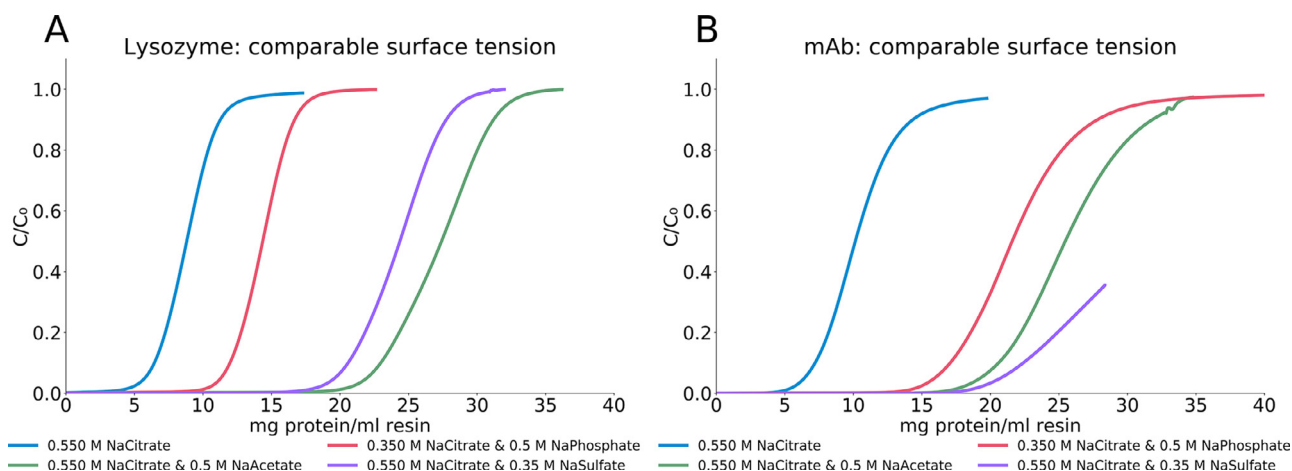
Fig. 1. Breakthrough curves for lysozyme (A, left) and mAb (B, right) at a sample concentration of 5 mg*ml^{-1} using different buffer systems with comparable surface tension as the mobile phase and a TOYOPEARL Butyl-650 M HIC column. DBC was determined for a residence time of 10 min.

and target value. Based on these measurements, the buffers listed in Table 1 (right-hand side) were then chosen as the appropriate buffers for chromatographic experiments for comparing the binding capacities of a HIC column when different dual salt mixtures with similar surface tension are used as the mobile phases.

At first glance, it might seem counterintuitive that for two of the dual salt buffer systems (citrate + sulfate and citrate + acetate), the addition of 0.3 M or 0.5 M of the secondary salt resulted in surface tension values that are almost identical to the one obtained for 0.55 M citrate alone. In this context, it has to be stated that the surface tension of a mixed salt system is not the sum of the contributions of the individual salts present in the mixture. Instead of being additive, the mixture's surface free energy, which determines the surface tension, is reduced by an excess of the component with the lower surface free energy, which is enriched in the surface layer [36]. In a dual salt mixture, the salt with the lower surface tension increment determines the mixture's surface tension. This phenomenon was also observed by Baumgartner et al. It led them to state that in their mixtures of kosmotropic and chaotropic salt, "the surface tension seems to be more influenced by the chaotropic salt" [3].

This behavior is also the reason why it was not possible to achieve a surface tension value more similar to the reference point for the mixture of citrate and phosphate, even by further reducing the concentration of phosphate present in the solution down to 0.1 M. It was, therefore, decided to keep the concentration of phosphate at its original value of 0.5 M in order to have a meaningful amount of secondary salt in the solution and instead, slightly decrease the amount of citrate in the buffer, which resulted in a surface tension value still within the acceptable range of ± 1 mN*m^{-1}.

4.2. Binding capacity in buffers with equal surface tension

Based on the relationship described in Eq. (1), it could be expected that different buffers at the same pH and with similar surface tension values would have the same hydrophobic energy and, hence, lead to the same dynamic binding capacity of the HIC resin. This expectation was put to the test by measuring the dynamic binding capacity of a Toyopearl Butyl 650-M column for lysozyme (Fig. 1 A) and the mAb (Fig. 1 B) in breakthrough experiments using the dual salt buffers with comparable surface tension (Table 1) as mobile phases. Table 2 provides a list with the DBC values calculated at 10 % BT for all the individual curves.

For all the dual salt systems investigated in these experiments, the measured binding capacity was noticeably higher than for citrate alone. The resulting DBC values varied strongly between the different buffers (Fig. 1 and Table 2). While this confirms, to some degree, previous observations of dual salt systems leading to higher binding capacities in HIC, the results are still slightly different to what Senczuk et al. reported. Our study of the dual salt system with phosphate as a secondary salt does not lead to the largest increase in binding capacity, as was previously reported [1]. Among the dual salt systems investigated, higher binding capacities did not correlate with the slight differences in buffer surface tension remaining after concentration adjustment. Therefore, it seems unlikely that these small variations in surface tension are the cause for the observed phenomenon.

4.3. The ionic strength of the buffers

The results described in the previous section indicated that the surface tension of the mobile phase solution might not be the decisive influencing factor when it comes to the dynamic binding capacities of a HIC column. Thus the influence of ionic strength on protein binding was investigated. The salt concentration in the buffer systems was adjusted to ionic strength values comparable to the reference buffer (0.55 M citrate pH 6.0).

Eqs. (2) and (3) were used to calculate the ionic strength. The citrate concentration in the buffers was then adjusted to get a value that closely matched the reference (ionic strength of 3.1 M). For the buffer containing the secondary salt sulfate, we have decided to adjust the secondary salt concentration to 0.5 M to match the secondary salt concentration of all dual salt systems. Since pH adjustment to pH 6.0 required the addition of significant amounts of NaOH, which, when taken into account, led to the new citrate concentrations and ionic strength values listed in Table 3.

4.4. Binding capacity in buffers with equal ionic strength

The DBC was studied with lysozyme, GFP, and mAb at sample concentrations of approx. 5 mg*ml^{-1} (Fig. 2). Dynamic binding capacities differ substantially between the mono- and dual salt systems (Table 4). For lysozyme and GFP, the breakthrough curves of dual salt systems group closer together. For mAb, dynamic binding capacities differ vastly depending on the secondary salt. Altogether, differences are less pronounced compared to the buffers of equal surface tension, especially in the case of lysozyme. All proteins exhibit the lowest binding capacity in the mono salt buffer 0.55 M

Table 2

Comparing capacities at 10 % BT for lysozyme, mAb, and GFP when solubilized in buffers sharing comparable surface tension. The DBC was determined for a residence time of 10 min. Differences between the lowest and highest binding capacities are shown, where either all buffers or only dual salt buffers are compared to each other.

Buffer	Buffer Surface tension [mN*m^{-1}]	DBC$_{10\%}$ for lysozyme [mg*ml^{-1}]	DBC$_{10\%}$ for mAb [mg*ml^{-1}]
0.55 M Citrate	73.5	7	8
0.55 M Citrate + 0.50 M Acetate	73.4	23	21
0.35 M Citrate + 0.50 M Phosphate	74.3	12	17
0.55 M Citrate + 0.30 M Sulfate	73.7	21	22
Highest difference, all systems [%]	-	70	64
Highest difference, dual salt systems only [%]	-	48	23

Table 3

New citrate concentrations calculated to achieve dual salt systems sharing the same ionic strength considering the citrate buffer as a reference (3.1 M).

Buffer	Citrate concentration [M]	Ionic strength after pH adjustment [M]
0.55 M Citrate		3.1
Citrate + 0.50 M Acetate	0.463	2.9
Citrate + 0.50 M Phosphate	0.441	2.8
Citrate + 0.50 M Sulfate	0.329	2.8
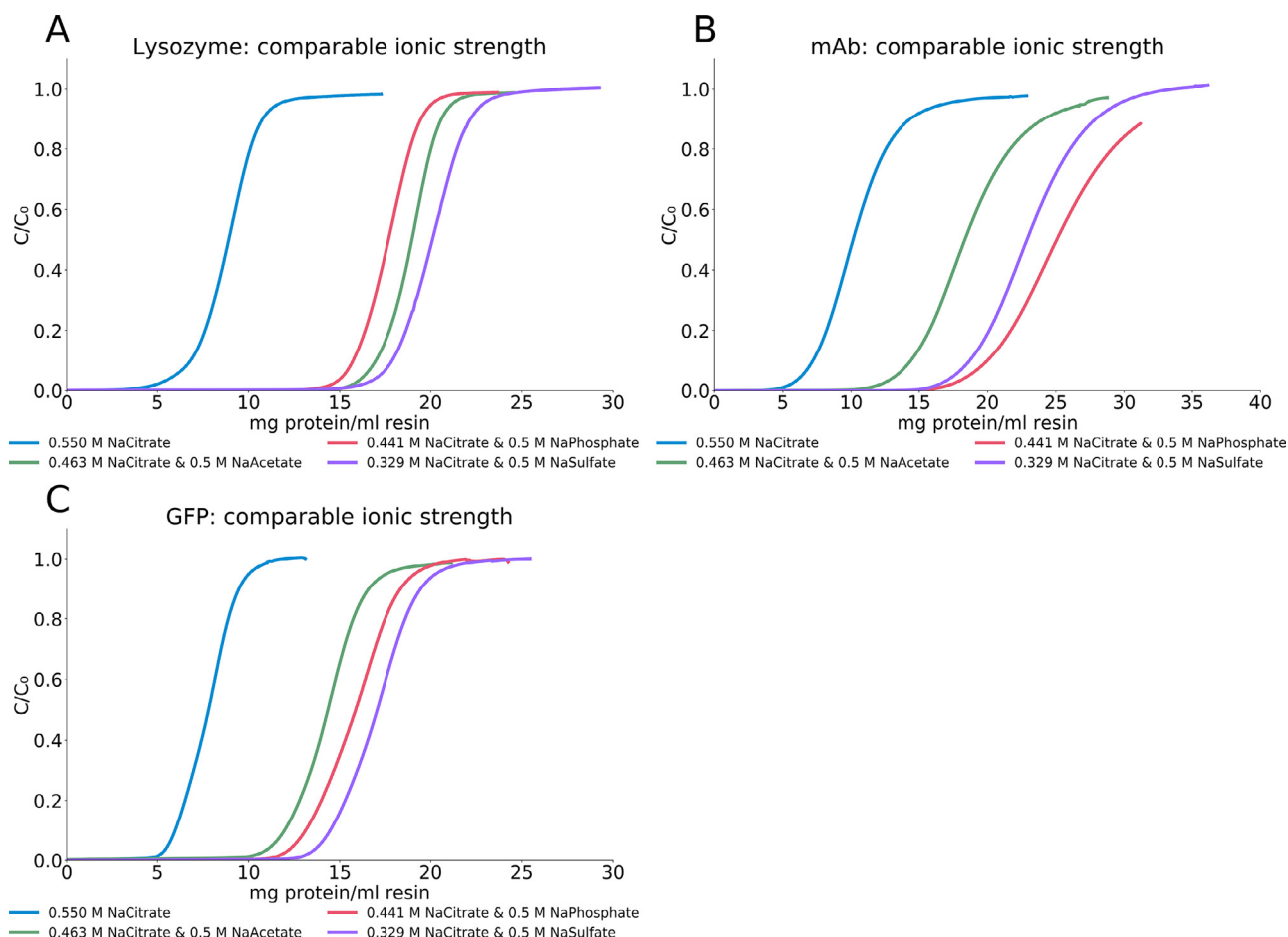
Fig. 2. Breakthrough curves for lysozyme (A, top left), mAb (B, top right) and GFP (C, bottom left) at a sample concentration of approx. 5 mg*ml^{-1} using different buffer systems with matching ionic strength as the mobile phase and a TOYOPEARL Butyl-650 M HIC column. DBC was determined for a residence time of 10 min.

sodium citrate. The breakthrough curves with the secondary salt sulfate induce the highest dynamic binding capacities for lysozyme and GFP, whereas it ranks close second for mAb. Besides, it is difficult to deduce trends for the investigated systems, and further analytics are needed to gain better understanding of driving forces governing binding to the stationary phase.

4.5. Adsorption behavior, internal structure, protein-protein interactions, and binding topology in buffers with equal ionic strength

The breakthrough experiments showed that ionic strength seems to be the more decisive factor for the DBC. Nevertheless, ionic strength alone is not sufficiently describing the phenomenon. Therefore, we have conducted SAXS and adsorption isotherm ex-

Table 4

Comparing capacities at 10 % BT for lysozyme, mAb, and GFP when solubilized in buffers sharing comparable ionic strength. The DBC was determined for a residence time of 10 min. Differences between the lowest and highest binding capacities are shown, where either all buffers or only dual salt buffers are compared to each other.

Buffers	DBC$_{10\%}$ for lysozyme [mg*ml^{-1}]	DBC$_{10\%}$ for mAb [mg*ml^{-1}]	DBC$_{10\%}$ for GFP [mg*ml^{-1}]
0.55 M Citrate	7	8	6
0.463 M Citrate + 0.50 M Acetate	17	14	12
0.441 M Citrate + 0.50 M Phosphate	16	20	13
0.329 M Citrate + 0.50 M Sulfate	18	19	14
Highest difference, all systems [%]	61	60	57
Highest difference, dual salt systems only [%]	11	30	14

periments to investigate possible explanations for the differences in dynamic binding capacities. Firstly, we hypothesize that the protein structure could be altered in the respective buffer, resulting in either an expanded or collapsed conformation. This would then result in modulation of the protein's footprint on the chromatographic resin and therefore cause differences in the dynamic binding capacities. Alternatively, protein-protein interactions could be responsible for modulating the surface coverage, allowing closer packing when protein-protein interactions are attractive and looser packing when protein-protein interactions are repulsive, respectively. Moreover, attractive protein-protein interaction could trigger multilayer formation. In order to investigate the internal structure and intermolecular interactions, the model proteins were analyzed via SAXS. Furthermore, adsorption isotherms were performed to evaluate the impact of protein-protein interaction on protein adsorption. Lastly, the protein-resin adduct was analyzed using SAXS. The self-avoiding random walk model was fitted into the pair density distribution function. The resulting model parameters were analyzed to investigate the protein topology on the chromatographic resin.

4.5.1. SAXS: proteins in buffers of equal ionic strength

In Fig. 3, SAXS traces of the model proteins in the investigated mono and dual salt buffers are shown. Moreover, the theoretical scattering profile of PDB crystal structures 1dpx, 1hzh and 1gfl are depicted. Notably, the intermediary and high q-range of all SAXS curves (~ 0.4 nm^{-1} < q) are comparable to the crystal structure's theoretical scattering curve. However, noise increases substantially at q = 1.5 nm^{-1}, resulting in more significant deviations from the theoretical scattering curve. This is believed to be due to the high electronic contrast. Since SAXS traces are comparable between 0.4 and 1.5 nm^{-1}, real-space distances of 4.1-15.7 nm are accordingly (as their reciprocal relation is given by Eq. (17), which includes the intramolecular distances of mAb and GFP (D$_{max}$ mAb and GFP: 16.4 nm [37] and 7 nm [38]) but exceeds that of lysozyme (D$_{max}$ of lysozyme: 4.0 nm [39]). This indicates comparable intramolecular structures of mAb and GFP > 4.1 nm in all investigated buffer systems.

In the low q-range (q > 0.2 nm^{-1}), the scattering intensities differ substantially for mAb in different HIC buffers (Fig. 3 B). For lysozyme and GFP (Fig. 3 A & B), differences in the low q-range are observable but less pronounced. Generally, the low q-range is dominated by long-range correlations, indicating the respective buffer's modulation of protein-protein interactions. To classify whether the interactions are attractive or repulsive, the theoretical scattering profiles of the crystal structures of the corresponding model proteins were calculated and compared to the experimental data in the low q-range. Lysozyme shows attractive interactions (Fig. 3 A), whereas mAb shows both attractive, neutral and repulsive behavior, respectively (Fig. 3 B). For GFP, no or minor repulsive interactions can be observed in the respective mono or dual salt buffers. Trends towards attraction and repulsion correlate with the pI of the model protein: the acidic GFP (pI = 5.8 [30]) exhibits no or weak repulsive interactions, mAb (pI = 7.9-9.1 [29]) both
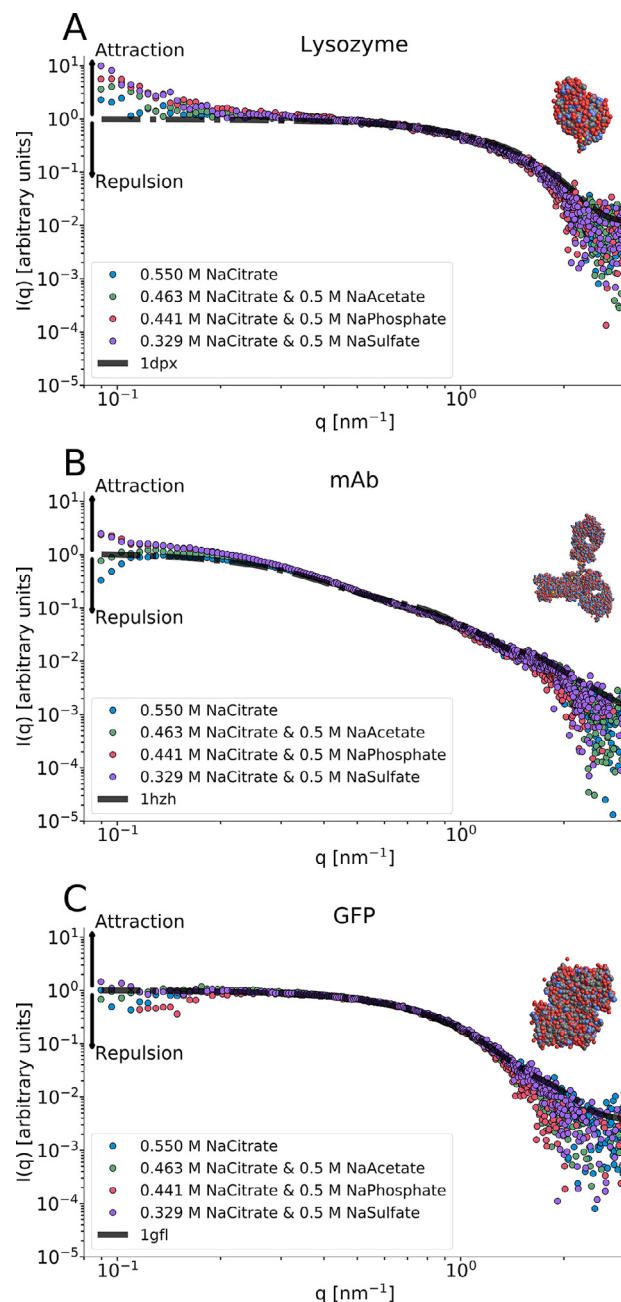
Fig. 3. SAXS profiles of lysozyme (A), the mAb (B), and GFP (C) in solution (5 mg*ml^{-1}). Attractive and repulsive categorizations are referred to as the theoretical scattering profile of the corresponding PDB. Respective PDBs are visualized in the top right corner for each protein.

pronounced attractive and repulsive interactions, respectively, and lysozyme (pI = 10.7 [28]) are dominated by attractive interactions in the dual salt buffers.

The attractivity (and vice versa repulsion) induced by the secondary salt follows a trend: the presence of divalent anions (SO_4^{2-} and HPO_4^{2-}) induce the highest attractive/lowest repulsive forces followed by the monovalent acetate anion. This trend is in line with the Hofmeister series [13]. The mono- and dual salt system's comparison reveals inconsistencies with the Hofmeister series: at pH 6, $citrate^{2-}$ and $citrate^{3-}$ are the predominant anion species in aqueous solution [40] and rather kosmotropic anions. ($citrate^{3-}$ > SO_4^{2-} > HPO_4^{2-} > $citrate^{2-}$ > CH_3COO^- > $citrate^-$ [13,41,42]) However, the single salt sodium citrate buffer induces higher repulsive/lower attractive interactions than the citrate and acetate system.

Ultimately, the SAXS analysis of the proteins in the respective buffer indicates that the internal structure of mAb and GFP > 4.1 nm is comparable. Moreover, protein-protein interactions depend on the kosmotropic nature of the secondary anion and the pI of the protein. mAb systems generally span the broadest range of protein-protein interactions, ranging from the repulsive to the attractive regime. Lysozyme systems are strictly in the attractive regime, whereas GFP shows no to slightly repulsive interactions. Attractive interactions correlate with dynamic binding capacities, as highly attractive systems (such as the systems with the secondary salt sulfate) coincide with higher dynamic binding capacities. More repulsive systems (especially citrate alone) coincide with low dynamic binding capacities. For mAb, both the variations in dynamic binding capacity (30 % for mAb's dual salt systems compared to 11–14 % for GFP and lysozyme, as seen in Table 4) and protein-protein interactions are high (Fig. 3), whereas they are smaller for the other two proteins. The single salt system 0.550 M citrate shows an interesting behavior. Judging from the protein-protein interaction data alone, we would postulate generally lower binding capacities than the dual salt system, as the citrate system is rather repulsive (Fig. 3). However, the difference for citrate alone to the system with the highest binding capacity is 57–61 %, but the difference between the lowest and highest binding capacity ranges from 11–30 % for the dual salt systems (Table 4). Although we only have a qualitative measure for protein-protein interactions at hand, this vast difference cannot be explained in the protein-protein interaction analysis (Fig. 3). This underlines the need for a quantitative comparison of protein-protein interactions and dynamic binding capacities.

Altogether, we hypothesize that protein-protein interactions could explain high dynamic binding capacities and play a crucial role in protein adsorption. In the following section, we will focus on the implications of protein-protein interactions in protein adsorption in general and investigate whether the binding mode of the protein is influenced.

4.5.2. Isotherms in buffers with equal ionic strength

Equivalent to the breakthrough curves (Fig. 2), adsorption isotherms were determined for the model proteins in mono- and dual salt buffers of equal ionic strength (Fig. 4). Generally, the ranking of the binding capacities in the adsorption isotherm experiments is comparable to the breakthrough curves for GFP and mAb. For lysozyme, however, this is not the case except for the mono salt buffer. The 0.55 M citrate buffer induces the lowest binding in the adsorption isotherms and breakthrough experiments.

As discussed above, most model proteins exhibit protein-protein interactions in the investigated systems, where GFP shows the weakest protein-protein interactions. Factoring in the protein-protein interactions from our SAXS analysis, Langmuir adsorption isotherm behavior is not expected for systems exhibiting protein-
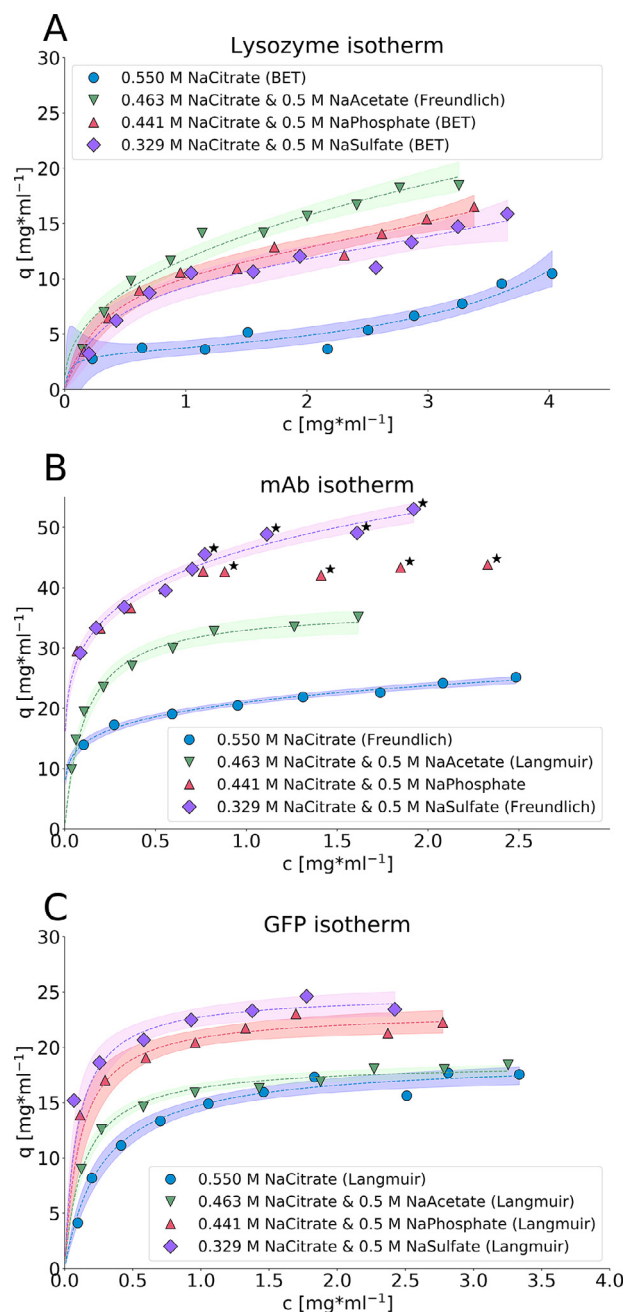
Fig. 4. Adsorption isotherms for lysozyme (A, top), mAb (B, middle), and GFP (C, bottom). A total volume of 250 μl was incubated for 24 h in 96 well plates at a slurry conc. of 10 % and 5 %, respectively. Data points where a resin concentration of 5 % where used are denoted with a star. 95 % confidence intervals are displayed in the corresponding color. Time effects were tested by reducing the incubation time to 3 h for the mAb in 0.441 M citrate & 0.5 M phosphate. As seen in Fig. S2, Supplementary Material, the difference between 3 and 24 h is small.

protein interactions, which is true for the majority of the experiments (Fig. 4).

When only the adsorption isotherm data is considered, the Langmuir model describes the GFP adsorption isotherms reasonably well (Fig. 4 A). Considering also the SAXS data; GFP in solution showed the lowest protein-protein interaction of all investigated model proteins. Only GFP in citrate and citrate plus phosphate shows weak repulsive protein-protein interaction (Fig. 3 C). Since the protein-protein interaction analysis here is only qualitative, it is challenging to state whether the measured protein-

protein interactions are high enough to diminish the model's validity or they can be neglected to allow for a good fit.

Adsorption isotherms of the mAb only follow Langmuir behavior when acetate is employed as a secondary salt (Fig. 4 B), which is in line with the protein-protein interaction data from the SAXS analytics (Fig. 3 B). When phosphate and sulfate are employed as secondary salts, a non-Langmuirian ascent can be observed that can be fitted well with the Freundlich isotherm. When phosphate is employed as a secondary salt, a non-Freundlich plateau is eventually reached, making both models unsuitable for the description of the isotherm. For the secondary salt sulfate, however, a plateau could not be reached. Here, we could not collect data at higher mobile phase concentrations due methodological limitations. Lastly, the 0.55 M citrate buffer induces the Freundlich type binding for mAb. This non-Langmuirian behavior is also in line with our protein-protein interaction data since the mAb is in the repulsive regime when 0.55 M citrate is used as a buffer.

The adsorption isotherm experiments with lysozyme reveal Freundlich and BET behavior, respectively (Fig. 4 A). For the lysozyme experiments, non-Langmuirian behavior is also in line with the SAXS data since a strictly attractive regime is observed for lysozyme in all investigated systems (Fig. 3 A). Adsorption isotherms that follow the BET model indicate multilayer formation, but it is unclear whether the multilayer forming interactions are reversible or irreversible.

Conclusively, we hypothesize that either the surface coverage is increased or multilayer formation does occur in systems that follow the Freundlich and BET isotherm model, respectively, being consistent with our protein-protein interaction data. However, it cannot be stated whether reversible self-association or irreversible aggregation occurs. Furthermore, GFP in citrate only and citrate plus phosphate could show pseudo-Langmuirian behavior or too little repulsive interaction to impact the protein adsorption.

4.5.3. SAXS: protein-resin adduct fitted via SARW model

For the analysis of the protein-resin adduct, the chromatographic resin was incubated for 15 h with either mAb, GFP or only buffer, respectively. The resin suspensions were measured via SAXS and a self-avoiding random walk model was fitted into the resulting pair density distribution function after inverse Fourier transform of the scattering data (Fig. S3, Supplementary Material). The resulting model parameters are presented in Fig. 5 A, as well as Fig. S4 (Supplementary Material).

Fig. 5 A shows that the excluded volume decreases when protein (GFP and mAb) is loaded onto the resin. When comparing the bound model protein's impact, the resulting excluded volume parameter is lower for resin incubated with mAb compared to GFP. Besides the impact of the loaded protein, the excluded volume parameter depends on the buffering system. For either model protein, the excluded volume parameter is significantly higher in the mono salt system (0.55 sodium citrate) than all other dual salt systems. Furthermore, the excluded volume parameter is lowest for systems incubated with the dual salt buffer citrate plus sulfate. This buffer results in a significantly lower excluded volume parameter compared to all others in mAb systems. Moreover, it induces a significantly lower excluded volume parameter for GFP systems compared to citrate alone and citrate plus acetate.

Altogether, the excluded volume parameter correlates inversely with the equilibrium binding capacity determined via the adsorption isotherms. This of course raises the question how protein adsorption could impact the excluded volume parameter of the adduct as a whole. Generally, the excluded volume parameter can be correlated with the accessible surface area, as the accessible surface area encompasses the excluded volume [43]. Therefore, we believe that the reduction of the excluded volume parameter can be best understood with the reduction of the accessible surface
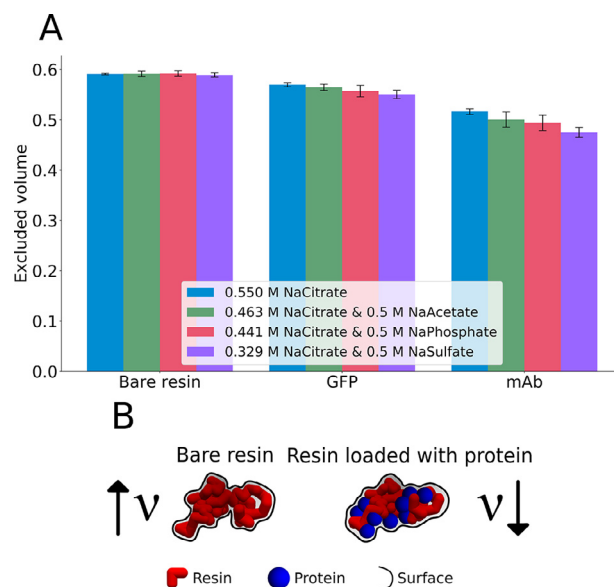
Fig. 5. A: Self-avoiding random walk (SARW) excluded volume parameter (ν) deduced from SAXS measurements of resin slurry (5 %) incubated with protein at 5 mg*ml^{-1} for 15 h. The average of three independent experiments is shown, including standard deviation. B: Conceptual visualization of the impact of protein binding on a SARW polymer. As proteins deposit in the cavities of the chromatographic resin, the excluded volume parameter (ν) of the protein-resin adduct decreases.

area. When a fractal object is considered, this is most likely caused by the deposition of the protein in the cavities of the chromatographic resin. Deposition of proteins in the cavities of the chromatographic resin would decrease overall accessible surface area (Fig. 5 B).

On the other hand, preferential binding of the protein to flat or convex regions of the chromatographic resin would increase the accessible surface area and, therefore, the excluded volume parameter of the whole object, which could not be observed. This curvature dependency was previously highlighted in a theoretical work [44]. There, concave hemicylindrical carbon nanotubes were simulated in water, and they were more hydrophobic than their convex counterpart. When we now also consider the SAXS analytics of the proteins in solution, buffer-dependent protein-protein interactions could play a role in the topology of the protein-resin adduct. Protein-protein interactions could lead to increased deposition onto already occupied cavities and decreased surface coverage due to repulsion, respectively. Altogether, we believe that the excluded volume parameter decreases due to the deposition of the protein in the cavities of the chromatographic resin. Nevertheless, this hypothesis is only based on theoretical considerations and demands further validation.

Similarly, the path length of the resulting self-avoiding random walk increases when mAb and GFP are loaded onto the resin, whereas the increase is more pronounced for mAb than GFP. In contrast to the excluded volume parameters, only two buffering systems show significantly different path lengths, namely mAb incubated with citrate alone exhibited shorter path lengths than citrate plus sulfate (Fig. S4, Supplementary Material).

5. Conclusion

The ionic strength of dual salt HIC buffers is a more decisive parameter for dynamic binding capacities than their surface tension. However, dynamic binding capacities still differ up to 30 % depending on the secondary salt employed, and the model protein used, even with comparable ionic strength of the buffering systems. To gain better mechanistic insight into dual salt systems in HIC, SAXS

analytics have been used to investigate the model proteins in the respective dual salt systems alone and when bound to the chromatographic resin.

We conclude that protein-protein interactions increase surface coverage for mAb and trigger multilayer formation for lysozyme, as the adsorption isotherms show a deviation from Langmuirian behavior, respectively. Protein-protein interactions are modulated in general agreement with the Hofmeister series and the pI of the model protein. The excluded volume parameter correlates with the maximum isotherm binding capacities. We hypothesize that the decrease of the excluded volume parameter is caused by the deposition of proteins in the cavities of the chromatographic resin. Furthermore, we postulate that attractive protein-protein interactions can enhance deposition in said cavities, as it allows closer packing due to the formation of attractive clusters and multilayers, respectively.

The protein's internal structure is not responsible for the increased binding capacity. The internal solution structure of mAb and GFP at distances > 4.1 nm is comparable in the investigated buffers, suggesting unaltered protein conformation.

Declaration of Competing Interest

The authors declare that they have no known competing financial interests or personal relationships that could have appeared to influence the work reported in this paper.

CRediT authorship contribution statement

Leo A. Jakob: Conceptualization, Methodology, Formal analysis, Investigation, Data curation, Writing – original draft, Visualization. **Beate Beyer:** Conceptualization, Formal analysis, Investigation, Methodology, Writing – original draft. **Catarina Janeiro Ferreira:** Investigation, Writing – original draft. **Nico Lingg:** Methodology, Writing – review & editing. **Alois Jungbauer:** Conceptualization, Writing – review & editing, Supervision, Project administration. **Rupert Tscheließnig:** Conceptualization, Formal analysis, Writing – review & editing, Supervision.

Acknowledgments

Supplementary materials

Supplementary material associated with this article can be found, in the online version, at doi:10.1016/j.chroma.2021.462231.

References

[1] A.M. Senczuk, R. Klinke, T. Arakawa, G. Vedantham, Y. Yigzaw, Hydrophobic interaction chromatography in dual salt system increases protein binding capacity, Biotechnol. Bioeng. 103 (5) (2009) 930–935, doi:10.1002/bit.22313.

[2] E. Müller, J. Vajda, D. Josic, T. Schröder, R. Dabre, T. Frey, Mixed electrolytes in hydrophobic interaction chromatography, J. Sep. Sci. 36 (8) (2013) 1327–1334, doi:10.1002/jssc.201200704.

[3] K. Baumgartner, S. Amrhein, A. Oelmeier Stefan, J. Hubbuch, The influence of mixed salts on the capacity of HIC adsorbers: a predictive correlation to the surface tension and the aggregation temperature, Biotechnol. Prog. 32 (2) (2015) 346–354, doi:10.1002/btpr.2166.

[4] A. Werner, H. Hasse, Experimental study and modeling of the influence of mixed electrolytes on adsorption of macromolecules on a hydrophobic resin, J. Chromatogr. A 1315 (2013) 135–144, doi:10.1016/j.chroma.2013.09.071.

[5] E. Hackemann, H. Hasse, Influence of mixed electrolytes and pH on adsorption of bovine serum albumin in hydrophobic interaction chromatography, J. Chromatogr. A 1521 (2017) 73–79, doi:10.1016/j.chroma.2017.09.024.

[6] C. Horváth, W. Melander, I. Molnár, Solvophobic interactions in liquid chromatography with nonpolar stationary phases, J. Chromatogr. (125) (1976) 129–156.

[7] I. Molnár, Searching for robust HPLC methods – CSABA Horváth and the Solvophobic theory, Chromatographia 62 (13) (2005) s7–s17, doi:10.1365/s10337-005-0645-1.

[8] M.E. Lienqueo, A. Mahn, J.C. Salgado, J.A. Asenjo, Current insights on protein behaviour in hydrophobic interaction chromatography, J. Chromatogr. B Analyt Technol. Biomed. Life Sci. 849 (1-2) (2007) 53–68, doi:10.1016/j.jchromb.2006.11.019.

[9] M. Baca, J. De Vos, G. Bruylants, K. Bartik, X. Liu, K. Cook, S. Eeltink, A comprehensive study to protein retention in hydrophobic interaction chromatography, J. Chromatogr. B Analyt. Technol. Biomed. Life Sci. 1032 (2016) 182–188, doi:10.1016/j.jchromb.2016.05.012.

[10] R. Majumdar, P. Manikwar, J.M. Hickey, H.S. Samra, H.A. Sathish, S.M. Bishop, C.R. Middaugh, D.B. Volkin, D.D. Weis, Effects of salts from the Hofmeister series on the conformational stability, aggregation propensity, and local flexibility of an IgG1 monoclonal antibody, Biochemistry 52 (19) (2013) 3376–3389, doi:10.1021/bi400232p.

[11] A.Y. Xu, M.M. Castellanos, K. Mattison, S. Krueger, J.E. Curtis, Studying excipient modulated physical stability and viscosity of monoclonal antibody formulations using small-angle scattering, Mol. Pharm. 16 (10) (2019) 4319–4338, doi:10.1021/acs.molpharmaceut.9b00687.

[12] B.J. Dear, J.A. Bollinger, A. Chowdhury, J.J. Hung, L.R. Wilks, C.A. Karouta, K. Ramachandran, T.Y. Shay, M.P. Nieto, A. Sharma, J.K. Cheung, D. Nykypanchuk, P.D. Godfrin, K.P. Johnston, T.M. Truskett, X-ray scattering and coarse-grained simulations for clustering and interactions of monoclonal antibodies at high concentrations, J. Phys. Chem. B 123 (25) (2019) 5274–5290, doi:10.1021/acs.jpcb.9b04478.

[13] C.P. Schneider, D. Shukla, B.L. Trout, Arginine and the Hofmeister Series: the role of ion-ion interactions in protein aggregation suppression, J. Phys. Chem. B 115 (22) (2011) 7447–7458, doi:10.1021/jp111920y.

[14] O. Matsarskaia, F. Roosen-Runge, G. Lotze, J. Moller, A. Mariani, F. Zhang, F. Schreiber, Tuning phase transitions of aqueous protein solutions by multivalent cations, Phys. Chem. Chem. Phys. PCCP 20 (42) (2018) 27214–27225, doi:10.1039/c8cp05884a.

[15] J. Chen, S.M. Cramer, Protein adsorption isotherm behavior in hydrophobic interaction chromatography, J. Chromatogr. A 1165 (1-2) (2007) 67–77, doi:10.1016/j.chroma.2007.07.038.

[16] A.P. Minton, Effects of excluded surface area and Adsorbate clustering on surface adsorption of proteins. II. Kinetic models, Biophys. J. 80 (4) (2001) 1641–1648, doi:10.1016/S0006-3495(01)76136-X.

[17] B.B. Langdon, M. Kastantin, R. Walder, D.K. Schwartz, Interfacial protein-protein associations, Biomacromolecules 15 (1) (2014) 66–74, doi:10.1021/bm401302v.

[18] R.A. Latour, The Langmuir isotherm: a commonly applied but misleading approach for the analysis of protein adsorption behavior, J. Biomed. Mater Res. A 103 (3) (2015) 949–958, doi:10.1002/jbm.a.35235.

[19] Q. Meng, J. Wang, G. Ma, Z. Su, Isotherm type shift of hydrophobic interaction adsorption and its effect on chromatographic behavior, J. Chromatogr. Sci. 51 (2) (2013) 173–180, doi:10.1093/chromsci/bms123.

[20] A. Ebadi, J.S. Soltan Mohammadzadeh, A. Khudiev, What is the correct form of BET isotherm for modeling liquid phase adsorption? Adsorption 15 (1) (2009) 65–73, doi:10.1007/s10450-009-9151-3.

[21] S. Brunauer, P.H. Emmett, E. Teller, Adsorption of Gases in Multimolecular Layers, J. Am. Chem. Soc. 60 (2) (1938) 309–319, doi:10.1021/ja01269a023.

[22] N. Codina, D. Hilton, C. Zhang, N. Chakroun, S.S. Ahmad, S.J. Perkins, P.A. Dalby, An expanded conformation of an antibody fab region by X-Ray scattering, molecular dynamics, and smfret identifies an aggregation mechanism, J. Mol. Biol. 431 (7) (2019) 1409–1425, doi:10.1016/j.jmb.2019.02.009.

[23] M.C. Thompson, B.A. Barad, A.M. Wolff, H. Sun Cho, F. Schotte, D.M.C. Schwarz, P. Anfinrud, J.S. Fraser, Temperature-jump solution X-ray scattering reveals distinct motions in a dynamic enzyme, Nat Chem. (2019), doi:10.1038/s41557-019-0329-3.

[24] J. Plewka, G.L. Silva, R. Tscheliessnig, H. Rennhofer, C. Dias-Cabral, A. Jungbauer, H.C. Lichtenegger, Antibody adsorption in protein-A affinity chromatography - *in situ* measurement of nanoscale structure by small-angle X-ray scattering, J. Sep. Sci. 41 (22) (2018) 4122–4132, doi:10.1002/jssc.201800776.

[25] G.L. Silva, J. Plewka, H. Lichtenegger, A.C. Dias-Cabral, A. Jungbauer, R. Tscheliessnig, The pearl necklace model in protein a chromatography: molecular mechanisms at the resin interface, Biotechnol. Bioeng. 116 (1) (2019) 76–86, doi:10.1002/bit.26843.

[26] B. Hammouda, Small-angle scattering from branched polymers, Macromol. Theory Simul. 21 (6) (2012) 372–381, doi:10.1002/mats.201100111.

[27] R. Haider, B. Sartori, A. Radeticchio, M. Wolf, S. Dal Zilio, B. Marmiroli, H. Amenitsch, μDrop: a system for high-throughput small-angle X-ray scat-

tering measurements of microlitre samples, J. Appl. Crystallogr. 54 (1) (2021), doi:10.1107/s1600576720014788.

[28] T. Sakaguchi, T. Wada, T. Kasai, T. Shiratori, Y. Minami, Y. Shimada, Y. Otsuka, K. Komatsu, S. Goto, Effects of ionic and reductive atmosphere on the conformational rearrangement in hen egg white lysozyme prior to amyloid formation, Colloids Surf B Biointerf. 190 (2020) 110845, doi:10.1016/j.colsurfb.2020.110845.

[29] L. Magnenat, A. Palmese, C. Fremaux, F. D'Amici, M. Terlizzese, M. Rossi, L. Chevalet, Demonstration of physicochemical and functional similarity between the proposed biosimilar adalimumab MSB11022 and Humira(R), MAbs 9 (1) (2017) 127–139, doi:10.1080/19420862.2016.1259046.

[30] A.M. dos Santos, Thermal effect on Aequorea green fluorescent protein anionic and neutral chromophore forms fluorescence, J. Fluoresc 22 (1) (2012) 151–154, doi:10.1007/s10895-011-0941-0.

[31] W. Wang, S. Singh, D.L. Zeng, K. King, S. Nema, Antibody structure, instability, and formulation, J. Pharm. Sci. 96 (1) (2007) 1–26, doi:10.1002/jps.20727.

[32] B.H. Zimm, The Scattering of Light and the Radial Distribution Function of High Polymer Solutions, J. Chem. Phys. 16 (12) (1948) 1093–1099, doi:10.1063/1.1746738.

[33] G. Beaucage, Determination of branch fraction and minimum dimension of mass-fractal aggregates, Phys. Rev. E 70 (3) (2004) 031401, doi:10.1103/PhysRevE.70.031401.

[34] M.A. Blanco, H.W. Hatch, J.E. Curtis, V.K. Shen, Evaluating the effects of hinge flexibility on the solution structure of antibodies at concentrated conditions, J. Pharm. Sci. 108 (5) (2019) 1663–1674, doi:10.1016/j.xphs.2018.12.013.

[35] O. Glatter, A new method for the evaluation of small-angle scattering data, J. Appl. Crystallogr. 10 (5) (1977) 415–421, doi:10.1107/S0021889877013879.

[36] J.W. Gibbs, THE COLLECTED WORKS OF J. Willard Gibbs, Yale University Press, New Haven, 1948.

[37] C.R. Mosbaek, P.V. Konarev, D.I. Svergun, C. Rischel, B. Vestergaard, High concentration formulation studies of an IgG2 antibody using small angle X-ray scattering, Pharm. Res. 29 (8) (2012) 2225–2235, doi:10.1007/s11095-012-0751-3.

[38] D.P. Myatt, L. Hatter, S.E. Rogers, A.E. Terry, L.A. Clifton, Monomeric green fluorescent protein as a protein standard for small angle scattering, Biomed. Spectrosc. Imaging 6 (3-4) (2017) 123–134, doi:10.3233/bsi-170167.

[39] C. Kulsing, A.Z. Komaromy, R.I. Boysen, M.T. Hearn, On-line determination by small angle X-ray scattering of the shape of hen egg white lysozyme immediately following elution from a hydrophobic interaction chromatography column, Analyst 141 (20) (2016) 5810–5814, doi:10.1039/c6an00851h.

[40] C. Gervais, C.A. Grissom, N. Little, M.J. Wachowiak, Cleaning marble with ammonium citrate, Stud. Conserv. 55 (3) (2013) 164–176, doi:10.1179/sic.2010.55.3.164.

[41] C. Drummond, L. Pérez-Fuentes, D. Bastos-González, Can polyoxometalates Be considered as superchaotropic ions? J. Phys. Chem. C 123 (47) (2019) 28744–28752, doi:10.1021/acs.jpcc.9b08324.

[42] F. Hofmeister, Zur Lehre von der Wirkung der Salze, Archiv für experimentelle Pathologie und Pharmakologie 24 (4) (1888) 247–260, doi:10.1007/BF01918191.

[43] T.J. Richmond, Solvent accessible surface area and excluded volume in proteins: Analytical equations for overlapping spheres and implications for the hydrophobic effect, J. Mol. Biol. 178 (1) (1984) 63–89, doi:10.1016/0022-2836(84)90231-6.

[44] E. Xi, V. Venkateshwaran, L. Li, N. Rego, A.J. Patel, S. Garde, Hydrophobicity of proteins and nanostructured solutes is governed by topographical and chemical context, Proc. Natl. Acad. Sci. USA 114 (51) (2017) 13345–13350, doi:10.1073/pnas.1700092114.

Taylor & Francis
Taylor & Francis Group

∂ OPEN ACCESS   Check for updates

Increase in cysteine-mediated multimerization under attractive protein–protein interactions

Leo A. Jakob[a], Tomás Mesurado[a], Alois Jungbauer[a,b] (iD), and Nico Lingg[a,b] (iD)

[a]Department of Biotechnology, Institute of Bioprocess Science and Engineering, University of Natural Resources and Life Sciences, Vienna, Austria; [b]Austrian Centre of Industrial Biotechnology, Vienna, Austria

ABSTRACT

The CASPON enzyme became an interesting enzyme for fusion protein processing because it generates an authentic N-terminus. However, the high cysteine content of the CASPON enzyme may induce aggregation via disulfide-bond formation, which can reduce enzymatic activity and be considered a critical quality attribute. Different multimerization states of the CASPON enzyme were isolated by preparative size exclusion chromatography and analyzed with respect to multimerization propensity and enzymatic activity. The impact of co-solutes on multimerization was studied in solution and in adsorbed state. Furthermore, protein–protein interactions in the presence of different co-solutes were measured by self-interaction chromatography and were then correlated to the multimerization propensity. The dimer was the most stable and active species with 50% higher enzymatic activity than the tetramer. Multimerization was mainly governed by a cysteine-mediated pathway, as indicated by DTT-induced reduction of most caspase multimers. In the presence of ammonium sulfate, attractive protein–protein interactions were consistent with those observed for higher multimerization when the cysteine-mediated pathway was followed. Multimerization was also observed under attractive conditions on a chromatographic stationary phase. These findings corroborate common rules to perform protein purification with low residence time to avoid disulfide bond formation and conformational change of the protein upon adsorption.

Introduction

Circularly permuted caspase-2, in particular CASPON enzyme, became a potentially interesting industrial enzyme for fusion protein processing.[1–3] This cysteine-dependent protease is the essential element of a platform process for the production of recombinant proteins.[3] The CASPON enzyme is a mutant of human caspase-2 (wtCasp2)[1,4] and exhibits increased enzymatic activity as well as manufacturability compared to wtCasp2.[1,2,5] The high manufacturability of the CASPON enzyme is partially due to the use of a solubility tag.[2] Figure 1 shows the wtCasp2 crystal structure (Figure 1(A), PDB accession number: 1PYO)[4] and an AlphaFold prediction of the CASPON enzyme structure (Figure 1(B & C)).[6–8] The most notable difference is the large, relatively unstructured solubility tag of the CASPON enzyme (Figure 1(C)). The core is structurally similar to wtCasp2, differing in only four amino acids.[1]

Human caspases are commonly active as dimers of heterodimers (Figure 1(A)). The multimerization state of the CASPON enzyme is expected to be dimeric due to circular permutation of the heterodimers into a single chain (Figure 1(B & C)).[9] As the CASPON enzyme dimer

contains 26 cysteines, cysteine-mediated multimerization may cause product loss during manufacturing as previously reported for other cysteine-bearing proteins.[10–12] The CASPON enzyme contains six free, exposed cysteine residues on its surface (Figure 1(C)).[4] These exposed cysteine residues can potentially form intermolecular disulfide bridges to caspase molecules and other cysteine-bearing molecules alike, resulting in the formation of multimers or aggregates. Moreover, since caspases are cysteine-dependent aspartate-directed proteases, the oxidation state of the cysteine in the active site critical to the enzymatic activity. Generally, solubility of large solutes, such as multimers, is decreased due to increased free energy of cavity formation.[13,14] Thus, the question arises whether cysteine-mediated multimerization and disulfide bond-based aggregates are a critical quality attribute for the CASPON enzyme.

Contrary to aggregation due to protein unfolding,[15–17] cysteine-mediated aggregation may not result in changes to the protein tertiary structure.[18] As a result, the native fold and enzymatic activity can be maintained. This also means that disulfide-linked multimers or aggregates can be reduced to their smallest functional multimerization state using reducing agents
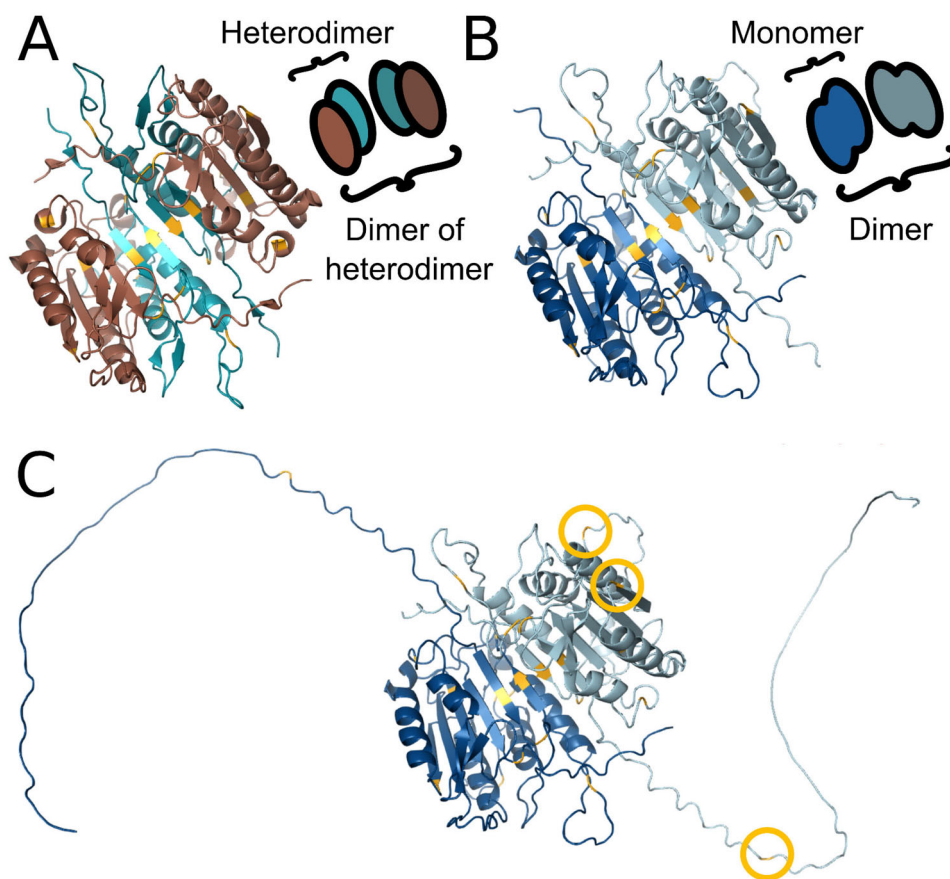
Figure 1. Comparison of the wtCasp2 crystal structure and an AlphaFold prediction of the CASPON enzyme including a cartoon representation of both proteins. Cysteine residues are marked in yellow. A: wtCasp2 (PDB accession: 1PYO). Small p12 subunits are depicted in teal, large p19 subunits are depicted in brown. B & C: AlphaFold prediction of the CASPON enzyme (panel C shows a zoomed view). CASPON enzyme monomers are marked dark blue and light blue, surface exposed cysteines of one monomer are circled in yellow.

such as dithiothreitol (DTT).[19,20] Therefore, protein aggregation through the cysteine-mediated pathway can be reversed during the manufacturing process or before use. Nonetheless, proteins recovered by reversing disulfide-linked multimerization may have lower product quality as native disulfide bonds may undergo chemical modifications such as β-elimination.[21,22]

Disulfide bond formation is a highly pH-dependent process due to higher nucleophilicity of cysteines' deprotonated thiolates.[23,24] Hence, conditions favoring the formation of aberrant disulfide bonds should be avoided when processing cysteine bearing peptides or proteins, that is, incubation of cysteine-bearing proteins above pH 7. In many bioprocesses, however, slightly basic conditions are prerequisites for numerous unit operations such as the purification of polyhistidine-tag bearing proteins using immobilized metal ion affinity chromatography (IMAC) and the purification of proteins with an isoelectric point in the neutral range using anion-exchange chromatography (AEX).

Co-solutes, such as ions, can induce attractive and repulsive protein–protein interactions,[25,26] potentially increasing spatial proximity of thiol moieties[24] and therefore cause multimerization. As proteins can reversibly associate under attractive conditions, the residence time and orientation of such reversible multimers dictate spatial proximity and residence time of intermolecular thiol/thiolate pairs. Therefore, protein-protein interactions can have a substantial impact on cysteine-mediated multimerization. Chaotropic salts such as guanidium

hydrochloride can cause aggregation by simultaneously destabilizing the tertiary and quaternary structures.[15,16]

The analysis of the aggregation state of a protein can be achieved by several techniques.[27–30] While native gel electrophoresis allows separation of proteins with different sizes, accurate determination of the size and quantity is difficult.[31] Sodium dodecylsulfate polyacrylamide gel electrophoresis (SDS-PAGE), on the other hand, is not suitable for the analysis of non-covalent aggregates due to the denaturing conditions used. SDS-PAGE may also have additional complications when analyzing proteins with high cysteine contents. For example, traces of oxidizing compounds can induce disulfide-bond formation and therefore obscure the native aggregation state.[32] High-performance size exclusion chromatography (HP-SEC) is the standard technique[30] that offers several advantages: elution of the protein in its native form and the possibility of integration with a multi-angle light scattering (MALS) detector, allowing determination of the molar mass irrespective of the shape of the protein.[31,33]

In this work, we studied the multimerization of CASPON enzyme, as well as the stability and enzymatic activity of its multimerization variants. Isolated CASPON enzyme species were characterized with respect to their molecular weight and enzymatic activity. The most stable and active species was exposed to a kosmotropic, neutral, as well as a chaotropic salt and its multimerization state was monitored over

time via HP-SEC. Multimerization rates were correlated to protein-protein interactions obtained by self-interaction chromatography experiments. Moreover, we investigated the difference between multimerization in the liquid phase versus in a chromatographic solid phase to elucidate the possible origin of CASPON enzyme multimerization variants. Overall, this study aims to assess whether multimerization is a critical quality attribute for the investigated protein in downstream processing, formulation and application as an industrial protease. In the broader context, this study can provide guidance in the manufacturing, formulation, and the of application of cysteine-bearing proteins.

Materials and methods

Buffer preparation

All employed chemicals were obtained from Merck KGaA (USA). pH of all buffers was adjusted using either 10 M NaOH or 25% HCl to achieve the desired pH value with a maximum deviation of ± 0.05. Phosphate buffered saline (PBS) used as a reference buffer contained 20 mM Na_2HPO_4 and 150 mM NaCl at pH 7. When investigating the impact of different salts on the multimerization behavior of the CASPON enzyme, solutions were buffered with 60 mM Na_2HPO_4.

Model protein: the CASPON enzyme

The model protein, the CASPON enzyme, was produced in-house. After expression of the protein in *E. coli*, a two-step purification process was applied. The purification procedure has been adapted from Lingg et al.[1] We have employed an additional SEC polishing step on an ÄKTA pure system (Cytiva, Sweden). Parameters of the SEC are shown in the supplementary materials (Table S1). For the preparation of CASPON enzyme dimer, SEC polishing loads were incubated for 15 min with either 25 mM TCEP or 25 mM DTT to maximize yield. After SEC polishing, the protein solution was either directly employed or further concentrated to up to 18 mg*ml^{-1} using Amicon Ultra-15 centrifugation tubes (Merck Millipore, USA) with a 10 kDa cutoff. The former preparation was used for the investigation of CASPON enzyme's multimerization behavior and the latter for further analysis of multimerization mechanisms, SIC experiments and the chromatographic binding experiments. For analysis of individual CASPON enzyme species, fractions at peak maximum (as indicated by 280 nm absorbance) were used. Extinction coefficients are 15.6 and 0.557 ml*mg^{-1}*cm^{-1} at 214 and 280 nm, respectively.

HP-SEC

A detailed description of HP-SEC parameters can be found in the supplementary materials (Table S2). In brief, a TSKgel G3000 SWXL analytical column was used at a flowrate of 0.4 ml*min^{-1} for all samples that did not contain imidazole. For imidazole containing samples, a Superdex 200 Increase 10/300 GL (Cytiva, Sweden) was used at a

flowrate of 0.5 ml*min^{-1}. For the determination of molar mass, MALS was performed on a DAWN HELEOS (Wyatt, USA) and analyzed with the ASTRA software (Wyatt, USA). Samples were filtered with a 0.22 µm filter prior to all injections and injection volume was 100 µl. Absorbance at 214 as well as at 280 nm were monitored depending on the concentration of the analyzed CASPON enzymes species.

FRET activity assay

A FRET assay was used for the determination of proteolytic enzymatic activity of the CASPON enzyme. The procedure was already described in literature [5]. In brief, 1 µM CASPON enzyme was incubated with 75 µM Abz-VDVAD↓SA-Dap(Dnp) (Bachem AG, Germany). Fluorescence was measured on an Infinite M200 Pro plate reader (Tecan Group AG, Switzerland) and the reaction buffer was 50 mM HEPES, 150 mM NaCl, pH 7.2. The initial slope of the fluorescence signal (excitation: 320 nm, emission 420 nm, gain: 110) was measured and enzymatic activity was calculated based on the slope of CASPON enzyme standards. Enzymatic activity units (U/g) correspond to the catalysis of 1 µmol substrate per minute and gram of the CASPON enzyme.

Multimerization in the presence of co-solutes

For analysis of the CASPON enzyme dimer multimerization over 7 days, two-fold stock solutions of buffers were used to achieve the desired salt concentration after 1:2 dilution, resulting in a protein concentration of 1 mg*ml^{-1}. After sample preparation, samples were incubated on a thermomixer (Thermo Fisher Scientific, USA) at 300 rpm at either 4 or 25 °C, whereas the impact of the shaking frequency was not investigated. After incubation, samples were directly analyzed via HP-SEC. Due to the long analysis time of HP-SEC and overall variability of the absorbance signal in the HP-SEC analysis, the relative content of the different species instead of the concentration of each species was compared between the co-solute conditions. Dimer depletion rates were calculated based on the decrease of dimer content over time, in which the decrease over 7 days were used for all conditions except for ammonium sulfate. For ammonium sulfate, rates were calculated at different time points at which 30-50% of dimer could still be detected. For testing reducibility of CASPON enzyme multimers that were formed either in the presence of ammonium sulfate or guanidine, CASPON enzyme dimer preparations with a concentration of 14-18 mg*ml^{-1} were directly diluted to 1 mg*ml^{-1} in the corresponding buffer and incubated at room temperature for 168 hours. 50 mM DTT was added to the samples to investigate the reducibility of formed multimers, incubated for 15 min and then further diluted to 0.2 mg*ml^{-1} for HP-SEC analysis. As a reference, H_2O was added instead of DTT.

Self-interaction chromatography

The CASPON enzyme was immobilized on a prepacked 1 ml HiTrap NHS-Activated HP affinity column (Cytiva, Sweden). The detailed coupling procedure can be found in the supplementary materials.

After coupling the protein to the column, unbound protein was determined photometrically to calculate surface coverage. For calculation of the surface coverage, we have followed the same procedure as earlier reported in literature[30]. The CASPON enzyme's radius was estimated combining the Einstein-Stokes equation and the relation derived by Tyn and Gusek[31]:

$$r_h = \frac{9.2*10^{-8}}{M_W^{\frac{1}{3}}} \quad (1)$$

Considering the molar mass of the CASPON enzyme dimer of 70.626 kDa (which is equivalent to a r_h of 3.29 nm as determined by Equation 1) and a surface area of 43.7 m²*ml⁻¹[34], the immobilized protein content of 18.1 mg*ml⁻¹ is equivalent to a surface coverage of 12 %.

For each condition in the SIC experiments, 50 µl of CASPON enzyme with a concentration of 1.5 g*l⁻¹ were injected in triplicates on a 1220 Infinity LC (Agilent Technologies, USA) HPLC system at a residence time of 10 min. The column was operated at either room temperature or 0-4 °C. Throughout our experiments on the HPLC system, air was frequently entrapped in the system, leading to ripples in the UV signal. Since the entrapment could not be avoided, affected chromatograms were smoothed by applying a gaussian filter using Mathematica 12.1 (Wolfram Research, Inc., USA). Smoothed chromatograms are marked as such.

For analysis of the protein, absorbance at 280 nm was used, except for conditions with a retention time of >1.5 CV or low overall signal, in which case absorbance at 214 nm was used. Figures containing absorption data at 214 as well as 280 nm are normalized according to their corresponding extinction coefficient.

For the calculation of B_{22}, the partition coefficient of the protein under interactive ($K_{overall}$) and non-interacting condition (K_{SEC}) is needed. Generally, the partition coefficient is equivalent to the retention factor and is given by Equation 2:

$$K = \frac{V_R - V_0}{V_t - V_0} \quad (2)$$

Where V_R is there retention volume of the protein in the mobile phase, V_0 is the extra particle volume, and V_t is the total volume of the mobile phase.

B_{22} is calculated by the following Equation 3:

$$B_{22} = \frac{(K_{SEC} - K_{overall})V_i}{N*M_W} \quad (3)$$

where V_i is the intra-particle pore volume, N is the number of immobilized proteins, and M_w is molar mass of CASPON enzyme dimer (70.626 kDa). We assumed that the CASPON enzyme can access the entire mobile phase and therefore K_{SEC} was set to 1. For the calculation of V_0 and V_t, extraparticle porosity ε and particle porosity ε_P are assumed to be 0.30[35] and 0.84[34], respectively.

Multimerization in IMAC

IMAC Sepharose FastFlow (Cytiva, Sweden) 50% resin slurry was incubated with the same volume of 50 mM NiSO₄ (thus two-fold resin volume). After incubating the IMAC resin with Ni²⁺, the resin was kept in 20% ethanol for storage. For binding experiments, the slurry was washed with equilibration buffer, which was either 60 mM Na₂HPO₄, 1 M ammonium sulfate, 20 mM imidazole, pH 8 or 60 mM Na₂HPO₄, 1 M sodium chloride, 20 mM imidazole, pH 8. 20 mM imidazole was used to suppress unspecific binding. The CASPON enzyme dimer stock (17 mg*ml⁻¹) was diluted with equilibration buffer to achieve a protein concentration of 2.78 mg*ml⁻¹, which was further diluted to a final protein concentration of 2.5 mg*ml⁻¹ by addition of the 50% slurry. Final resin concentration was 5% and total volume was 200 µl. After addition of the chromatographic resin to the protein solution, the solution was incubated for 30 min on a tube rotator at 300 rpm (Antylia Scientific, USA) for binding. After removal of 100 µl of the supernatant, the mixture was washed two times with 700 µl equilibration buffer and then incubated without withdrawing the liquid from the second wash for 6 h on the tube rotator at 300 rpm. Finally, 750 µl of the supernatant were withdrawn and 200 µl of IMAC elution buffer (300 mM imidazole, 20 mM Na₂HPO₄, 300 mM NaCl) were added to the slurry to elute the bound protein. After filtration of the eluted protein, HP-SEC analysis was performed using Superdex 200 Increase as stated above. Each experimental condition was performed in triplicates.

Results & discussion

Caspon enzyme multimerization states: stability, enzymatic activity and reducibility

Figure 2(A) shows HP-SEC chromatograms of three independent CASPON enzyme preparations. A heterogenous size distribution of the product was observed in the SEC fingerprints. Suspected multimers were further isolated by preparative SEC (Figure 2(B)) and the fractions were subsequently analyzed with HP-SEC-MALS (Figure 2(C & D)). The HP-SEC-MALS analysis revealed that the main fraction consists of the CASPON enzyme dimer, since the molecular weight determined through light scattering was consistent with the theoretical molecular weight (experimental: 71,500 Da, theoretical: 70,626 Da, Figure 2(B & C)). Similarly, the CASPON enzyme tetramer could be identified (experimental: 143,000 Da, theoretical: 141,252 da, Figure 2(B & C)). Higher order multimers were also identified; however, they could not be resolved and showed a broad distribution of molar masses, indicating the presence of hexameric and higher forms of the CASPON enzyme (Figure 2(C)). Separation of higher order multimers could probably be achieved by HP-SEC columns with a larger
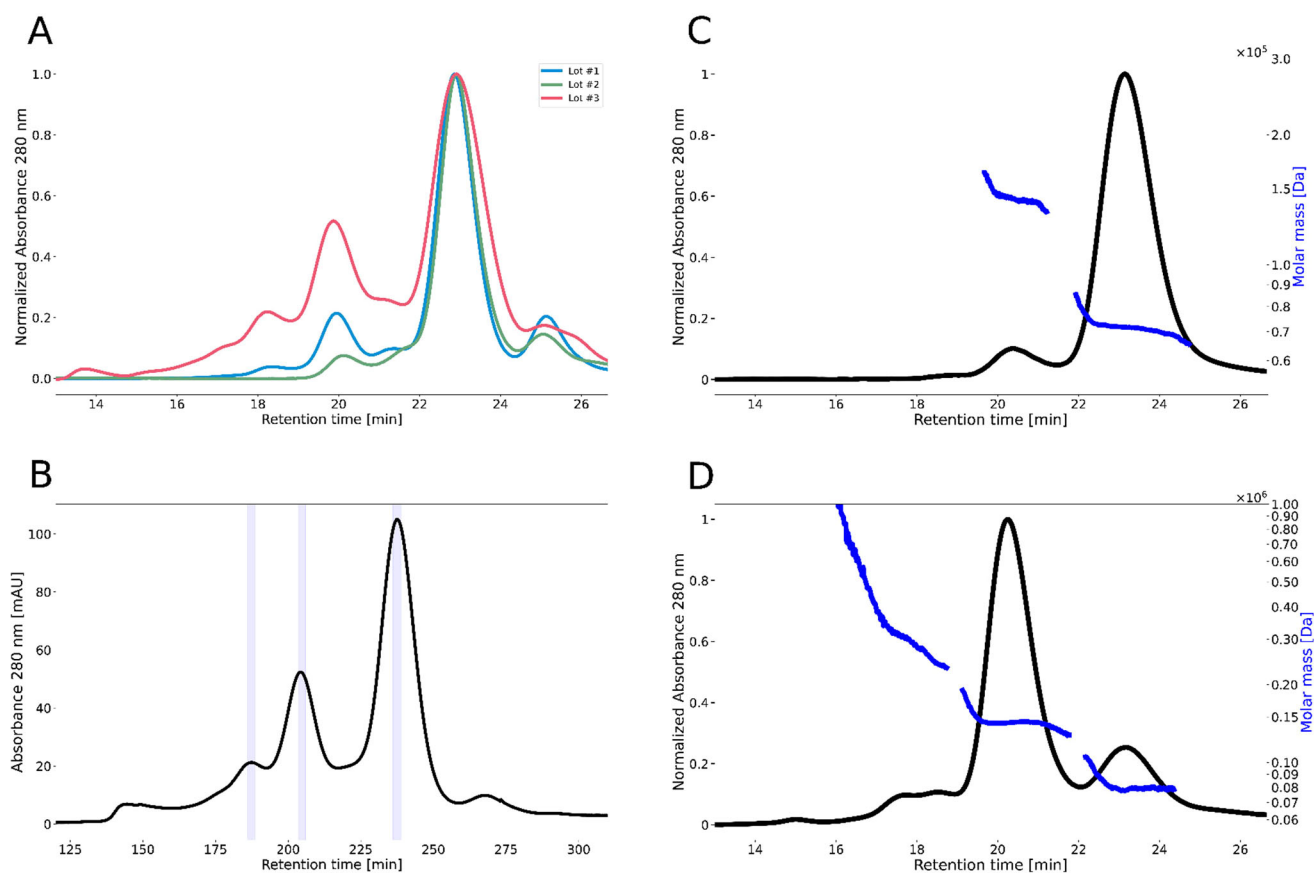
Figure 2. (A) HP-SEC chromatograms of different CASPON enzyme preparations. (B) Preparative SEC chromatogram. Highlighted areas (blue) of peak 1, 2 and 3 were fractionated and further analyzed. HP-SEC MALS of dimeric (C) and tetrameric (D) CASPON enzyme fraction corresponding to fractions 1 and 2 in preparative SEC, respectively. MW of different CASPON enzyme species shown in the HP-SEC-MALS analysis.

pore diameter. However, the focus of this study was on the dimeric species since it is the most active and hence most relevant multimerization state. For the isolated fractions, SDS-PAGE could not differentiate different size variants and showed mostly monomer with a minor dimer band (Figure S3, supplementary material).

To determine whether heterogeneous multimerization of the product affects product quality, CASPON enzyme dimers, tetramers, and the broad higher order multimer fractions were separated via preparative SEC. The resulting CASPON enzyme fractions were immediately transferred to 4 °C, stored at the initial elution concentration and analyzed for their enzymatic activity and stability over a time course of 48 h.

Figure 3(A) shows the time course of the multimerization state and the corresponding recovery. SEC profiles of the CASPON enzyme dimer do not change significantly over 48 h, whereas the multimer profiles of the tetramer fraction change significantly. After 48 h, residual dimeric and tetrameric CASPON enzyme in the mainly tetrameric fraction multimerized to higher order multimers. This suggests that dimers have a stable multimerization state, while higher order multimers are more transient in nature. This is also reflected in the recovery, as the recovery of dimeric fraction is high (96%), while recoveries of tetrameric and higher order fraction decreases to under 40% after 48 h. Since SEC only shows soluble multimers or aggregates up to a certain size, it is likely that the observed loss in area stems from the

formation of very large or insoluble aggregates. Interestingly, multimerization of tetrameric and higher order species was higher even though the sample concentration was lower compared to that of the dimeric fraction. It appears that increasing multimer size correlates with decreased stability in the investigated phosphate buffer. This could be due to higher free energy of cavity formation. It was shown that free energy of cavity formation in water correlates for length scales >1 nm with the surface area,[13] which could explain decreased stability of higher order multimers.

Enzymatic activity was monitored over the course of two days for the dimeric and tetrameric fraction (Figure 3(B)). For the higher order multimers, enzymatic activity could not be determined since protein concentration was too low for the assay. Concentration via membrane concentrators of this fraction resulted in multimerization itself (data not shown), hence the activity measurement of the original higher order multimer fraction was not feasible. Generally, the CASPON enzyme dimer exhibits a higher enzymatic activity than the tetramer fraction. Furthermore, enzymatic activity decreases can be observed for both fractions, where the relative loss in enzymatic activity is more pronounced in the tetrameric fraction. Oxidation of cysteines in the active sites could be the cause of reduced enzymatic activity. The cysteine in the active site can be oxidized via dissolved oxygen, but can also be involved in cross-linking between the tetrameric or higher order multimers, therefore decreasing
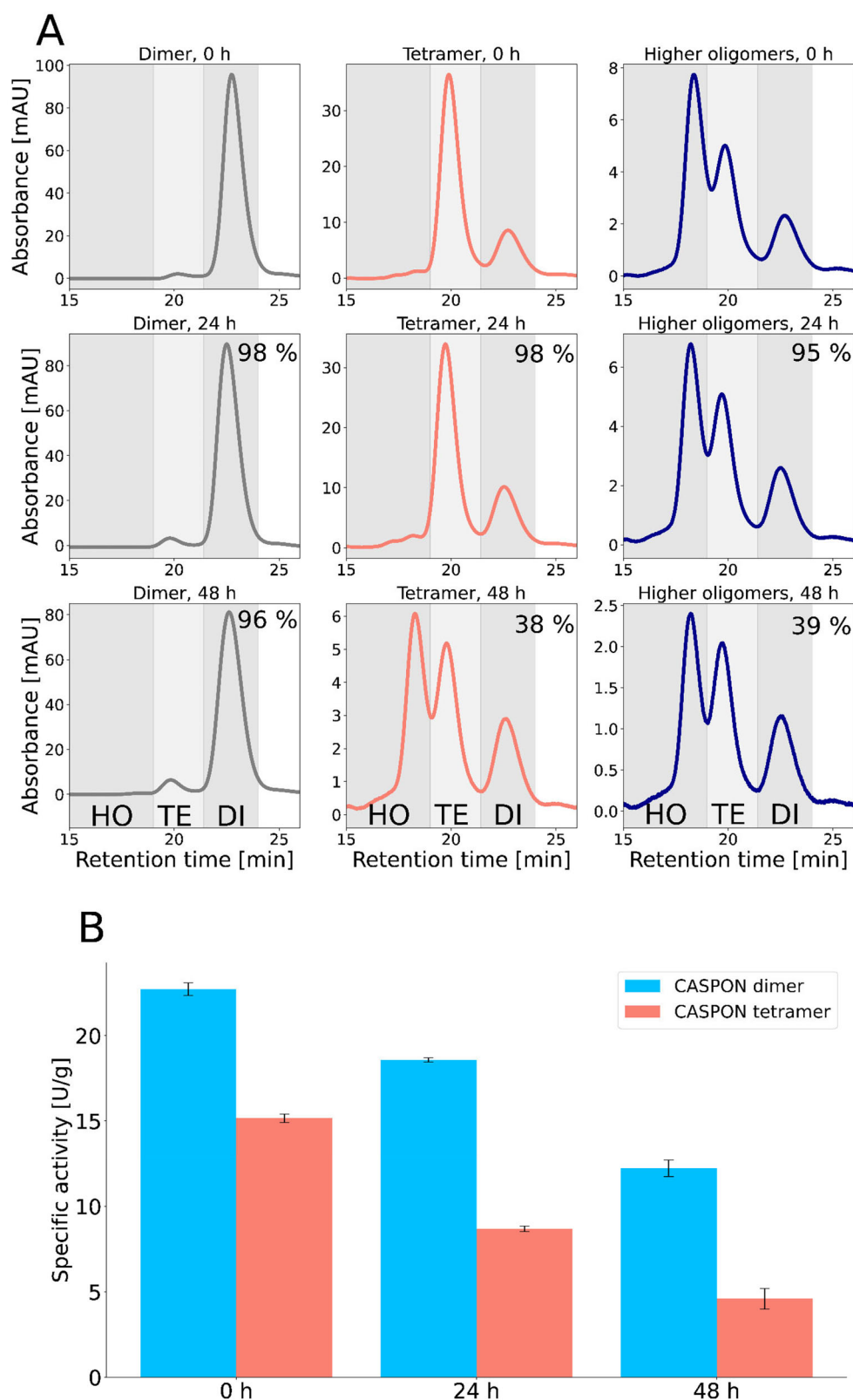
Figure 3. (A) Time course of SEC profiles of the CASPON enzyme dimer tetramer and multimers species at 4 °C. Initial protein concentrations vary between the samples, hence the y-axes of the chromatograms are scaled to show the relative distribution of size variants. The percentage values in the 24 h and 48 h chromatograms are recovery values relative to 0 h. Size variants identified with SEC-MALS are highlighted and marked: higher order multimer (HO), tetramer (TE) and dimer (DI). (B) Time course of enzymatic activity of the dimeric and tetrameric CASPON enzyme fraction at 4 °C.

the total number of functional active sites. Since tetramer and higher multimer fractions show decreased enzymatic activity and stability, maintaining the CASPON enzyme in the dimeric state is beneficial.

In order to investigate the multimerization pathway, dimer, tetramer, and higher order multimer fractions were incubated with 10 mM DTT. Enzymatic activity and SEC profiles were compared to those of untreated samples, shown in Figure 4.

Note that peaks after 30 min are DTT associated (Figure S2, supplementary materials) and the protein concentration varied for each sample. All investigated samples showed a higher dimer content after DTT treatment as tetramer and higher order multimer content decrease in the normalized chromatograms (Figure 4) and the area of the dimer fraction in the raw
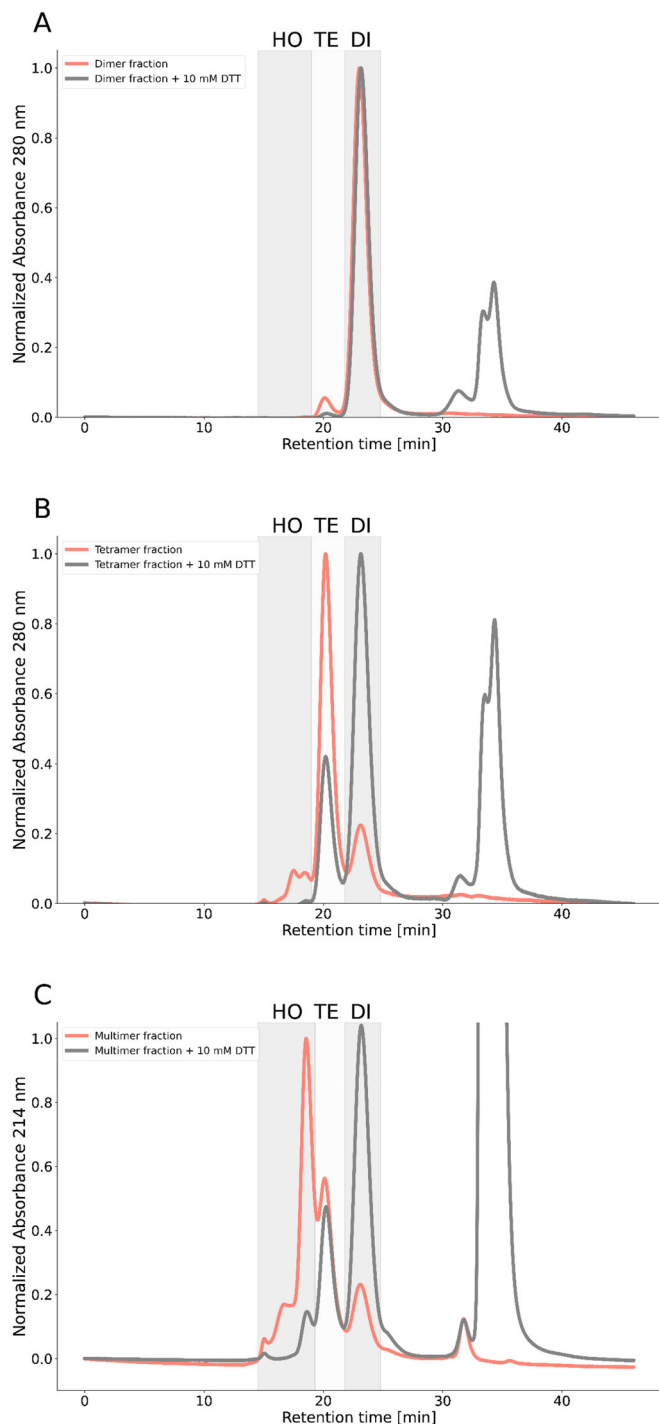
Figure 4. Effect of DTT on tetramers and higher order fractions: SEC-HPLC chromatograms of the dimeric fraction (0.9 g*l^{-1}) that exhibited a 188% increase in enzymatic activity (A), tetrameric (0.4 g*l^{-1}) with a 12.5% increase (B) and heterogenous higher order multimer fraction (0.2 g*l^{-1}) (C). Samples were either incubated with 10 mM DTT or were directly analyzed. Size variants identified with SEC-MALS are highlighted and marked: higher order multimer (HO), tetramer (TE) and dimer (DI). Corresponding raw data can be found in the supplementary materials (Figure S1).

chromatograms increases (Figure S1). This effect is more pronounced for the tetramer and higher order multimer fractions. Enzymatic activity of the dimeric and tetrameric fraction was increased after addition of DTT. This increase was most pronounced for the dimeric fraction (188%) and moderate for the tetrameric fraction (13%). Protein concentration was again too low for the determination of the enzymatic activity of the higher order multimer fraction. The CASPON enzyme monomer cannot be detected throughout the experiment. Moreover, we have analyzed all fractions with and without DTT using SDS-PAGE (Figure S3, supplementary material). In the SDS-PAGE analysis, only the CASPON enzyme monomer and very low amounts of the dimer could be detected for all investigated samples. Altogether, we believe that SDS-PAGE is not a suitable analytical method for investigating disulfide-bond linked CASPON enzyme multimers.

Reduction of CASPON enzyme tetramers and higher order multimers is a strong indication for multimerization formed by covalent disulfide bridges. As indicated by the AlphaFold prediction (Figure 1(C)), the cysteine close to the hexa-histidine tag appears to be exposed in a flexible region, which could be the most prominent site for disulfide bond formation. However, tetrameric and higher order multimers were only partly reduced, hence it is not clear whether cysteine-mediated multimerization is accompanied by another multimerization mechanism or more reducing agent would be needed. Other recombinant proteins have also been reported to undergo cysteine-dependent multimerization.[10,11,20,36] For monoclonal antibodies, cysteine-dependent multimerization can occur during manufacturing[36] and after exposure to thermal stress,[11] correlating overall to free thiol content.[11,36] Cysteine-dependent multimerization in recombinant proteins derived from *E. coli* seems to be more prominent overall.[10,20]

Schweizer and coworkers reported that a disulfide bridge in the dimer interface stabilized the dimeric state in wtCasp2 (*4*). Interestingly, no monomerization occurred upon DTT addition. We hypothesize that the reduction of the internal disulfide bridge is either sterically hindered or non-covalent forces between the monomers are strong enough to keep the dimer intact in the employed buffer. With regards to enzymatic activity, the dimeric fraction experienced a higher replenishment of the enzymatic activity compared to the tetrameric fraction. This could be explained by preferential reduction of disulfide bonds compared to oxidized cysteine in the active site. SDS-PAGE is not suitable for the analysis of the size variants since tetrameric or higher species could not be detected irrespective of DTT addition. We hypothesize that harsh sample preparation and non-native conditions could alter the native multimerization state. Disulfide reshuffling and oxidation to higher order multimer species could occur which might be visible as slight smeared bands in the SDS-PAGE. Nevertheless, SDS-PAGE confirmed the high purity of the investigated samples and the absence of host cell impurities.

Multimerization behavior of dimeric CASPON enzyme

Since the dimeric species of the CASPON enzyme is most stable and active, we further investigated its multimerization

behavior in the presence of kosmotropic, neutral and chaotropic salts (ammonium sulfate, sodium chloride and guanidium hydrochloride, respectively). We have selected a pH range of 6-8 to study multimerization behavior. At this practically relevant pH range, the protonation state of cysteines varies from partially protonated and fully protonated to partially deprotonated and fully deprotonated at pH 6 and 8, respectively[23]. Temperatures for incubation were set to either 4 °C or 25 °C to emulate conventional temperatures in downstream processing. During this experiment, minor peaks occurred at higher retention times than the dimeric species and due to their later retention time compared to the dimer in SEC, we identified the species as the CASPON enzyme monomer.

Figure 5 shows the evolution of the multimeric state of the CASPON enzyme with respect to different salt exposure, pH, and temperature. As expected, multimerization is higher at 25 °C compared to 4 °C for all salts. In the presence of 1 M ammonium sulfate and 1 M sodium chloride, multimerization increases with solution pH, with ammonium sulfate inducing more pronounced multimerization. Highest multimerization was observed in the presence of 1 M ammonium sulfate at pH 8 and 25 °C, where multimerization was over 90% after 3 days. In comparison, multimer content was below 20% after incubation for 3 days with sodium chloride at pH 8 and 25 °C. For 1 M guanidium chloride, temperature had a tremendous impact on multimerization. Almost no multimerization was observed at 4 °C, whereas multimerization can be observed for all tested pH values at 25 °C. Ammonium sulfate and sodium chloride also induce monomerization compared to the reference. However, monomer content was lower than 20% throughout the experiment for those two salts. Multimerization behavior does not correlate with pH when the enzyme is incubated with guanidium hydrochloride. pH 6 induced pronounced monomerization in the presence of guanidium hydrochloride as indicated by a maximum monomer content of over 20%. While a high monomer content was observed throughout the experiment at 4 °C, monomer content decreases abruptly after one day at 25 °C. After one day, decreased monomer content coincides with increased multimerization.

In the presence of 1 M ammonium sulfate and 1 M sodium chloride, multimerization increases at higher pH and thus higher thiolate content. This indicates a predominantly cysteine-dependent multimerization because of higher reactivity of thiolates. However, multimerization rates differ substantially between ammonium sulfate and sodium chloride. These effects are generally in accordance with the Hofmeister series.[37] High monomer content at pH 6 indicates an overall destabilization of the monomer-monomer interface that is further enhanced by disruption of non-covalent interactions by guanidine.[16,17,38] Interestingly, guanidine induced monomerization followed by multimerization at 25 °C. Since guanidine can potentially cause unfolding of the protein, we hypothesize that formed multimers could have an altered tertiary structure and hence follow a denaturing multimerization pathway. At 4 °C however, monomerization occurs in the presence of guanidine while

multimerization does not occur. Thus, the disruption of the dimer interface is not necessarily accompanied by unfolding of the CASPON enzyme which is potentially increased at 25 °C. Lastly, the reference experiment shows that the CASPON enzyme dimer is stable for at least one day in PBS with a comparably low ionic strength.

As previously mentioned, cysteine-dependent multimerization can also occur in IgG1 and IgG2; however, it is much lower compared to the multimerization of CASPON enzyme in the reference PBS buffer. Even after thermal stress exposure for 12 weeks at 45 °C, total aggregate content of an anti-streptadivin antibody preparation was below 10% and reducible aggregate content was 2–5%.[11] On the other hand, cysteine-mediated multimerization appears to be more prominent when overexpressing recombinant, cysteine-bearing proteins in E. coli. Depending on the protein of interest[10,20] and E. coli strain,[20] disulfide-linked aggregate content directly after purification varies from under 10% to a considerably higher aggregate content.[10,20] When incubating the cysteine-bearing extracellular domain of human CD83 at room temperature, higher cysteine-dependent multimerization can be observed, where disulfide-linked aggregate content reaches 30–70%.[10] This is considerably higher compared to the multimerization of the CASPON enzyme in the low ionic strength reference conditions. In PBS, the CASPON enzyme preparation contains under 20% aggregate content after 7 days.

To further investigate the differences of multimerization caused by ammonium sulfate and guanidine, we incubated the CASPON enzyme over 168 h (7 days) at room temperature with these salts. For guanidine, pH 6 was selected due to prominent monomerization followed by multimerization (Figure 5). For ammonium sulfate, pH 8 showed highest multimerization content after 7 days and thus represented an interesting condition. After incubation over 7 days, both preparations were analyzed with and without DTT.

Figure 6 shows the resulting HP-SEC chromatograms. After incubation with ammonium sulfate, the overall signal is lower than 90% compared to all other samples. Nevertheless, addition of DTT reduces higher order multimers back to dimers (and to a much smaller extent, monomers), indicating strictly cysteine-mediated multimerization. Guanidine on the other hand causes less multimerization compared to ammonium sulfate and incubation with reductant cannot reduce all higher order multimers. Furthermore, monomer content is highest of all investigated samples, indicating that after monomerization of the CASPON enzyme, monomers can covalently link via disulfide bridges to non-native dimers or higher order multimers. After DTT addition, the total UV area of the SEC chromatogram of guanidine treated samples is considerably lower compared to that of the samples incubated with ammonium sulfate, indicating a higher proportion of non-reducible higher order multimers that are too large to be detectable after 0.22 μm filtration. We suggest that guanidine induces a denaturing pathway and mixed pathway due to its salting in effect, leading to the formation of multimers with an altered tertiary structure.
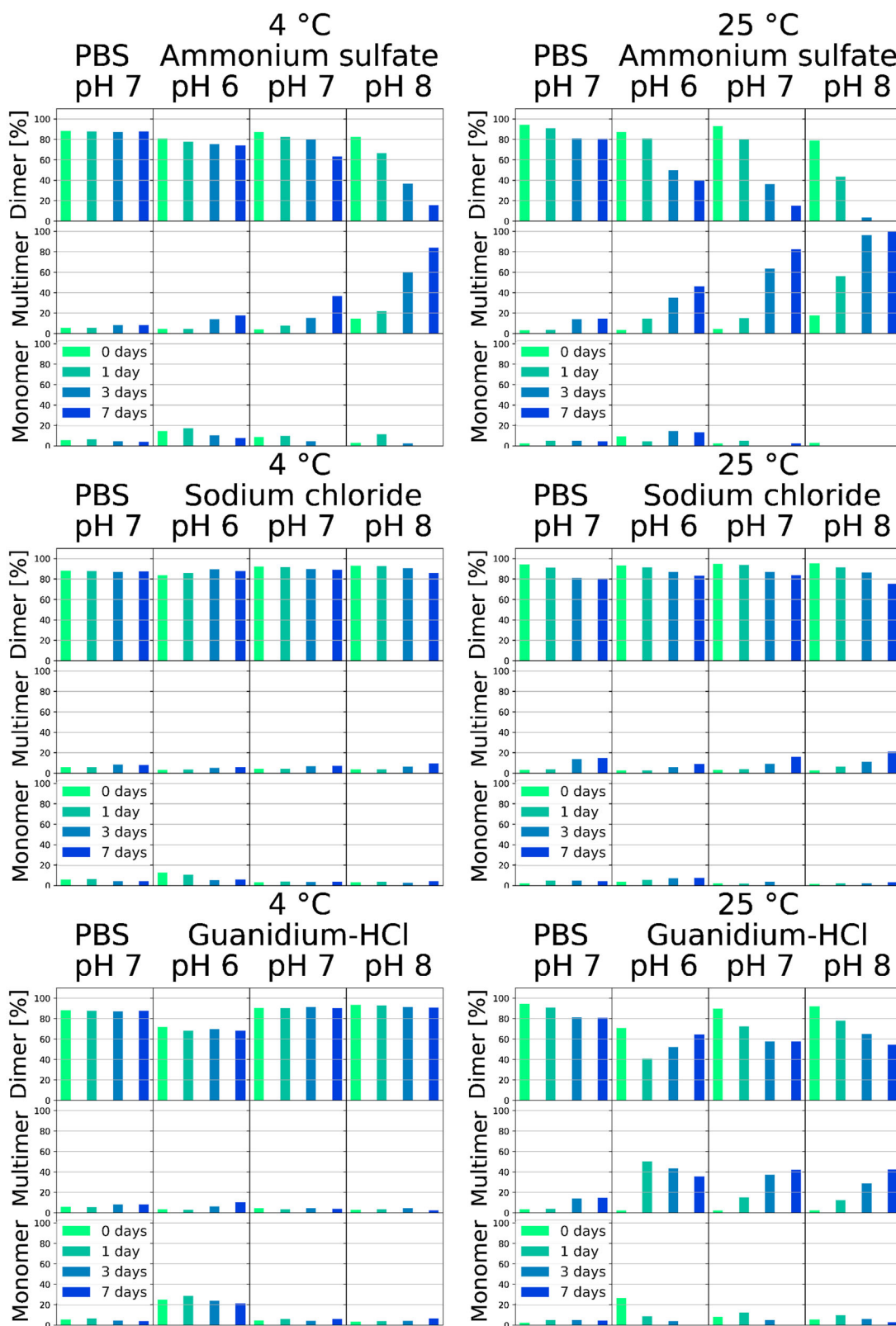
Figure 5. Impact of pH and different additives on multimerization (1 M salt, 60 mM phosphate). Left: 4 °C. Right: 25 °C.

Protein–protein interactions

In this section, we investigate the correlation between protein-protein interactions and multimerization rates. Protein-protein interactions were determined by SIC experiments, where dimeric CASPON enzyme was present as an analyte in the mobile phase and as a ligand in the stationary phase. As a reference, highly interactive conditions were also tested with a column that carried immobilized Tris instead of the CASPON enzyme.

Firstly, 1 M ammonium sulfate induces strong attractive protein-protein interactions that cannot be quantified using
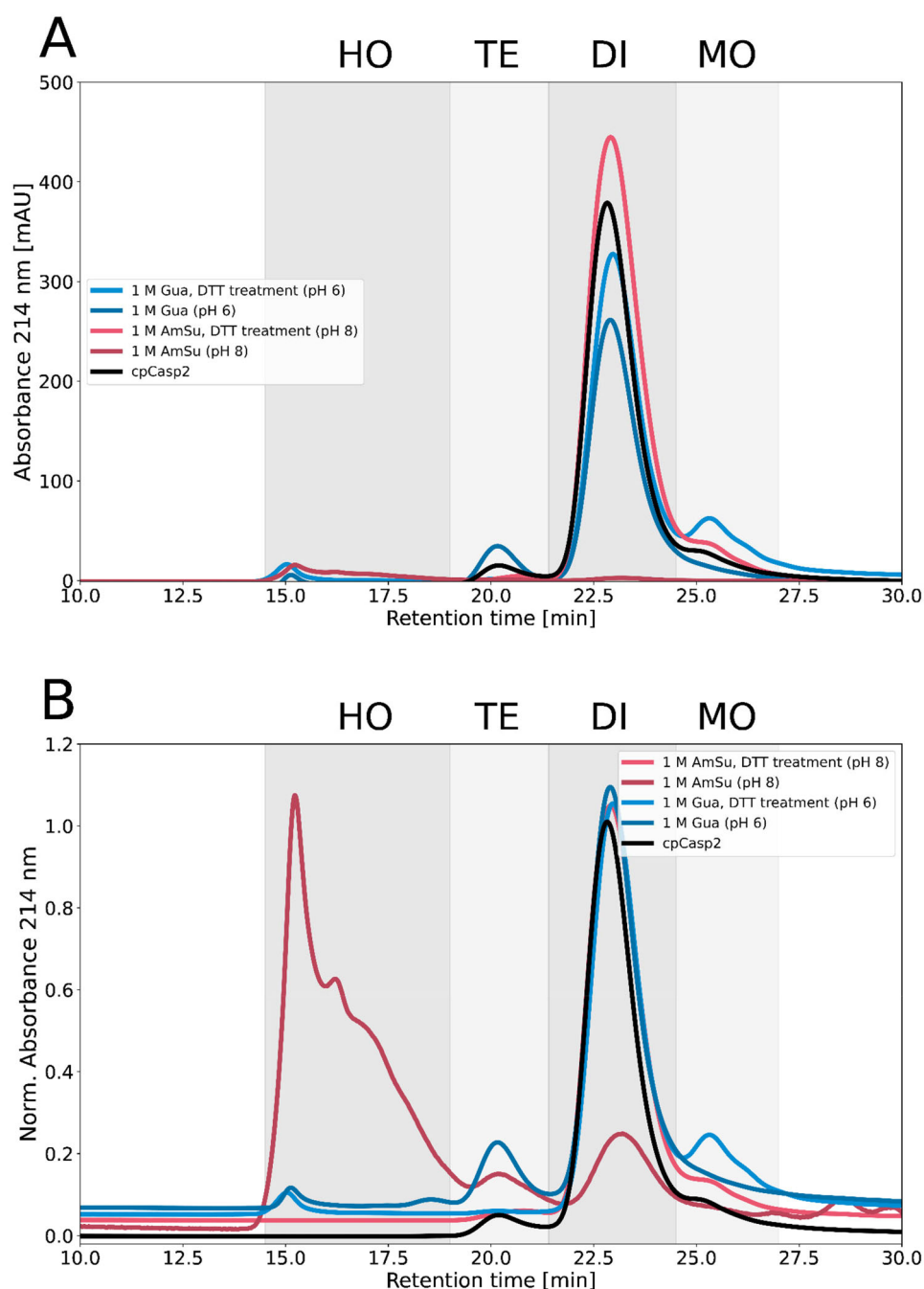
Figure 6. HP-SE chromatograms of the CASPON enzyme incubated with 1 M ammonium sulfate (pH 8) and 1 M guanidium hydrochloride (pH 6) for 7 d. Comparison of reduced (incubation with 10 mM DTT) to untreated samples. A) Raw data at 214 nm absorbance and B) chromatograms normalized to largest peaks. Size variants highlighted and marked: monomer (MO), dimer (DI), tetramer (TE) and higher order multimer (HO).

SIC due to backbone interactions (Figure 7) and low recovery (Table 1), respectively. As seen in Figure 7, protein retention is higher at increasing pH values. Furthermore, retention increases with increasing temperature with the CASPON enzyme as a ligand and with Tris as a ligand. Overall, retention on NHS Sepharose with immobilized CASPON enzyme is higher compared to that on the bare column with Tris as a ligand in addition to recoveries dropping below 22%. It cannot be stated whether the enzyme binds irreversibly or reversibly to the SIC column. Initially, formed multimers could be reversible due to protein-protein interactions as reported in literature[39] and become irreversible as disulfide bonds form over time. Once again, higher pH values likely increase reaction rates of disulfide bond formation due to higher concentration of thiolate anions on the surface of the protein. Moreover, protein-protein interactions may additionally contribute to higher multimerization rates at higher pH. Interestingly, binding of the CASPON enzyme to Tris-Sepharose at pH 8 and 25 °C appears to change the interactions with protein remaining in the mobile phase. After each injection, retention time increases and recovery decreases, suggesting successive deposition of the CASPON enzyme and increased interactivity of the stationary phase to the CASPON enzyme in the mobile phase.
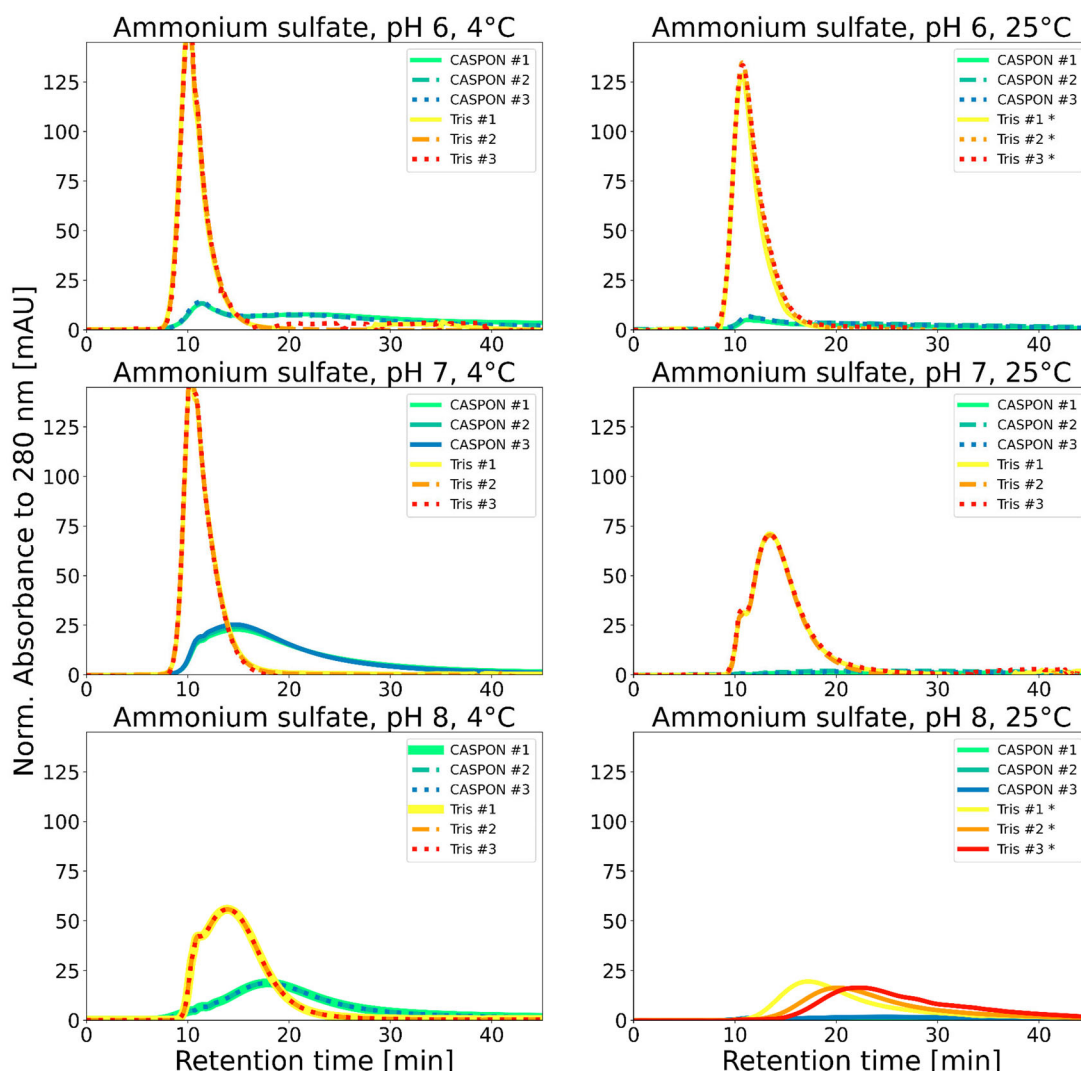
Figure 7. SIC experiments in presence of 1 M ammonium sulfate, 60 mM phosphate buffer with different ligand (either CASPON enzyme or Tris). Successive injections are numbered from 1 to 3. Chromatograms marked with an asterisk (*) were smoothed using a gaussian filter.

Table 1. Recovery for SIC experiments for 1 M ammonium sulfate, 60 mM phosphate buffer on two different ligands (Tris or CASPON enzyme).

pH	Ligand	Recovery at 4 °C	Recovery at 25 °C
6	CASPON enzyme	54.7 ± 3.9	21.7 ± 4.3
	C(O)-Tris	94.3 ± 1.3	95.6 ± 1.0
7	CASPON enzyme	66.9 ± 1.8	13.7 ± 3.6
	C(O)-Tris	101 ± 1.0	90.2 ± 1.5
8	CASPON enzyme	55.1 ± 0.8	5.2 ± 1.5
	C(O)-Tris	88.6 ± 6.2	51.3 ± 4.1

Table 2. B_{22} for CASPON enzyme incubated with PBS, 1 M NaCl and 1 M guanidium HCl. Positive B_{22} values indicate repulsive interactions.

				B_{22} [mol*l^{-1}*g^{-2}]		
	PBS		NaCl		Guanidium HCl	
pH	4 °C	25 °C	4 °C	25 °C	4 °C	25 °C
6			0.50	0.34	2.64	2.74
7	1.07	1.54	2.75	2.64	3.04	2.94
8			2.92	2.78	2.85	2.94

Secondly, 1 M sodium chloride and 1 M guanidine buffers induce weak repulsive protein-protein interactions and dimer depletion showed no correlation to B_{22} in the presence of those two salts (Figure S4, supplementary materials). Protein-protein interactions were comparable at different temperatures (Table 2). In the presence of sodium chloride, protein-protein interactions are increasingly repulsive with increasing pH. When guanidine is employed, protein-protein interactions are equally repulsive irrespective of pH.

While multimerization was highly temperature dependent in the presence of guanidinium hydrochloride and sodium chloride, increasing protein-protein interactions did not correlate with increasing temperature. For sodium chloride, increasing temperature could simply allow faster kinetics and thus increase dimer depletion rates. For guanidine, protein-protein interactions were not indicative of multimerization whatsoever. This suggests that protein-protein interactions might not be a useful parameter in predicting multimerization via a denaturing multimerization mechanism.

The impact of protein-protein interactions on multimerization in the adsorbed phase was investigated by batch adsorption of CASPON enzyme on Ni Sepharose FF resin. The protein was adsorbed for 6 h under either highly attractive (1 M ammonium sulfate, pH 8) or slightly repulsive (1 M
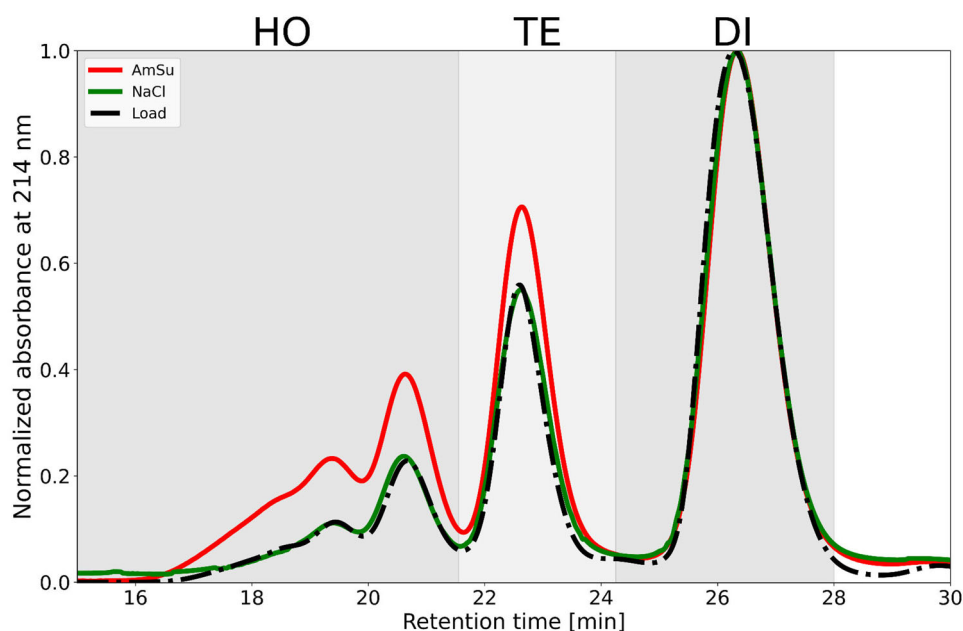
Figure 8. SEC chromatograms of IMAC eluates after 6 h incubation. Ammonium sulfate induces strong protein-protein interactions, whereas sodium chloride induces weakly repulsive interactions. Size variants identified with SEC-MALS are highlighted and marked: dimer (DI), tetramer (TE) and higher order multimer (HO). Raw data and normalized chromatograms of the remaining two injections for each condition can be found in the supplementary material (Figure S5).
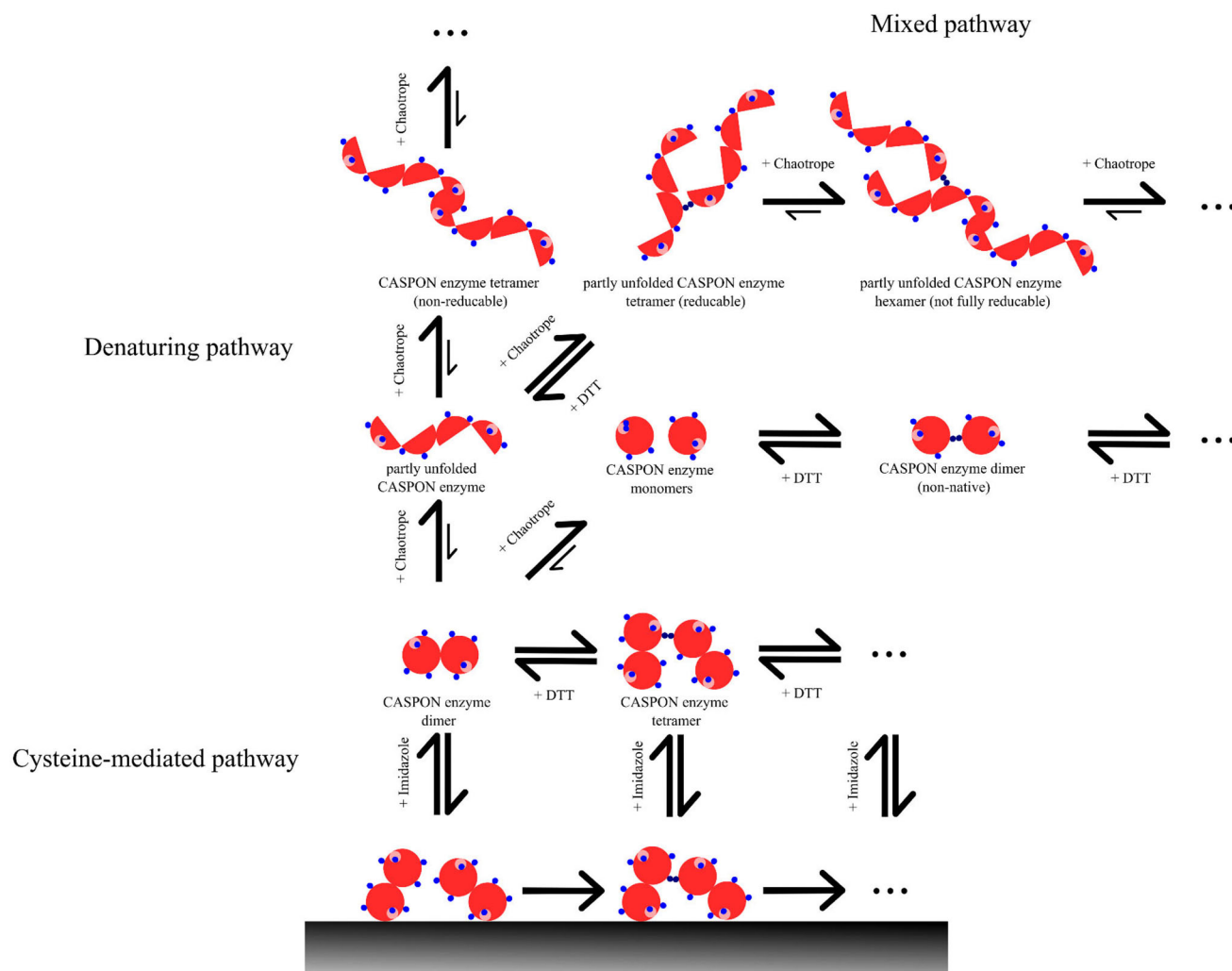

Figure 9. Proposed pathways for CASPON enzyme multimerization, monomerization and denaturation. Grey bar on the bottom indicates an IMAC stationary phase. Blue dots: cysteine, neighboring dark blue dots: disulfide bridges, small light-red dots: active site.

NaCl, pH 8) conditions and subsequently eluted and evaluated. This contact time is typical for a purification process using IMAC.[40–42]

Figure 8 shows normalized HP-SEC chromatograms (raw data can be found in supplementary materials, Figure S5) of the eluted CASPON enzyme after adsorption in the presence of different salts. The relative dimer content in the eluate is equal to that of the load at 57% when incubated with 1 M sodium chloride. In the presence of 1 M ammonium sulfate, the relative dimer content decreases from 57% in the load to 45% in the eluate. Multimerization still occurs in the adsorbed phase under attractive conditions. Immobilized proteins can still interact with other proteins in close proximity. Unfortunately, mass balances were difficult to determine and were unreliable due to the low volume of stationary phase, leading to low recoveries (Table S3).

Mechanism of action

Understanding multimerization mechanism can facilitate process development and improvement for cysteine-bearing proteins, specifically for the CASPON enzyme. In a manufacturing process, reductants could be added to buffers in certain downstream unit operations (ion-exchange chromatography, hydrophobic interaction chromatography, buffer exchange, filtration) if a strictly cysteine-mediated multimerization mechanism is followed (Figure 9). This could ultimately increase product yield due to reduction of disulfide-bond linked multimers. If target protein aggregates are reversed during the process, potential chemical modifications of the product must be monitored. In the final formulation, low reductant concentration could reduce the active center to replenish the enzymatic activity and reverse newly formed multimers. Reductants show pH-dependent activity which could limit their application to defined pH ranges.[43]

The addition of chaotropic and denaturing reagents such as guanidine is rare except for refolding processes.[44] Nevertheless, the enzyme could enter a denaturing or mixed pathway (Figure 9) in several unit operations that can cause partial unfolding. Partial unfolding of proteins can be observed upon adsorption in HIC[45,46] or ion-exchange chromatography (IEX).[15,47] In general, multimers obtained from the denaturing pathway are more problematic than reducible multimers as their tertiary structure and hence activity might be affected.

Aside from the CASPON enzyme, some general considerations must be made for other cysteine-bearing proteins. Firstly, in-silico tools could help to identify potentially redundant cysteines and avoid cysteine-dependent multimerization a priori when conducting protein design. Secondly, cysteine removal might not always be possible, in which case special emphasis should be put on stability and activity of the protein in presence of the selected reductant. Dedicated stability experiments should be performed by employing analytical techniques to monitor changes of the native state (e.g., SEC) and the denatured state (e.g., reversed-phase HPLC).

Conclusion

Dimeric CASPON enzyme is the most stable and active multimerization species. Under standard process conditions, i.e., in PBS at 25 °C for up to 24 h, multimerization of the dimer is negligible, indicating that multimerization is not a critical quality attribute in its application as a protease for tag removal. Generally, multimerization of the CASPON enzyme follows two different pathways or a combination thereof, namely a cysteine-mediated pathway or a denaturing pathway. In the cysteine-mediated pathway, CASPON enzyme multimers are linked via disulfide bonds and the formed multimers are reduceable. Here, protein-protein interactions correlate with dimer depletion rates, where 1 M ammonium sulfate induced highest dimer depletion. In the denaturing pathway, the CASPON enzyme partly unfolds and binds to other proteins to form non-reducible multimers. In the presence of chaotropic guanidine, the CASPON enzyme follows both the denaturing pathway and the cysteine-mediated pathway in a weakly repulsive regime. The multimerization also occurs when binding CASPON enzyme to IMAC Sepharose FF under attractive conditions, indicating that multimerization occurs during downstream processing. Multimerization propensity must be considered when processing such cysteine-bearing proteins. The addition of reductants such as DTT can be considered to reverse multimerization and restore the native state of the protein. This work is in line with common rules to execute protein purification with low contact time and low residence time to avoid disulfide bond formation and conformational change of the protein upon adsorption.

Supplementary materials

Table S1: Preparative SEC parameters with HiLoad Superdex 200 pg (Cytiva, Sweden). Table S2: Detailed HPLC parameters for samples containing imidazole (Superdex 200 Increase 10/300 GL) and without imidazole (TSKgel G3000 SWXL). Figure S1: Chromatogram raw data for Figure 3. Figure S2: Injection of 10 mM DTT solution after incubation at RT for 160 min. Figure S3: SDS-PAGE analysis of dimeric, tetrameric and higher order multimer fraction (NuPAGE (Invitrogen, USA) 4–12% Bis-Tris with MES running buffer). 1: Protein standards. 2: dimer fraction. 3: dimer fraction, 10 mM DTT. 4: dimer fraction, 180 mM DTT. 5: tetramer fraction. 6: tetramer fraction, 10 mM DTT. 7: tetramer fraction, 180 mM DTT. 8: higher order multimer fraction. 9: higher order multimer fraction, 10 mM DTT. 10: higher order multimer fraction, 180 mM DTT. 11: Protein standards. Figure S4: B_{22} plotted over dimer depletion rate for sodium chloride and guanidium hydrochloride at 4 and 25 °C. Table S3: Mass balances and binding capacities for IMAC binding experiments. Figure S5: All SEC chromatograms of IMAC eluates after 6 h incubation. Top: raw data. Bottom: normalized data. Ammonium sulfate induces strong protein-protein interactions, whereas sodium chloride induces weakly repulsive interactions.

ORCID

Alois Jungbauer http://orcid.org/0000-0001-8182-7728
Nico Lingg http://orcid.org/0000-0002-3574-6991

References

[1] Lingg, N.; Kröß, C.; Engele, P.; Öhlknecht, C.; Köppl, C.; Fischer, A.; Lier, B.; Loibl, J.; Sprenger, B.; Liu, J.; et al. CASPON Platform Technology: Ultrafast Circularly Permuted Caspase-2 Cleaves Tagged Fusion Proteins before All 20 Natural Amino Acids at the N-Terminus. *N Biotechnol.* **2022**, *71*, 37–46. DOI: 10.1016/j.nbt.2022.07.002.

[2] Cserjan-Puschmann, M.; Lingg, N.; Engele, P.; Kröß, C.; Loibl, J.; Fischer, A.; Bacher, F.; Frank, A.-C.; Öhlknecht, C.; Brocard, C.; et al. Production of Circularly Permuted Caspase-2 for Affinity Fusion-Tag Removal: Cloning, Expression in Escherichia coli, Purification, and Characterization. *Biomolecules* **2020**, *10*, 1592. DOI: 10.3390/biom10121592.

[3] Lingg, N.; Cserjan-Puschmann, M.; Fischer, A.; Engele, P.; Kröß, C.; Schneider, R.; Brocard, C.; Berkemeyer, M.; Striedner, G.; Jungbauer, A. Advanced Purification Platform Using Circularly Permuted Caspase-2 for Affinity Fusion-Tag Removal to Produce Native Fibroblast Growth Factor 2. *J. Chem. Technol. Biotechnol.* **2021**, *96*, 1515–1522. DOI: 10.1002/jctb.6666.

[4] Schweizer, A.; Briand, C.; Grutter, M. G. Crystal Structure of Caspase-2, Apical Initiator of the Intrinsic Apoptotic Pathway. *J. Biol. Chem.* **2003**, *278*, 42441–42447. DOI: 10.1074/jbc.M304895200.

[5] Öhlknecht, C.; Petrov, D.; Engele, P.; Kröß, C.; Sprenger, B.; Fischer, A.; Lingg, N.; Schneider, R.; Oostenbrink, C. Enhancing the Promiscuity of a Member of the Caspase Protease Family by Rational Design. *Proteins* **2020**, *88*, 1303–1318. DOI: 10.1002/prot.25950.

[6] Jumper, J.; Evans, R.; Pritzel, A.; Green, T.; Figurnov, M.; Ronneberger, O.; Tunyasuvunakool, K.; Bates, R.; Žídek, A.; Potapenko, A.; et al. Highly Accurate Protein Structure Prediction with AlphaFold. *Nature* **2021**, *596*, 583–589. DOI: 10.1038/s41586-021-03819-2.

[7] Evans, R.; O'Neill, M.; Pritzel, A.; Antropova, N.; Senior, A.; Green, T.; Žídek, A.; Bates, R.; Blackwell, S.; Yim, J. Protein Complex Prediction with AlphaFold-Multimer. *bioRxiv* **2022**, DOI: 10.1101/2021.10.04.463034.

[8] Mirdita, M.; Schütze, K.; Moriwaki, Y.; Heo, L.; Ovchinnikov, S.; Steinegger, M. ColabFold - Making Protein Folding Accessible to All. *bioRxiv* **2022**, DOI: 10.1101/2021.08.15.456425.

[9] Garcia-Calvo, M.; Peterson, E. P.; Rasper, D. M.; Vaillancourt, J. P.; Zamboni, R.; Nicholson, D. W.; Thornberry, N. A. Purification and Catalytic Properties of Human Caspase Family Members. *Cell Death Differ.* **1999**, *6*, 362–369. DOI: 10.1038/sj.cdd.4400497.

[10] Zhang, L.; Moo-Young, M.; Chou, C. P. Molecular Manipulation Associated with Disulfide Bond Formation to Enhance the Stability of Recombinant Therapeutic Protein. *Protein Expr. Purif.* **2011**, *75*, 28–39. DOI: 10.1016/j.pep.2010.08.006.

[11] Franey, H.; Brych, S. R.; Kolvenbach, C. G.; Rajan, R. S. Increased Aggregation Propensity of IgG2 Subclass over IgG1: role of Conformational Changes and Covalent Character in Isolated Aggregates. *Protein Sci.* **2010**, *19*, 1601–1615. DOI: 10.1002/pro.434.

[12] Tang, P.; Tan, Z.; Ehamparanathan, V.; Ren, T.; Hoffman, L.; Du, C.; Song, Y.; Tao, L.; Lewandowski, A.; Ghose, S.; et al. Optimization and Kinetic Modeling of Interchain Disulfide Bond Reoxidation of Monoclonal Antibodies in Bioprocesses. *MAbs.* **2020**, *12*, 1829336. DOI: 10.1080/19420862.2020.1829336.

[13] Chandler, D. Interfaces and the Driving Force of Hydrophobic Assembly. *Nature* **2005**, *437*, 640–647. DOI: 10.1038/nature04162.

[14] Sedov, I.; Magsumov, T. The Gibbs Free Energy of Cavity Formation in a Diverse Set of Solvents. *J. Chem. Phys.* **2020**, *153*, 134501. DOI: 10.1063/5.0021959.

[15] Guo, J.; Carta, G. Unfolding and Aggregation of Monoclonal Antibodies on Cation Exchange Columns: effects of Resin Type, Load Buffer, and Protein Stability. *J. Chromatogr. A* **2015**, *1388*, 184–194. DOI: 10.1016/j.chroma.2015.02.047.

[16] Povarova, O. I.; Kuznetsova, I. M.; Turoverov, K. K. Differences in the Pathways of Proteins Unfolding Induced by Urea and Guanidine Hydrochloride: molten Globule State and Aggregates. *PLoS One.* **2010**, *5*, e15035. DOI: 10.1371/journal.pone.0015035.

[17] Syed, S. B.; Khan, F. I.; Khan, S. H.; Srivastava, S.; Hasan, G. M.; Lobb, K. A.; Islam, A.; Hassan, M. I.; Ahmad, F. Unravelling the Unfolding Mechanism of Human Integrin Linked Kinase by GdmCl-Induced Denaturation. *Int. J. Biol. Macromol.* **2018**, *117*, 1252–1263. DOI: 10.1016/j.ijbiomac.2018.06.025.

[18] Swaminathan, R.; Ravi, V. K.; Kumar, S.; Kumar, M. V.; Chandra, N. Lysozyme: A Model Protein for Amyloid Research. *Adv Protein Chem Struct Biol* **2011**, *84*, 63–111.

[19] Bondos, S. E.; Bicknell, A. Detection and Prevention of Protein Aggregation before, during, and after Purification. *Anal. Biochem.* **2003**, *316*, 223–231. DOI: 10.1016/S0003-2697(03)00059-9.

[20] Dotson, P. P.; 2nd Karakashian, A. A.; Nikolova-Karakashian, M. N. Neutral Sphingomyelinase-2 is a Redox Sensitive Enzyme: role of Catalytic Cysteine Residues in Regulation of Enzymatic Activity through Changes in Oligomeric State. *Biochem. J.* **2015**, *465*, 371–382. DOI: 10.1042/BJ20140665.

[21] Liu, H.; May, K. Disulfide Bond Structures of IgG Molecules: structural Variations, Chemical Modifications and Possible Impacts to Stability and Biological Function. *MAbs.* **2012**, *4*, 17–23. DOI: 10.4161/mabs.4.1.18347.

[22] Grassi, L.; Cabrele, C. Susceptibility of Protein Therapeutics to Spontaneous Chemical Modifications by Oxidation, Cyclization, and Elimination Reactions. *Amino Acids.* **2019**, *51*, 1409–1431. DOI: 10.1007/s00726-019-02787-2.

[23] Poole, L. B. The Basics of Thiols and Cysteines in Redox Biology and Chemistry. *Free Radic. Biol. Med.* **2015**, *80*, 148–157. DOI: 10.1016/j.freeradbiomed.2014.11.013.

[24] Trivedi, M. V.; Laurence, J. S.; Siahaan, T. J. The Role of Thiols and Disulfides on Protein Stability. *Curr. Protein Pept. Sci.* **2009**, *10*, 614–625. DOI: 10.2174/138920309789630534.

[25] Matsarskaia, O.; Roosen-Runge, F.; Lotze, G.; Moller, J.; Mariani, A.; Zhang, F.; Schreiber, F. Tuning Phase Transitions of Aqueous Protein Solutions by Multivalent Cations. *Phys. Chem. Chem. Phys.* **2018**, *20*, 27214–27225. DOI: 10.1039/c8cp05884a.

[26] Jakob, L. A.; Beyer, B.; Janeiro Ferreira, C.; Lingg, N.; Jungbauer, A.; Tscheließnig, R. Protein-Protein Interactions and Reduced Excluded Volume Increase Dynamic Binding Capacity of Dual Salt Systems in Hydrophobic Interaction Chromatography. *J. Chromatogr. A* **2021**, *1649*, 462231. DOI: 10.1016/j.chroma.2021.462231.

[27] Arakawa, T.; Kita, Y. Protection of Bovine Serum Albumin from Aggregation by Tween 80. *J Pharm Sci* **2000**, *89*, 646–651. DOI: 10.1002/(SICI)1520-6017(200005)89:5<646::AID-JPS10>3.3.CO;2-A.

[28] Wang, W. Instability, Stabilization, and Formulation of Liquid Protein Pharmaceuticals. *Int. J. Pharm.* **1999**, *185*, 129–188. DOI: 10.1016/S0378-5173(99)00152-0.

[29] Charman, S. A.; Mason, K. L.; Charman, W. N. Techniques for Assessing the Effects of Pharmaceutical Excipients on the Aggregation of Porcine Growth Hormone. *Pharm. Res.* **1993**, *10*, 954–962.

[30] Fekete, S.; Beck, A.; Veuthey, J. L.; Guillarme, D. Theory and Practice of Size Exclusion Chromatography for the Analysis of Protein Aggregates. *J. Pharm. Biomed. Anal.* **2014**, *101*, 161–173. DOI: 10.1016/j.jpba.2014.04.011.

[31] Ye, H. Simultaneous Determination of Protein Aggregation, Degradation, and Absolute Molecular Weight by Size Exclusion Chromatography-Multiangle Laser Light Scattering. *Anal. Biochem.* **2006**, *356*, 76–85. DOI: 10.1016/j.ab.2006.05.025.

[32] Achilli, C.; Ciana, A.; Minetti, G. Oxidation of Cysteine-Rich Proteins during Gel Electrophoresis. *J. Biol. Methods.* **2018**, *5*, e104. DOI: 10.14440/jbm.2018.275.

[33] Housmans, J. A. J.; Wu, G.; Schymkowitz, J.; Rousseau, F. A Guide to Studying Protein Aggregation. *Febs J.* **2021**. DOI: 10.1111/febs.16312.

[34] Tarmann, C.; Jungbauer, A. Adsorption of Plasmid DNA on Anion Exchange Chromatography Media. *J. Sep. Sci.* **2008**, *31*, 2605–2618. DOI: 10.1002/jssc.200700654.

[35] Carta, G.; Jungbauer, A. *Protein Chromatography: Process Development and Scale-Up*; Editor Ed.∘Eds.; Protein Chromatography: Process Development and Scale-Up, Weinheim, Germany, 2010.

[36] Chung, W. K.; Russell, B.; Yang, Y.; Handlogten, M.; Hudak, S.; Cao, M.; Wang, J.; Robbins, D.; Ahuja, S.; Zhu, M. Effects of Antibody Disulfide Bond Reduction on Purification Process Performance and Final Drug Substance Stability. *Biotechnol. Bioeng.* **2017**, *114*, 1264–1274. DOI: 10.1002/bit.26265.

[37] Schneider, C. P.; Shukla, D.; Trout, B. L. Arginine and the Hofmeister Series: The Role of Ion-Ion Interactions in Protein Aggregation Suppression. *J. Phys. Chem. B* **2011**, *115*, 7447–7458. DOI: 10.1021/jp111920y.

[38] Balamurugan, K.; Prakash, M.; Subramanian, V. Theoretical Insights into the Role of Water Molecules in the Guanidinium-Based Protein Denaturation Process in Specific to Aromatic Amino Acids. *J. Phys. Chem. B* **2019**, *123*, 2191–2202. DOI: 10.1021/acs.jpcb.8b08968.

[39] Godfrin, P. D.; Zarraga, I. E.; Zarzar, J.; Porcar, L.; Falus, P.; Wagner, N. J.; Liu, Y. Effect of Hierarchical Cluster Formation on the Viscosity of Concentrated Monoclonal Antibody Formulations Studied by Neutron Scattering. *J. Phys. Chem. B* **2016**, *120*, 278–291. DOI: 10.1021/acs.jpcb.5b07260.

[40] Lingg, N.; Ohlknecht, C.; Fischer, A.; Mozgovicz, M.; Scharl, T.; Oostenbrink, C.; Jungbauer, A. Proteomics Analysis of Host Cell Proteins after Immobilized Metal Affinity Chromatography: Influence of Ligand and Metal Ions. *J. Chromatogr. A* **2020**, *1633*, 461649. DOI: 10.1016/j.chroma.2020.461649.

[41] Riguero, V.; Clifford, R.; Dawley, M.; Dickson, M.; Gastfriend, B.; Thompson, C.; Wang, S.-C.; O'Connor, E. Immobilized Metal Affinity Chromatography Optimization for Poly-Histidine Tagged Proteins. *J. Chromatogr. A* **2020**, *1629*, 461505. DOI: 10.1016/j.chroma.2020.461505.

[42] Zhang, C.; Fredericks, D.; Longford, D.; Campi, E.; Sawford, T.; Hearn, M. T. Changed Loading Conditions and Lysate Composition Improve the Purity of Tagged Recombinant Proteins with Tacn-Based IMAC Adsorbents. *Biotechnol. J.* **2015**, *10*, 480–489. DOI: 10.1002/biot.201400463.

[43] Santarino, I. B.; Oliveira, S. C. B.; Oliveira-Brett, A. M. Protein Reducing Agents Dithiothreitol and Tris(2-Carboxyethyl)Phosphine Anodic Oxidation. *Electrochem. Commun.* **2012**, *23*, 114–117. DOI: 10.1016/j.elecom.2012.06.027.

[44] Rathore, A. S.; Bade, P.; Joshi, V.; Pathak, M.; Pattanayek, S. K. Refolding of Biotech Therapeutic Proteins Expressed in Bacteria: review. *J. Chem. Technol. Biotechnol.* **2013**, *88*, 1794–1806. DOI: 10.1002/jctb.4152.

[45] Beyer, B.; Jungbauer, A. Conformational Changes of Antibodies upon Adsorption onto Hydrophobic Interaction Chromatography Surfaces. *J. Chromatogr. A* **2018**, *1552*, 60–66. DOI: 10.1016/j.chroma.2018.04.009.

[46] Muca, R.; Kołodziej, M.; Piątkowski, W.; Carta, G.; Antos, D. Effects of Negative and Positive Cooperative Adsorption of Proteins on Hydrophobic Interaction Chromatography Media. *J. Chromatogr. A* **2020**, *1625*, 461309. DOI: 10.1016/j.chroma.2020.461309.

[47] Guo, J.; Zhang, S.; Carta, G. Unfolding and Aggregation of a Glycosylated Monoclonal Antibody on a Cation Exchange Column. Part I. Chromatographic Elution and Batch Adsorption Behavior. *J. Chromatogr. A* **2014**, *1356*, 117–128. DOI: 10.1016/j.chroma.2014.06.037.